THE EFFECT OF PARTICLE SHAPE ON JUST-SUSPENDED SPEED OF MIXTURES OF SOLIDS AT HIGH CONCENTRATIONS

A THESIS SUBMITTED TO
THE GRADUATE SCHOOL OF NATURAL AND APPLIED SCIENCES
OF
MIDDLE EAST TECHNICAL UNIVERSITY

BY
BAŞAK KÜTÜKCÜ

IN PARTIAL FULFILLMENT OF THE REQUIREMENTS
FOR
THE DEGREE OF MASTER OF SCIENCE
IN
CHEMICAL ENGINEERING

JUNE 2017

Approval of thesis:

THE EFFECT OF PARTICLE SHAPE ON JUST-SUSPENDED SPEED OF MIXTURES OF SOLIDS AT HIGH CONCENTRATIONS

submitted by **BAŞAK KÜTÜKCÜ** in partial fulfillment of the requirements for the degree of **Master of Science in Chemical Engineering Department, Middle East Technical University** by,

Prof. Dr. Gülbin Dural Ünver ________________
Dean, Graduate School of **Natural and Applied Sciences**

Prof. Dr. Halil Kalıpçılar ________________
Head of Department, **Chemical Engineering**

Asst.Prof. Dr. İnci Ayrancı ________________
Supervisor, **Chemical Engineering Dept., METU**

Examining Committee Members:

Prof. Dr. Yusuf Uludağ ________________
Chemical Engineering Dept., METU

Asst. Prof. Dr. İnci Ayrancı ________________
Chemical Engineering Dept., METU

Assoc. Prof. Dr. Görkem Külah ________________
Chemical Engineering Dept., METU

Asst. Prof. Dr. Erhan Bat ________________
Chemical Engineering Dept., METU

Asst. Prof. Dr. Suna Ertunç ________________
Chemical Engineering Dept., Ankara University

Date: June 19, 2017

I hereby declare that all information in this document has been obtained and presented in accordance with academic rules and ethical conduct. I also declare that, as required by these rules and conduct, I have fully cited and referenced all material and results that are not original to this work.

Name, Last name: Başak Kütükcü

Signature :

ABSTRACT

THE EFFECT OF PARTICLE SHAPE ON JUST-SUSPENDED SPEED OF MIXTURES OF SOLIDS AT HIGH CONCENTRATIONS

Kütükcü, Başak

M. Sc., Department of Chemical Engineering

Supervisor: Asst. Prof. Dr. İnci Ayrancı

June 2017, 103 pages

Solid-liquid mixing is a common application in the chemical industry. For solid-liquid mixing operations, it is important to determine the impeller speed which provides the maximum contact surface between the phases at minimum power consumption. This impeller speed is called just suspended speed, N_{js}. N_{js} can be determined experimentally by visual observation or pressure gauge measurement method. If the mixing system is at the design stage or if it is not possible to apply experimental methods, the correlations in literature are used to predict N_{js}. Most of the studies on this subject have been done with unimodal slurries of spherical particles at low solids concentrations, and some with mixed slurries of spherical particles at high concentrations. But industrial applications generally consist of mixtures containing many solid phases and irregularly shaped particles at high concentrations.

In this study, the aim was to test the applicability of the correlations in literature for mixed slurries that have non-spherical particles at high concentrations and to test the applicability of pressure gauge measurement method at conditions that are different than literature conditions.

First, the suspension behaviour of mixed slurries with non-spherical particles was investigated. The results showed that spherical particles are harder to suspend. To investigate whether a correction is required in correlations, the N_{js} predictions of

Ayranci's correlation were compared for the unimodal slurries with spherical and non-spherical particles. Ayranci's correlation was chosen because the most accurate N_{js} predictions were obtained with this correlation compared to the other correlations in literature without any shape consideration. It was seen that the predictions with Ayranci's correlation are at almost the same accuracy for both spherical and non-spherical particles. Nevertheless, to obtain more accurate results for non-spherical particles, the performance of aspect ratio, circularity, convexity, Wadell's sphericity and Corey's shape factor was compared to incorporate particle shape mathematically. It was decided that Wadell's sphericity is the most convenient factor to represent the effect of particle shape on solids suspension in stirred tanks. With this, the standard deviations in the predictions decreased.

The mixed slurry N_{js} was measured experimentally and these results were compared with the predictions using the power model. A correction on the power model was recommended for the slurries that show networking effect. This correction allowed for the prediction data to follow the experimental data more closely. When the correction for the particle shape in Ayranci's correlation was introduces, the standard deviations in the prediction of mixed slurries decreased.

Finally, the applicability of pressure gauge measurement method was tested at conditions that are beyond the limits that it was developed initially. The problems encountered with collection and analysis of data at these out-of-limit applications and the solutions to overcome them are reported. Also, the visual observation method and the pressure gauge measurement method were compared with a large data set for the first time, in this study.

Keywords: Solids suspension, just suspended speed, particle shape, pressure gauge measurement method, high concentrations, stirred tanks, mixing

ÖZ

YÜKSEK KONSANTRASYONLU KATI SIVI KARIŞIMLARINDA PARTİKÜL ŞEKLİNİN MİNİMUM KARIŞTIRMA HIZINA ETKİSİ

Kütükcü, Başak

Yüksek Lisans, Kimya Mühendisliği Bölümü

Tez Yöneticisi: Yrd. Doç. Dr. İnci Ayrancı

Haziran 2017, 103 sayfa

Katı-sıvı karıştırma kimya endüstrisinde sıkça karşılaşılan bir uygulamadır. Katı-sıvı karıştırma operasyonlarında minimum güç tüketiminde, fazlar arasındaki maksimum temas yüzeyini sağlayan karıştırıcı hızını belirlemek önemlidir. Bu hız minimum karıştırma hızı, N_{js}, olarak adlandırılır. N_{js} deneysel olarak görsel ölçümler veya basınç farkı ölçümü yöntemi ile belirlenebilir. Karıştırma sistemi tasarım aşamasındaysa ya da deneysel yöntemleri uygulamak mümkün değil ise N_{js} tahmini için literatürde yer alan korelasyonlar kullanılmaktadır. Bu konu hakkında yapılan akademik çalışmaların çoğu düşük konsantrasyonlarda tek katı faz içeren ve küresel partiküllü karışımlar ile, bir kısmı ise yüksek konsantrasyonlarda iki katı faz içeren küresel partiküllü karışımlar ile yapılmıştır. Ancak endüstriyel uygulamalar çeşitli şekillerdeki çok sayıdaki katı fazını yüksek konsantrasyonlarda içeren karışımlardan oluşmaktadır.

Bu çalışmada yüksek konsantrasyonda küresel olmayan partiküllerden oluşan iki katı fazlı katı-sıvı karışımları için literatürdeki korelasyonların uygulanabilirliğinin ve basınç ölçümü yönteminin literatürde yer alan koşullardan farklı koşullarda uygulanabilirliğinin test edilmesi amaçlanmıştır.

Öncelikle, küresel olmayan partiküllerden oluşan iki katı fazlı karışımların süspansiyon davranışı incelenmiştir. Sonuçlar küresel partiküllerin daha zor süspanse

olduklarını göstermiştir. Tek katı fazlı katı-sıvı karışımları için Ayrancı'nın korelasyonunun küresel ve küresel olmayan partiküller ile verdiği sonuçlar karşılaştırılmıştır. Ayrancı'nın korelasyonunun her iki partikül tipi için de neredeyse aynı doğrulukta tahminler verdiği görülmüştür. Ayrancı'nın korelasyonu'nun seçilmesinin sebebi herhangi bir şekil düzenlemesi yapılmadan literatürde tek katı fazlı katı-sıvı karışımları için yer alan diğer korelasyonlara kıyasla en iyi sonucu vermesidir. Yine de küresel olmayan partiküller için daha iyi bir tahmin sağlamak için, en boy oranı, dairesellik, dış bükeylik, Wadell'in küreselliği ve Corey'in şekil faktörünün partikül şeklini matematiksel olarak ifade etme performansı karşılaştırılmıştır. Karıştırmalı tanklarda partikül şeklini ifade eden en uygun faktörün Wadell'in küreselliği olduğuna karar verilmiştir. Bu düzeltme ile Ayrancı'nın korelasyonu ile yapılan tahminlerdeki standart sapma azalmıştır.

İki katı fazlı karışımların N_{js}'leri deneysel olarak ölçülmüş ve bu sonuçlar güç modeli kullanılarak elde edilen N_{js} tahminleri ile karşılaştırılmıştır. Ağ etkisi gösteren katı-sıvı karışımlarının N_{js} tahminleri için güç modeline bir düzeltme önerilmiştir. Bu düzeltme katı-sıvı karışımlarının N_{js} tahminlerinin deneysel verileri takip edebilmesini sağlamıştır. Ayrancı'nın korelasyonundaki şekil düzeltmesi ile birlikte iki katılı katı-sıvı karışımlarının N_{js} tahminlerinin standart sapması düşmüştür.

Son olarak, basınç farkı ölçümü yönteminin, geliştirildiği koşullardan daha geniş koşullarda uygulanabilirliği test edilmiştir. Yöntemin limitleri dışında yapılan bu çalışmada, veri toplarken ve analiz edilirken karşılaşılan problemler ve çözüm önerileri rapor edilmiştir. Aynı zamanda ilk defa bu çalışma ile görsel yöntem ve basınç farkı ölçümü yöntemi karşılaştırılması geniş bir veri seti ile yapılmıştır.

Anahtar kelimeler: Katı süspansiyonları, minimum karıştırma hızı, partikül şekli, basınç farkı ölçümü yöntemi, yüksek konsantrasyon, karıştırmalı tank, karıştırma

Dedicated to my mother, Esma Kütükcü, my father, Ersin Kütükcü,
and my brother, Başar Kütükcü

ACKNOWLEDGMENTS

First, I am grateful to my supervisor Asst. Prof. Dr. İnci Ayrancı for her guidance, patience, encouragement and helps on all parts of my study. Her positive perspective motivated me every time. I learned a lot and improved myself thanks to her during this study.

I would like to state my sincere thanks to Esra Demirkol and Nilay Yazıcı for their great friendship. Although they live away from me, I always felt their support and positive energy.

Özge Kalender and Yiğit Akgün are my dear friends that I have gained in my graduate education. I thank them for their friendship and support. Also, I would like to thank to beloved Arda Yılmaz for his love and support. He was always there to make me happy and hopeful when I needed.

Finally, I would like to express my deepest gratitude to my parents, Esma Kütükcü and Ersin Kütükcü, and my brother Başar Kütükcü. I always felt their support and love throughout my life. I thank them for believing and encouraging me every time.

This study is supported by TUBITAK and METU BAP, I also thank for these financial supports. TUBITAK Grant no: 115C033, BAP Grant no: 07-02- 2014-007-711.

TABLE OF CONTENTS

LIST OF FIGURES

LIST OF TABLES

LIST OF SYMBOLS

Roman Characters

A: projected area of particle

A_b: area of the tank bottom

A_c: the area of an imaginary particle that has the smallest possible perimeter in which the indentations are not present

A': Ayranci's geometry related constant

a: minor axis of a particle

B: breadth of particle

b: major axis of a particle

C: off-bottom clearance of the impeller (m) or constant for networking mechanism used in Equation (4.2)

C_b: volume fraction at near bottom of tank (volume of solids/volume of slurry)

C_D: drag coefficient

D: diameter of impeller (m)

d_{proj}: diameter of projected area

d_p: particle diameter (m)

d_{mass}: mass equivalent diameter (m)

d_{min} : minimum dimension of particle (m)

d_{med} : medium dimension of particle (m)

d_{max} : maximum dimension of particle (m)

F: force applied on particle (N)

F_z: Zingg factor

$F_{pressure}$: the force due to the pressure exerted by the amounts of liquid and solid phases

F_{total}: the total force that applies on the bottom of the tank

$F_{direct\ contact}$: the force that applies on the bottom of the tank due to direct contact of particles

g: acceleration of gravity (m/s^2)

H: height of liquid (m)

K: the large side of rectangle surrounding area of a particle (m)

L: the distance between two farthest points of a particle (m)

M: the short side of rectangle surrounding the area of a particle (m)

M_l: mass of liquid

M_s: mass of suspended solid particles

M_t: total mass of solid particles

m: exponent on shape factor term

m_{pellet}: mass of pellet (kg)

N_{js}: just suspended speed (rpm)

$N_{js,mix}$: just suspended speed of mixed slurries (rpm)

$N_{js,1}$: just suspended speed of unimodal slurry of component 1 (kg/m^3)

$N_{js,2}$: just suspended speed of unimodal slurry of component 2 (kg/m^3)

$N_{js,\ measured}$: just suspended speed that is determined by measurement (kg/m^3)

$N_{js,\ PGM}$: just suspended speed that is determined by pressure gauge measurement method (kg/m^3)

$N_{js,\ visual}$: just suspended speed that is determined by visual observation method (kg/m^3)

N_p: power number

n: exponent of concentration term used in Equation (1.4)

P: perimeter of the projected area of particle (m)

$P_{ellipse}$: perimeter of the fitted ellipse (m)

P_{smooth}: smoothed perimeter of the projected area of particle (m)

P_{rough}: rough perimeter of the projected area of particle (m)

R: the shortest side of a rectangle which has equal perimeter and area to projected area of a particle (m)

R_{El}: elongation ratio

R_{Fl}: flatness ratio

r: the distance between where the force is applied to particle and where the torque acting on particle is measured (m)

S: Zwietering constant

T: diameter of tank (m)

U_t: terminal settling velocity (m/s)

u_s: sedimentation velocity (m/s)

V: volume of particle

X: Zwietering's solids loading (mass of solids/mass of liquid *100)

X_w: solids weight concentration (mass of solids/mass of slurry*100)

X_v: solids volume concentration (volume of solids/volume of slurry*100)

x: exponent of concentration term used in Equation (1.3)

Z: constants used in Equation (1.2)

z: constant used in Equation (1.6)

Greek Characters

ρ_s: density of solid (kg/m^3)

ρ_l: density of liquid (kg/m^3)

$\rho_{sl:}$ density of slurry (kg/m^3)

$\rho_{sl,1:}$ density of unimodal slurry of component 1 (kg/m^3)

$\rho_{sl,2:}$ density of unimodal slurry of component 2 (kg/m^3)

$\rho_{sl,mix:}$ density of mixed slurry (kg/m^3)

$\Delta\rho$: density difference of solid and liquid phases, (ρ_s - ρ_l) (kg/m^3)

ΔS_s: the surface area of a sphere which has the same volume as particle (m^2)

ΔS_r: the surface area of particle (m^2)

μ_l : viscosity of liquid

υ: kinematic viscosity of liquid (m^2/s)

v': turbulent eddy fluctuation velocity in vicinity of solid surface (m/s)

ε_{mf}: voidage at minimum fludization velocity

δ: constant used in Equation (1.5)

γ: constant used in Equation (1.5)

β: constant used in Equation (1.5)

α: dimensionless energy damping constant in Equation (1.3)

τ: torque acting on particle (N.m)

φ: Shape factor

φ_C: Corey's shape factor

φ_W: Wadell's sphericity

φ_H: Heywood's shape factor

φ_V: Volumetric shape factor

φ_{mass}: Mass shape factor

φ_{stokes}: Stokes shape factor

Abbreviations

AR: aspect ratio

ABS: acrylonitrile butadiene styrene

BG: big glass beads

El: elongation

Grit St: grit steel particles

LG: large glass beads

LAl: large aluminum oxide particles

Plt Cp: plate shaped copper particles

PGM: pressure gauge measurement method

Re: Reynolds number

Re_t: Reynolds number of turbulent eddies

Re_{ter}: Reynolds number at terminal velocity

Re_E: Reynolds number of turbulent eddies

Rod Cp: rod shaped copper particles

SAl: small aluminum oxide particles

SG: small glass beads

Sph St: spherical steel particles

TPE: thermoplastic elastomer

CHAPTER 1

INTRODUCTION

1.1 Definition of Mixing

Mixing can be defined as reduction of inhomogeneity to achieve desired process results (Atiemo-Obeng and Penney, 2004). The inhomogeneities can correspond to concentration, phase or temperature distribution, and they can affect the process objectives such as mass transfer rate, reaction yield or properties of products.

The research about industrial mixing is critical because setting up a mixing process, reaching products which have desired properties and maintaining an efficient process is only possible with the development of fundamental understanding of mixing processes, which can be done through research.

In the development step of a process which includes mixing operations, if mixing scale-up fails to produce the required product quality or production yield;

- the cost of production can increase significantly,
- selling of the product can be delayed or canceled because of insufficient time and cost to correct the mixing problem.

The cost of appropriate evaluation and solving the mixing issues at the process development stage is less than the cost associated with these problems. Even if the mixing requirements are scaled up correctly, some new methods and alternative mixing designs for critical applications may need to be developed for more complex problems.

Single phase mixing has no applications, but multiphase mixing is common operation in the chemical industry. The aim, examples and significance of mixing can be explained as follows for most common types of industrial multiphase mixing.

Gas-Liquid Contacting: There are many processes which are based on the mass transfer between gas and liquid phase. In these processes, absorption and desorption are the main transfer mechanisms. An example of the gas-liquid reaction is the chlorination of liquid benzene and other hydrocarbons with gaseous chlorine (Levenspiel, 1998). In this example, gas chlorine absorbs into the liquid phase to react with hydrocarbons. According to reaction kinetics, short or long contact time can be necessary for efficient operation. This means that a careful design of a mixing system is critical.

Immiscible Liquid-Liquid Mixing: These systems contain two or more mutually insoluble liquids as separate phases. These phases are the dispersed – or drop – phase and the continuous – or matrix – phase. Some examples of these systems are emulsification, nitration, sulfonation, alkylation, hydrogenation, and halogenation. The rate of chemical reactions is often mass transfer controlled and affected by interfacial area. Therefore, the total area of drop phase affects mass transfer and the rate of chemical reactions. For example; in stirred vessels drop size distribution and resultant average drop size can be controlled by selection of the impeller type, the position of the impeller and impeller speed (Atiemo-Obeng and Penney, 2004).

Rotor–stator mixers, static mixers, decanters, settlers, centrifuges, homogenizers, extraction columns, and electrostatic coalescers are the other examples of industrial process equipment used to contact liquid–liquid systems.

Solid-Liquid Mixing: Solids can be settling or floating in industrial applications. The highly concentrated solid-liquid suspensions are called as slurry. The main aim of creating a suspension is to promote the maximum rate of mass transfer.

Solids suspension operations are typically carried out in stirred tanks. Pumped liquid jets and static mixers are also being used to suspend low concentrations of relatively slow settling solids and to disperse fine solids into polymers (Atiemo-Obeng and Penney, 2004).

In this study, suspension of settling solids was investigated. In the next section, some information was given about operations based on solid-liquid mixing, types of suspension and critical parameters to design a mixing system for solids suspension.

1.2 Solid-Liquid Mixing

Industrial processes have many unit operations based on solid-liquid mixing. Dispersion of solids, crystallization and precipitation, solid catalyzed reactions, dissolution and leaching, absorption, desorption and ion exchange, suspension and polymerization are examples of solid-liquid mixing operations. The objective of the process is often to provide maximum mass transfer. To satisfy this objective the surface area between the solid and liquid phases should be maximum, and this objective should be achieved at minimum power consumption for an efficient operation (Atiemo-Obeng and Penney, 2004).

The requirement of maximizing the contact surface for an efficient operation can be better understood with some more detailed descriptions of operations mentioned above. For example, in a dispersion process the aim is to suspend and disperse solid particles and aggregates by an agitator in the fluid and to maintain a uniform suspension. In a dissolution process, the solid particles become smaller and finally disappear as a solute in the liquid phase. Leaching means extracting some chemicals from the solid particles by taking advantage of solubility of the chemicals in the liquid. Similarly, in desorption and absorption, there are mass transfer phenomena from the solid to the liquid and vice versa. In solid catalyzed reaction operations, the reaction occurs at the surface of the catalyst so reactants should absorb to surfaces and products should be desorbed from the surfaces; therefore, it is important to maintain a uniform suspension for uniform distribution of reactants and products and maximum mass transfer area between solid and liquid phases. Precipitation and crystallization starts with only liquid phase and then solid particles form and grow. During these operations, the most important things are to minimize particle breakage or attrition and to control the particle size distribution and uniformity of mixture.

The solid-liquid mixing operations are often carried out in agitated tanks. The state of suspension can be characterized experimentally by visual or pressure measurement based methods. The degree of solids suspension is categorized into three groups: on-bottom motion or partial suspension, complete off-bottom suspension and uniform suspension. These are illustrated in Figure 1.

At the state of on-bottom motion suspension, the particles are in motion, but they are not fully suspended. Most particles are in constant contact with the tank base. On-bottom motion suspension is often used for dissolution of solids. If the solids used can dissolve in the liquid phase easily, this suspension state is ideal.

At uniform suspension, particle size distribution and particle concentration are uniform at every point of the tank. If the process objective requires a uniform distribution as in crystallization reactions, this is the suspension state that should be maintained.

At complete off-bottom suspension, the particles are just-suspended of the bottom of the tank, allowing for the interaction of the entire surface area of the solids with liquid. If the process objective is mass transfer only, then the complete off-bottom suspension should be maintained. This state is the most commonly used state of suspension for solid-liquid mixing operations in industrial applications (Atiemo-Obeng and Penney 2004).

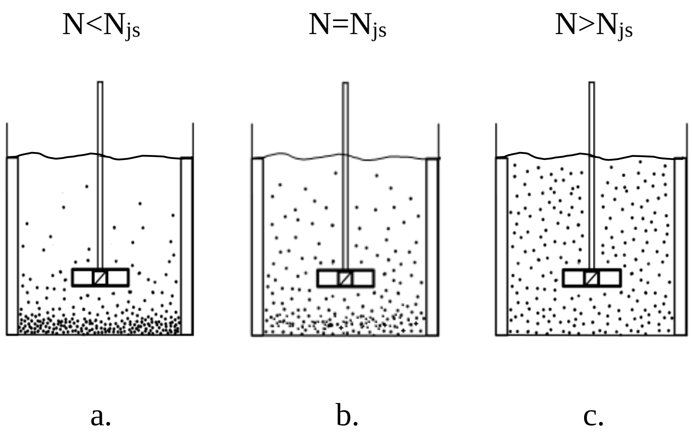

Figure 1. (a) On-Bottom Motion Suspension or Partial Suspension, (b) Complete Off-Bottom Suspension, (c) Uniform Suspension

The state of complete suspension is generally characterized by Zwietering criterion: when no particle remains stationary on the tank bottom for more than 1 to 2 s, the complete off-bottom suspension is achieved. The impeller speed for this condition is defined as just suspended speed, N_{js} (Zwietering, 1958).

Considering studies about solid-liquid mixing so far, the parameters which affect N_{js} can be listed as:

- Densities of solid and liquid phase,
- Particle size,
- Diameter of the tank and the impeller,
- Impeller type,
- Off-bottom clearance,
- Baffle width,
- Solids loadings,
- Shape of tank bottom,
- Liquid height.

The most commonly used state of suspension is complete off-bottom suspension so studies are generally based on this state of suspension. In the next section, the methods to determine just suspended speed are explained.

1.3 The Methods to Determine the Just Suspended Speed

The just suspended speed is either determined by experimentally for a small scale of the industrial system and then scaled-up, or by using the correlations available in the literature. In this section first the experimental methods, and then the correlations are explained in detail.

1.3.1 Experimental Methods

N_{js} is most commonly measured by **observing the bottom** of the tank which is in line with Zwietering's definition. This method; however, has some drawbacks. It is observer-dependent. The results may vary between observers. (Atiemo-Obeng and Penney, 2004). The accuracy of the measured N_{js} ranges from 7 % to 38 % between observers, depending on the particle types in the slurry, the colour contrast between particles and the liquid phase is important (Ayranci and Kresta, 2011).

Another visual observation method is based on **measurement of cloud height** of the suspension as defined by Einenkel and Mersmann (1977). When solids are suspended, interface forms between the clear liquid at the top of the tank and the solids rich volume, just below. Einenkel and Mersmann (1977) proposed that the impeller speed that provides a cloud height of approximately 90% of the total liquid height is the just suspended. This visual method does not appear more reliable than Zwietering's method. First of all, it considers the particle motion in the axial position in the tank, rather than the bottom of the tank. The bottom view clearly gives more information about the suspension state. Even if the particles may seem suspended when observed from the side, the bottom view can show that most are still stationary at the tank base. Second, if the suspension contains various sizes of particles, the easy to suspend particles can reach the top of the tank easily although some hard to suspend particles are still on the bottom of the tank. Because of these, the cloud height method is unreliable, and cannot be used to accurately determine the just suspended speed.

These visual methods are very simple; however, they are required the use of transparent tanks. It is possible to use transparent tanks in laboratory scale equipment, but it is not practical for larger-scale tanks (Kasat and Pandit 2005). These methods are also observer-dependent.

These drawbacks revealed the need for new measurement methods which are independent of the observer, and applicable to any type of tank. Micale (2002) proposed **pressure gauge measurement** method. This method is based on the measurement of changes in the pressure at the bottom of the tank, while the impeller speed is increasing. When the impeller is running, the fluid motion causes the pressure at the bottom of the tank to increase. The vertical forces due to force exchange between impeller and fluid or friction on the vessel lateral and baffles contribute to bottom pressure are called as dynamic head effects.

When particles are suspended in liquid, the forces acting on the base become greater with respect to the state when there are no particles. This is because the distribution of the particles into the liquid phase changes the apparent density of the fluid and increases pressure captured by a sensor placed at the bottom of the tank (Micale et al. 2002). As shown in Figure 2 while the apparent density of fluid increases, pressure increase would have a greater gradient. For instance, the apparent density of water increases from 1000 to 1060 kg/m^3 for the mixture which includes 10 wt % glass, from 1000 to 1200 kg/m^3 for the mixture which includes 30 wt % glass. Once all the particles are suspended in the liquid, the pressure increase is only due to the dynamic head effects. After the complete suspension of all particles pressure increase becomes only dependent on kinetic energy transferred from the impeller to the slurry, therefore the pressure increase becomes proportional to the square of the impeller speed and the pressure data can be represented by a second-order parabola. This parabola helps to determine pressure differences at just suspension condition, the pressure increase due to the dynamic head effects at each impeller speed and the N_{js}. The detailed information about the application of pressure gauge measurement method is given in Chapters 3 and 4.

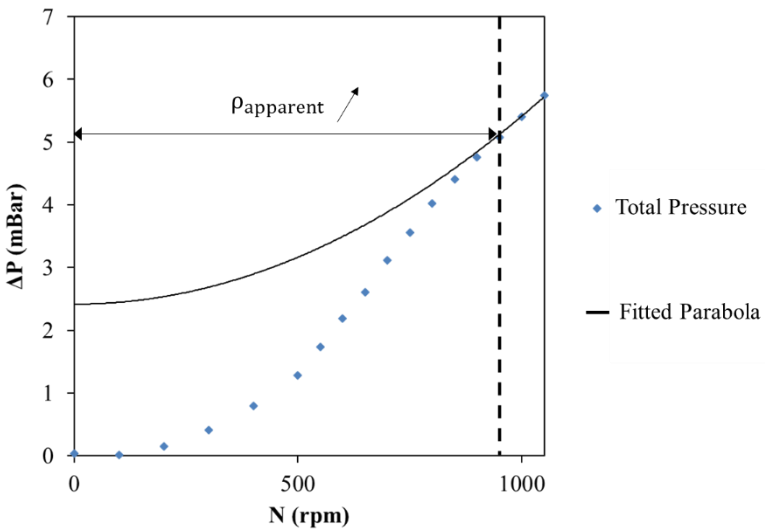

Figure 2. A typical plot of pressure change at the bottom of the tank with increasing impeller speeds. The second order parabola that represents the cases at and above N_{js} is also shown.

The pressure gauge measurement method is observer independent. This is a major advantage compared to the other methods available in the literature. This method was used in three studies in the literature, all of which were limited to single solid phase slurries with low N_{js} values. The method was not tested for high solids concentrations - therefore high N_{js} - slurries, and slurries with more than one solid phase. The application of the method to these extreme conditions is tested in this thesis.

1.3.2 Correlations

Experimental methods can be used to determine just suspended speed during the operation. In design stage of a mixing system, the need for empirical correlation arises.

Zwietering (1958) proposed a correlation to calculate N_{js} using a very large data set that he collected for several impellers and tank geometries. Equation (1.1) was obtained via dimensional analysis, except for the kinematic viscosity and density terms. After all the exponents for the rest of the terms were found, experiments were conducted with five different impellers to find the exponent of kinematic viscosity and density term:

$$N_{js} = S\left[\frac{g(\rho_s - \rho_l)}{\rho_l}\right]^{0.45} \upsilon^{0.1} X^{0.13} d_p^{0.2} D^{-0.85} \qquad (1.1)$$

Here ρ_s and ρ_l are densities of solid and liquid phases, g is acceleration of gravity, υ is kinematic viscosity, X is solids loading term, d_p is diameter of particles, D is diameter of impeller and S is the geometry-related term which depends on the ratios of the impeller to tank diameter (D/T), clearance to tank diameter (C/T) and type of impeller. Zwietering’s correlation has been used as design equation for mixing processes since it was developed, but recently some critical analysis of this correlation showed its deficiencies, and new correlations were proposed that can be applied to slurries that show properties similar to the industrial cases.

Main deficiencies of the Zwietering correlation are summarized as follows (Ayranci and Kresta 2014):

- The Zwietering constant does not only depend on impeller type, impeller size, clearance but also the shape of the tank bottom, geometry of baffles and particle type. It also cannot express the effects of impeller type, impeller size, clearance correctly.

- There is a viscosity term in the Zwietering correlation, but this term is arguable because of lack of experiments that are conducted with a wide viscosity range.

- Solids concentration term leads to unreasonable results when solids concentration is too low and its exponent cannot represent all range of solids concentration.

The studies to solve these problems which restrict the use of Zwietering's correlation are listed below.

The effect of geometry and scale cannot be expressed with Zwietering constant, S:

Ayranci et al. (2012) stated that effect of geometry and scale could not be represented with Zwietering's constant, S. If the mixing systems with the same geometry but different scales are compared, the difference between N_{js} values of these two systems cannot be predicted with only $D^{-0.85}$. The mechanism of solids suspension should be further investigated to predict the effect of scale-up on N_{js} (Ayranci et al., 2012).

As mentioned above, the impeller type, impeller size and clearance affect the Zwietering constant. Wong et al. (2015) stated that some impellers like pitched blade turbines and propellers can create double loop flow which causes a significant increase in N_{js} at systems that have larger C/D ratio than 0.75. Zwietering's correlation did not consider such effects. Also, the new impeller types that work better for solids suspension were developed afterwards; therefore, the impellers used by Zwietering are different from those used today (Wong et al. 2015).

Ibrahim et al. (2015) reached the conclusion that the Zwietering constant deviates less than 20 % from the result of correlation in the condition that C/D ratio is lower than 0.25 and solids loading is lower than 20 wt %. At higher solids loadings and C/D ratio, deviation of S values can reach up to 70 %. Also, it was observed that deviation of

Zwietering constant is affected more by off-bottom clearance and solids loading when using certain types of impellers. It can be understood from these inferences that Zwietering constant is not sufficient to predict N_{js} of mixtures at wide concentration and clearance ranges accurately.

The viscosity term is not reliable for mixtures which have fluids more viscous than water:

Ibrahim and Nienow (1994) found that the Zweitering's correlation is likely to fail, with an error as large as 90 % when a high viscosity liquid than 1 Pa.s is used. Zwietering's experiments contain liquids which have viscosities between $0.31x10^{-3}$ and $9.3x10^{-3}$ Pa.s. the viscosity range is not wide enough to determine an exponent on the viscosity term that can represent the effect of viscosity for fluids larger than 1 Pa.s viscosity. Solids suspension has applications for high viscosity fluids with varying rheological properties. The effect of viscosity and rheology should be considered for solids suspension applications. When there is a large amount of dispersed fine particles in suspension, it causes shear-thinning non-Newtonian behaviour. In such a situation suspension of coarse particles are affected by the non-Newtonian flow of the fluid+fine solids (Wu et al. 2001).

The solids loading term may cause non-physical results:

Myers et al. (2013) conducted experiments for different particle types with about 25 particles of each type, separately. They observed that N_{js} of 25 particles is 72 % of N_{js} of 1 wt% solids. This is a significant N_{js}; however, the correlation predicts zero N_{js}. This shows that the solids loading term may give non-physical results.

At high concentrations, the Zwietering correlation fails to represent experimental data:

The particle-particle interaction is not only effective for the mixtures that contain solid components which have varying sizes and densities but also for unimodal slurries at high solids loading. Myers et al. (2013) determined three new exponents for Zwietering's solids loading. According to their findings, the exponent of X should be 0.097 at low solids loadings ($0<X\leq5$) to 0.22 at intermediate loadings ($5\leq X\leq25$) and 0.34 for the high loadings ($25\leq X\leq67$). Also, Ayranci and Kresta (2014) proposed new

exponents: 0.17, 0.23 and 0.32 for solids loading term for the entire solids concentration range they tested. Their exponents are grouped according to particle type.

In addition to critical studies mentioned above, there have been some other studies that proposed a new correlation to predict N_{js}. Baldi et al. (1978) proposed a theory based correlation to predict N_{js}. Their correlation is based on an energy balance that the required potential energy to lift a particle from the bottom of the tank is equal to the turbulent kinetic energy transferred to the particle, and the turbulent kinetic energy should be the energy of the turbulent eddies with similar sizes as the particle. They finally obtained Equation (1.2). Z values were obtained experimentally and given in graphs. Z values approach 1 for mixtures at concentrations higher than 2 wt %, therefore; N_{js} becomes independent from solid concentration.

$$N_{js} = \frac{1}{Z}\left(\frac{g(\rho_s - \rho_l)d_p}{\rho_l}\right)^{0.5} \frac{d_p^{\frac{1}{6}}}{N_p^{\frac{1}{3}} D^{\frac{2}{3}}} \frac{T}{D} \qquad Z \propto \left(\frac{\mu\, T}{\rho_l\, D^3 N_{js}}\right)^{-0.2} X^{-0.15} \qquad (1.2)$$

Davies (1986) wrote a force balance around one isolated particle and proposed another theory based correlation. According to his hypothesis, while a particle becomes suspended, the gravitational force of a particle is balanced by turbulent eddy forces acting on it. When he wrote the force balance, he used Baldi's hypothesis, so he assumed that eddy's size equal to particle diameter at the just suspended condition. Unlike Baldi's correlation, there is a concentration term in Davies' correlation. This term comes from the assumption that suspended particles distribute energy around them and this energy causes a decrease of turbulence. When he used turbulent velocity in his equations, he assumed that they are reduced locally to $(\frac{v'}{(1+\alpha C_b})$. α is dimensionless energy damping constant, C_b is the concentration at near bottom of the tank. C_b can be taken as equal to solids concentration at the state of just-suspended. The equation which is obtained with these assumptions is given in Equation (1.3), n depends on particle size.

$$N_{js} = 0.76\,(1+\alpha C_b)(1-C_b)^{x/2} N_p^{-1/3} d_p^{(1/6)} \left(\frac{g\Delta\rho}{\rho_l}\right)^{1/2} \left(\frac{H}{T}\right)^{1/3} \left(\frac{D}{T}\right)^{-1} D^{-2/3} \qquad (1.3)$$

Davies observed that C_b term can give compatible results with experimental data in the range of 0.08<C<0.1. Their data were not tested with the mixtures at concentrations higher than C_b=0.1.

Ayranci and Kresta (2014) examined Zwietering's correlation and determined its limits of applicability. They also aimed to propose a correlation considering Zwietering's findings and Baldi's hypothesis. When relationships between N_{js} and the parameters which are given by Zwietering is examined, it can be said that terms of density, particle size and viscosity are expressed partially correctly but experimental data is required to determine how the terms of clearance and solids loading should be.

Ayranci et al. (2012) found that the dominant mechanism for suspension of solids is the turbulent eddies for an impeller of T/3 diameter. This is in line with Baldi's hypothesis; therefore, to take account for his hypothesis, they used his exponents for d_p, D, T and N_p in their correlation. Then, they used experimental data to obtain a representative concentration term.

After the arrangements and data analysis, they found that Zwietering's constant (S) does not only depend on geometry, it is also a function of physical properties of fluid and particles and scale of the mixing system. It is stated that power per mass is constant for systems which are at different scale but have the same ratio of C/T and D/T. However, the amount of power per mass is affected by density and size of particles, density and viscosity of fluid, diameter and type of impeller. A' constant which can express these effects is found and given in Equation (1.4), after the modification of S. The condition of constant power per mass is ensured with A' so Equation (1.4) can be used on scale-up.

$$N_{js} = A'\left(\frac{g(\rho_s-\rho_l)}{\rho_l}\right)^{0.5}\frac{d_p^{\frac{1}{6}}X^n}{N_p^{\frac{1}{3}}D^{\frac{2}{3}}}\frac{T}{D} \qquad A' = S\frac{d_p^{\frac{1}{30}}N_p^{\frac{1}{3}}\upsilon^{0.1}}{D^{\frac{11}{60}}}\frac{D}{T}\left(\frac{g\Delta\rho}{\rho_l}\right)^{-0.05} \qquad (1.4)$$

Ayranci and Kresta (2014) found three possible n values 0.17, 0.23 and 0.32 which will be used in Equation (1.4) as the exponent of solids loading term. The exponent of 0.23 is the average exponent that represents the entire data set. Ayranci's correlation gives accurate results up to 35 wt % solids.

Grenville et al. (2016) proposed another correlation known as GMB. This correlation satisfies the rule of constant power per mass on scale up. First, they stated that required potential energy which particle has when it is lifted from the tank bottom is equal to turbulent kinetic energy transferred to the particle. Turbulent kinetic energy is a function of energy dissipation rate and length of the eddies. They accepted the truth of Baldi's hypothesis and assumed that length of eddies is equal to particle diameter. Then they obtained an equation that includes Reynolds number of turbulent eddies and Archimedes number.

The relationship between Re_E and Ar is examined with the experimental data. It was seen that there are two regimes: Re_E is proportional to $Ar^{1/2}$ and $Ar^{1/3}$. Particle size causes the formation of these regimes. The regimes show where turbulent eddies and particles interact. If they interact in inertial sub-range Re_E is proportional to $Ar^{1/2}$ but if they interact in viscous sub-range Re_E is proportional to $Ar^{1/3}$. They analyzed experimental data taken from regime which particles and eddies interact in inertial sub-range. Finally, Equation (1.5) is obtained and constants γ and δ are determined with regressions. The experiments conducted using the particles which have various sizes and densities, different clearances at various concentrations.

$$\frac{\mathrm{Re_E}}{\mathrm{Ar}^{1/2}} = \beta\, \mathrm{X_v^{\gamma}} \left(\frac{\mathrm{C}}{\mathrm{D}}\right)^{\delta} \tag{1.5}$$

The other exponents in Equation (1.6) taken from Davies' correlation directly. Z is 1.528 for pitch blade turbines and 1.213 hydrofoil impellers.

$$\mathrm{N_{js}} = \frac{\mathrm{z}}{\mathrm{N_p^{0.333} D^{0.667}}} \left(\frac{\mathrm{g}(\rho_s - \rho_l)}{\rho_l}\right)^{0.5} \mathrm{d_p^{0.167} X_v}^{0.154} \left(\frac{\mathrm{C}}{\mathrm{D}}\right)^{0.1} \tag{1.6}$$

These new correlations are significant developments for industrial operations based on solid-liquid mixing. But these can predict only N_{js} of slurries which include single phase.

When there are two or more solid phases, how N_{js} should be calculated is uncertain:

The industrial operations are composed of mixtures of solids with varying densities and particle sizes at high concentrations. The interaction between particles has an important impact on just suspended speed for the mixtures which contain two or more solid phases and high concentrations. Montante and Magelli (2007) carried out a computational study which includes mixtures that have two solid phases. In order to decide if there is any interaction between solid phases which can affect the N_{js} of mixtures, they compared the sum of suspended solid mass measured for unimodal and mixed slurries at various impeller speeds. According to their results, the presence of second solid phase does not affect the N_{js} because the sum of suspended solid mass for each unimodal slurry is equal to the solid mass of mixed slurry at certain impeller speeds. Thus, it can be said that N_{js} of binary mixtures is equal to N_{js} of unimodal slurry which is higher than other but their study includes mixtures at low solids concentrations (<5 wt %). Ayranci et al. (2013a) conducted a study to determine the accuracy of this inference for high concentrations - up to 35 wt % - and they proved that interactions between solid phases are so important that they affect N_{js}. These interactions become even more important for concentrations higher than 20 wt %. They proposed to use the momentum or power model to predict N_{js} of mixtures. These models based on the hypothesis that the required momentum or power to suspend mixture is equal to the sum of momentum or power of each solid phases. While momentum model generally gives results higher than experimental data, the results of power model are more accurate and acceptable. Power model which obtained by Ayranci et al. (2013) is given in Equation (1.7). Bao et al. (2013) conducted another experimental study to decide whether the visual N_{js} is equal to N_{js} calculated from the sum of power required to suspend each solid phase. According to their results, this theory is valid for binary and ternary solid mixtures but N_{js} obtained from the sum of power is 10 % higher than measured N_{js} for low-density (<1500 kg/m^3) solid mixtures and high density (>2400 kg/m^3) solid mixtures.

$$N_{js,mix} = \left(\frac{\rho_{sl,1} N_{js,1}^3 + \rho_{sl,2} N_{js,2}^3}{\rho_{sl,mix}}\right)^{1/3} \tag{1.7}$$

Ayranci and Kresta (2011) investigated particle-particle interactions and its effect on just suspended speed. N_{js} of mixtures generally increases when the solids loading increases except for conditions that the less dense component is smaller than or similar to the more dense component. In their study, it was observed that small and less dense particles create a network which enables denser and larger particle to be suspended more easily. Such suspension mechanism which includes the formation of a network is called networking mechanism. Power model can be applied with a standard deviation of 9 % except in cases involving network mechanism. In such cases, when solids concentration is higher than 20 wt %, an increase of concentration causes a decrease of N_{js}. Power model cannot calculate $N_{js,\ mix}$ correctly in such situations.

Some explanations and correlations were given to account for the parameters that affect solids suspension. Another parameter that has not yet been considered, but requires attention is particle shape. In research, often spherical particles are used; however, such particle shapes do not represent the slurries dealt with in the industry.

1.3 Motivation of Thesis

The industrial mixing applications involve both concentrated and mixed slurries with non-spherical or irregularly shaped particles. In literature, there are investigations about concentrated and mixed slurries but the effect of particle shape on N_{js} of unimodal and mixed slurries have not been expressed in correlations even if differently shaped particles were used for some of the tests. The aim of this study was to investigate how the N_{js} is affected by the particle shape and to represent the effect of particle shape in the prediction of N_{js} of unimodal and mixed slurries. Also, the visual method to measure the N_{js} of unimodal and mixed slurries is observer dependent. PGM method was used in this study with the aim of testing the applicability of PGM method to industrial applications with a large data set for mixed slurries at high concentrations.

CHAPTER 2

LITERATURE SURVEY

2.1 Behaviour of Non-Spherical Particles in Different Applications

The shape of the particle can affect the difficulty of lifting a particle from the bottom of the tank because it influences motion on the bottom, the interaction between the particles and fluid drag forces on the particles (Thorpe and Stevenson 2003).

There are some studies about the behaviour of non-spherical particles conducted in stirred tanks, pipes and fluidized bed reactors. The critical design parameter tested is the just suspended speed in stirred tanks, the deposition velocity – minimum velocity required to transport a slurry – in pipes, the minimum fluidization velocity in fluidized bed reactors. There are studies in the literature that show the relationship between the sphericity and drag coefficient or drag force. They are useful to comment on the behaviour of particles in applications mentioned above.

Leith (1987) studied to expand the range of use of Stoke's law which defines the drag force for spherical particles in a creeping flow. When he used an extension to Stoke's law, it was seen that as objects become less spherical, the surrounding flow field becomes less compared to around a sphere, causing drag on non-spherical objects to be higher than predicted. This result means that reduction of sphericity causes facilitating the drift.

Loth (2008) examined the relationship between the particle Reynolds number and drag coefficient (C_D) with the help of his experimental studies. In his study, it was observed that the particles which have the larger surface area than the surface area of the sphere which has the same volume as the particle, they have higher drag coefficient. The larger surface means less sphericity. When the value of drag coefficient becomes higher, particle settling velocity would be smaller. Equation (2.1) shows the formula of settling velocity and the relationship between settling velocity and drag coefficient is seen in this equation. As illustrated in Table 1, Oldshue (1983) categorized the mixing problems according to the settling velocity value that they have. For particles which have a free settling velocity of 0.1 to 6.0 ft/min, the power required for complete suspension and total uniformity is two and four times and a free settling velocity of 4 to 8 ft/min, the power ratios are 3 and 9 for complete suspension and total uniformity, according to this.

$$U_t = \sqrt{\frac{4\ g\ d_p\ (\rho_s - \rho_l)}{3\ \rho_l\ C_D}} \qquad (2.1)$$

Therefore, it can be considered that when sphericity decreases, C_D increases and this situation leads to the fact that the particles have lower settling velocity and less energy input for the state of complete suspension.

Table 1. The relationship between settling velocity of particle and required power to achieve suspension criteria (Oldshue, 1983, Atiemo-Obeng and Penney, 2004)

Suspension Criteria	Power ratio at settling velocity of 16-60 ft/min	Power ratio at settling velocity of 4-8 ft/min	Power ratio at settling velocity of 0.1-0.6 ft/min
On-bottom motion	1	1	1
Complete off-bottom suspension	5	3	2
Total uniformity	25	9	4
	As the settling velocity of particle decreases, to achieve complete off-bottom suspension is required less power →		

Ditl and Nauman (1992) conducted an experimental study with thin plate and disc shaped particles and concluded that thickness of the particles is the controlling dimension on N_{js}, their shape or major dimensions are not important. They observed that as the thickness of a particle increases, N_{js} increases. After a certain thickness, N_{js} is not affected by increasing thickness and remains constant.

Lambert and Smith (1996) conducted some experiments with buttons, tiddly winks and other, thicker, plastic disks in a stirred tank. They compared the visual N_{js} of the particles and the Zwietering prediction with their volume equivalent diameters. The measured data was higher than predicted data for non-spherical particles, but these data were equal to each other for spherical particles; therefore, they stated that Njs of non-spherical particles is higher than spherical particles. But they did not compare to visual Njs of spherical and non-spherical particles directly. They also stated that the friction force between the particle and bottom of the tank is much larger for flat particles compared to spherical particles. The spherical particles can roll easily.

The higher friction force between the particles and the bottom of the tank can have a negative effect on getting suspend of particles, but the flow direction area of a particle is also an important parameter for drag force on the particle. The larger flow direction area and the higher drag force can cause lower N_{js} value. It can be related to individual mass whether the drag force or friction force is important for a mixture. When the particles have bigger individual mass, friction force can become more important than drag force.

Hilton et al. (2010) specified that pressure drop obtained in fluidized beds with non-spherical particles are higher than in beds with volume equivalent spherical particles. The reasons for these situations are the reduced voidage and larger flow direction area of the non-spherical ones. They argued that the reduced voidage arises from that the face-on-face inter-particle contact is more likely for non-spherical particles. Also, they showed that fluidization velocities of non-spherical particles are lower than the velocities of spherical particles.

When all the particles are at rest on the bottom of the tank of a stirred tank, the reduced voidage can cause friction force between particles, and between particles and the bottom of the tank; therefore, the non-spherical particles may require higher N_{js}.

However, larger flow direction area of non-spherical particles can cause larger drag force and lower N_{js} values.

Parveen et al. (2013) have examined the effect of agglomerate shape on the stability in a fluidized bed. They proposed that spherical agglomerates are more stable than cylindrical agglomerates as spherical ones are exposed to less shear from bed turbulence. The torque acting on the particle is calculated as follows:

$$\tau = rF\sin\theta \tag{2.2}$$

where F is the force and r is the distance between where the force is applied and where the torque is measured. For cylindrical agglomerates, most of the acting forces create 90° angles with the breakage plane, while for spherical agglomerates, the forces do not create 90° angles, shown in Figure 3. This reduces the magnitude of the torque acting on the breakage plane of spherical agglomerates. This explains why spherical agglomerates were more stable than non-spherical ones (Parveen et al. 2013).

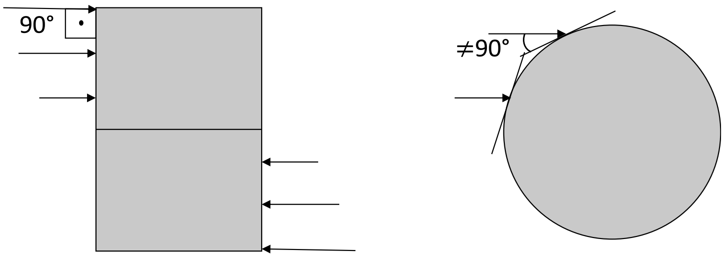

Figure 3. The comparison of forces acting on spherical and non-spherical particles adopted from Parveen et al. 2013.

If this situation is reviewed for an agitated tank, the high torque acting on the non-spherical particle lead to easier moving and lifting from the bottom of the tank, and this is desirable for an efficient solids suspension operation thus complete suspension can be obtained at lower stirrer speed.

Liu et al. (2008) conducted an experimental study providing information on the relationship between the minimum fluidization velocity and sphericity. Their results showed that equivalent spherical particles have higher minimum fluidization velocity.

Schaan et al. (1997) conducted an experimental study to determine the effect of particle shape on pipeline friction. They used three types of particle shape and they observed that as the angularity of particles increases, the velocity of particles with the fluid decreases. They stated that it is more difficult to convey particles which have higher sphericities with the fluid; because non-spherical particles cause higher force due to friction with the wall of the pipe.

Henthorn and Curtis (2005) observed that as the sphericity of particle in conveyed mixture becomes higher, pressure drop at vertical gas-solids pneumatic conveying line decreases. They stated that it is because the projection area of the particle affects the drag coefficient. The conveying of the spherical particles from the bottom to the top is more difficult than the conveying of the non-spherical particles so when they measured the pressure difference between the bottom and the top of the pipeline, it was lower for spherical particles.

Kruggel-Emden and Oschmann (2014) investigated the effect of particle shape on rope formation and dispersion in the pipeline during pneumatic conveying. In Figure 4, rope formation and dispersion are shown. The non-spherical particles which have larger projection area accelerated stronger at horizontal pipe section, but spherical particles have the lowest maximum velocity before entering the bend. On the other hand, the particles which have higher sphericities have the faster rope dispersion because of strong particle-fluid interaction, particle-particle collisions and large bend exit velocities. According to the result of this study, the non-spherical particles can drift with higher average velocity than the average velocity of spherical particles. On the other hand, the spherical particles do not slow down at the bend region because of the interaction with fluid and each other.

Figure 4. Schematic diagram of the simulation set-up adopted from Kruggel-Emden and Oschmann, 2014

2.2 Mathematical Definition of Particle Shape

In this study, suspension of non-spherical particles in a stirred tank is studied. The N_{js} correlations in the literature were evaluated to account for the effect of non-sphericity. This reveals the need for a factor which can express the particle shape numerically. Based on the literature, particle shape can be defined in terms of several different factors. These factors can be divided into three groups; 2D, 3D and measurement based shape factors.

2.2.1 2D Shape Factors

2D shape factors are preferable since only the images of the particles are required for their calculation. There are image analysis programs that enable to measure sizes of particles or calculate some ratios which identify their shape, so it becomes easy to determine 2D shape factors. The shape factors considered in the group of 2D shape factors are listed and explained below:

a) Aspect Ratio: It is introduced by Schneiderhöhn and defined as the ratio of minor axis to major axis of a particle which are perpendicular to each other. If the shape of the particle is indented, an ellipse can be fitted and axis can be measured from representative ellipse (Liu et al. 2008). This factor gives information about elongation, but it cannot distinguish some shapes, e. g. square and circle (Bouwman et al. 2004).

$$\mathrm{AR} = \frac{\mathrm{a}}{\mathrm{b}} \tag{2.3}$$

b) Elongation: It is defined as the ratio of the distance between two farthest points of the particle to the shortest side of a rectangle which has equal perimeter and area to projected area of the particle (Saad et al. 2011). The definition of this factor is also shown in Figure 5.

$$\mathrm{El} = \frac{\mathrm{L}}{\mathrm{R}} \tag{2.4}$$

Another definition of the elongation is given in Equation (2.5) a/b is the ratio of the minor axis to the major axis of the ellipse that has the same center as projected area of the particle (Emara and Ahmed 2009).

$$\mathrm{El} = \log 2\,\frac{\mathrm{a}}{\mathrm{b}} \tag{2.5}$$

c) Circularity: Circularity was first described by Cox; therefore it is also called Cox's roundness. Circularity is defined as a ratio that involves projected area and perimeter of this area (Radoičić et al. 2014). The definition is given in Equation (2.6). The measurements required to calculate circularity are significantly affected by the scale of measurement and the resolution of the image. This problem is often referred as the Coastline of Britain Problem (Bouwman et al. 2004).

$$\mathrm{Circularity} = \frac{4\,\pi\,\mathrm{A}}{\mathrm{P}^2} \tag{2.6}$$

Another definition of circularity is that the ratio of the perimeter of projected area to perimeter of a circle which has an equivalent area (Saad et al. 2011). The definition is given visually in Figure 5.

$$\mathrm{Circularity} = \frac{\mathrm{P}}{2\sqrt{\pi\,\mathrm{A}}} \tag{2.7}$$

d) Projection shape factor: This factor is a modified version of circularity which is given in Equation (2.6). The aim of modification is to decrease the dependence of shape factor to the scale of measurement and resolution of the image. When perimeter is measured, lines from the center to the periphery are drawn at 5º intervals and points that intersect the outer boundary and lines are merged in order to obtain perimeter which is smoother than the real perimeter (Bouwman et al. 2004).

$$\text{Projection Shape Factor} = \frac{4\,\pi\,A}{P_{smooth}^2} \tag{2.8}$$

e) Convexity: It is a factor that gives information about indentation of particles. Convexity can be defined as in Equation (2.9). It is a ratio that includes the projected area of the real particle and the area of the imaginary particle that has the smallest possible perimeter in which the indentations are not present. The definition is given visually in Figure 5. As the particles become concave, convexity decreases (Saad et al. 2011).

$$\text{Convexity} = \frac{A}{A + A_c} \tag{2.9}$$

f) Complexity: It gives information about angularity of a particle. An ellipse that is the least squares fit to the measured area is required to determine complexity. Complexity can be described as the ratio of the perimeter of projected area to perimeter of the fitted ellipse (Liu et al. 2008).

$$\text{Complexity} = \frac{P}{P_{ellipse}} \tag{2.10}$$

g) Compactness: This factor is defined as the ratio of projected area to the area of the rectangle surrounding this area. It is a measure of the deviation from rectangle or square of particle shape (Saad et al. 2011). The definition is given visually in Figure 5.

$$\text{Compactness} = \frac{A}{K\,M} \tag{2.11}$$

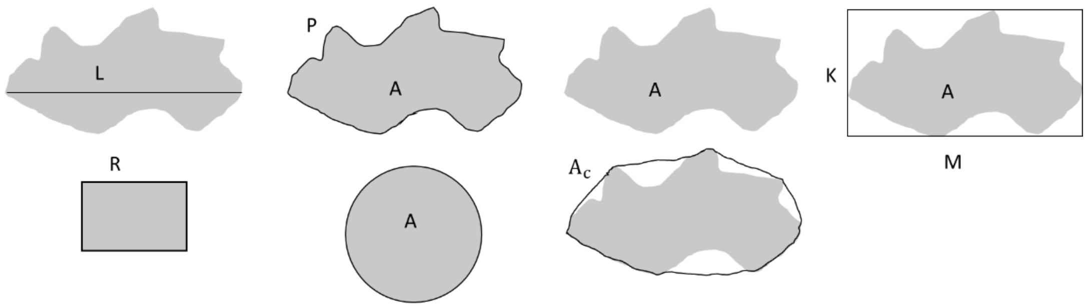

a. b. c. d.

Figure 5. Schematic representation of shape factors: a. Elongation, b. Circularity, c. Convexity and d. Compactness (adopted from Saad et al. 2011).

h) Roughness factor: Roughness of a particle has an influence on drag force, but it is not easy to measure the importance of this influence. It is thought that particle shape is more effective and important. The increase of the roughness of a particle causes the decrease of drag coefficient at low Reynolds number, but roughness becomes less important at high turbulence intensities (Loth 2008).

The definition of roughness factor involves the ratio of the smoothed perimeter to the rough perimeter. Smoothed perimeter is obtained like in definition of projection shape factor. Unlike smoothed perimeter, the rough perimeter is obtained by drawing lines from center to periphery are drawn at 1º intervals (Bouwman et al. 2004).

$$\text{Roughnes} = 1 - \frac{P_{\text{smooth}}}{P_{\text{rough}}} \tag{2.12}$$

2.2.2 3D Shape Factors

3D shape factors are factors that require knowledge of each dimension, surface area or volume of the particles. These can give more representative results, especially for flat particles when compared to 2D shape factors because there is a dimension that is not considered in the calculation of 2D shape factors. However, if this dimension is too small or too large, 2D shape factors can give misleading results.

a) Wadell's Sphericity: It is a 3D shape factor that is used commonly and is the most representative shape factor in fluid-particle systems (Radoičić et al. 2014). It is defined as the ratio of the area of a sphere which has the same volume as the real particle to the area of the real particle.

$$\varphi_w = \frac{\Delta S_s}{\Delta S_r} \tag{2.13}$$

b) Zingg Factor: This factor is introduced by Zingg and also known as dynamic shape factor. It is defined as the ratio of the elongation to the flatness. It provides representative results to be used in fluidization applications (Liu et al., 2008). Unlike sphericity, this factor can distinguish some shape differences. For example, an elongated cylinder and a square plate can have same sphericity but their shape is different and Zingg factor gives different results for these particle shapes. This difference leads to different behaviour in fluidized bed so it can be said that Zingg factor is a good approach to use in fluidized bed for non-spherical particles (Kruggel-Emden and Vollmari, 2016). R_{El} is elongation ratio, R_{Fl} is flatness ratio, L, B and H are the length, breadth and height of particle, respectively.

$$F_z = \frac{R_{El}}{R_{Fl}} = \frac{LH}{B^2} \tag{2.14}$$

If a particle is cylindrical or rod type $F_z > 1$, if it is a plate or disc-shaped $F_z < 1$.

c) Heywood's shape factor: It is defined as the ratio of the volume of the particle to the cube of projected diameter. Heywood's shape factor is equal to 0.524 for a sphere and its value decreases, as the flatness of particle increases (Daniel 1988). Projected area is obtained by the multiplication of the two main dimensions of the particle (Nikku et al. 2014).

$$\varphi_H = \frac{V}{d_{proj}^3} \qquad d_{proj} = \left(\frac{4(LH)}{\pi}\right)^{0.5} \tag{2.15}$$

d) Volumetric Shape Factor: It has a close definition to Heywood's shape factor. Volumetric shape factor defined as the ratio of the particle volume to the cube of the diameter of a sphere which has same projected area as the area of particle (Nikku et al. 2014, Mandø and Rosendahl, 2010).

$$\varphi_v = \frac{V}{d_p^3} \tag{2.16}$$

e) Corey's shape factor: It requires three lengths of particle perpendicular to each other and defined as the ratio of the minimum size of the particle to the geometrical mean of the maximum and medium sizes. It is a factor that is equal to 1 for cube and sphere. Although it is quite difficult to measure three dimensions of the particle, this factor is often used in fluidization applications (Nikku et al. 2014).

$$\varphi_c = \frac{d_{min}}{\sqrt{d_{med} d_{max}}} \tag{2.17}$$

Loth (2008) stated that it is the best factor to describe particle shape and suggested to be used instead of sphericity.

2.2.3 Measurement Based Shape Factors

There are some shape factors based on measurements of mass, surface area, settling velocity of particles, pressure drop or voidage in a fluidized bed. These factors can give information about movement properties of particles in a fluid with experimental data, but they are thought to be time-consuming methods to determine shape factor according to 2D and 3D methods (Bouwman et al. 2004).

a) Mass shape factor: It is the ratio of the diameter of the sphere which has the same mass as the particle to the diameter of the circle which has the same projected area as particle. Projected area can be measured from an image of the particle.

$$d_{mass} = \sqrt[3]{\frac{6m_{pellet}}{\rho_s \pi}} \qquad \varphi_{mass} = \frac{d_{mass}}{d_{proj}} \tag{2.18}$$

b) Stokes' shape factor: This factor is based on the comparison of the sedimentation velocity (u_s) and theoretical settling velocity. Sedimentation velocity of a particle can be measured in a viscous liquid and it is used to calculate Stoke's shape factor. Stokes shape factor can be calculated as:

$$\varphi_{stokes} = \frac{18\,\mu\,u_s}{(\rho_s - \rho_l)\,g\,d_{mass}^2} \tag{2.19}$$

c) Sphericity obtained from measurement of pressure drop: The pressure drop is measured throughout the fluidized bed. It also can be calculated with the Ergun equation and Wadell's sphericity (φ_w) can be obtained from this equation with the use of experimental pressure measurements (Radoičić et al., 2014).

$$-\frac{dP}{dz} = 150\frac{(1-\varepsilon)^2}{\varepsilon^3}\frac{\mu}{{\varphi_w}^2}U + 1.75\frac{(1-\varepsilon)}{\varepsilon^3}\frac{\rho_l}{\varphi_w}U^2 \tag{2.20}$$

d) Sphericity obtained from settling velocity measurement: The following equation is obtained a force balance around a particle and it shows that settling velocity is a function of the drag coefficient.

$$U_t = \sqrt{\frac{4\,g\,d_p\,(\rho_s - \rho_l)}{3\,\rho_l\,C_D}} \tag{2.1}$$

Drag coefficient is a function of sphericity. It can be expressed in different correlations which are given in Table 2. Approximately 100 experiments are required to obtain a representative settling velocity (Radoičić et al., 2014).

Table 2. The drag coefficient correlations that depend on sphericity

	$C_D = f(\varphi_w)$
Haider and Levenspiel:	$$C_D = \frac{24}{Re_{ter}}\left[1 + 8.716\, Re_t^{0.0964-0.5565}\exp(4.0655\,\varphi_w)\right] + \frac{73.69 Re_t \exp(-5.0748\varphi_w)}{Re_{ter} + 5.378\exp(6.2122\varphi_w)} \qquad (2.21)$$
Ganser:	$$\frac{C_D}{K_2} = \frac{24}{Re_{ter}K_1K_2}\left[1 + 0.1118\,(Re_{ter}K_1K_2)^{0.6567}\right] + \frac{0.4305}{1 + 3305/Re_{ter}K_1K_2} \qquad (2.22)$$ K_1 and K_2 are the shape-related factors.
Chien:	$$C_D = \frac{30}{Re_{ter}} + 67.289\exp(-5.03\varphi_w) \qquad (2.23)$$
Geldart:	$$U_t = K(U_t)_{sphere} \qquad (2.24)$$ K_1 and K_2 are the constants which depend on sphericity and they can be found in the literature.

e) Sphericity obtained from measurement of voidage at minimum fluidization: There are some empirical correlations proposed to determine sphericity which require the knowledge of voidage at minimum fluidization. They are shown in Table 3.

Table 3. The correlations used to calculate voidage at minimum fluidization

	$\varphi_w = f(\varepsilon_{mf})$
Wen & Yu:	I. $\varphi_w = \frac{14}{\varepsilon_{mf}^3}$ II. $\varphi_w = \left(\frac{1-\varepsilon_{mf}}{11\,\varepsilon_{mf}^3}\right)^{0.5}$ (2.25)
Narsimhan:	$\varphi_w = \frac{0.768-\varepsilon_{mf}}{0.42}$ (2.26)
Limas-Ballestrores:	$\varphi_w = \left(\frac{0.42}{\varepsilon_{mf}}\right)^{1/0.376}$ (2.27)

2.2.4 Selection of Shape Factors to Use in N_{js} Equations

Five shape factors were chosen to assess from listed factors above for using in N_{js} correlations to take account of particle shape effect on N_{js}. They are aspect ratio, circularity, convexity, Wadell's sphericity and Corey's shape factor. The following two criteria are taken into consideration during the selection of these factors.

- Being easy to measure: The shape factor which will be used for mixtures that have irregularly shaped particles so measurements should be repeated many of times to reach a representative shape factor. The factors easy to measure for irregular solid particles were chosen.

- Having the value smaller than 1: In experimental results, it was observed that N_{js} decreases as the shapes of particles deviate from the sphere, therefore; a shape factor which is maximum for sphere and decreases when the shape of particles begin to deviate from spherical is convenient for using in N_{js} correlation.

CHAPTER 3

EXPERIMENTAL PROCEDURE

3.1 Experimental Set-up

The experiments were conducted in a cylindrical, flat-bottom tank with a diameter (T) of 24 cm shown in Figure 6. There were four equally spaced baffles in the tank. The width of the baffles (W) was 1/10 of the tank diameter. A down pumping pitched blade turbine (PBT) with a diameter (D) of T/3 was used as impeller. The impeller was placed at the center of the tank and its clearance (C) was set to T/3. The liquid height was constant in all experiments and it was equal to the diameter of the tank.

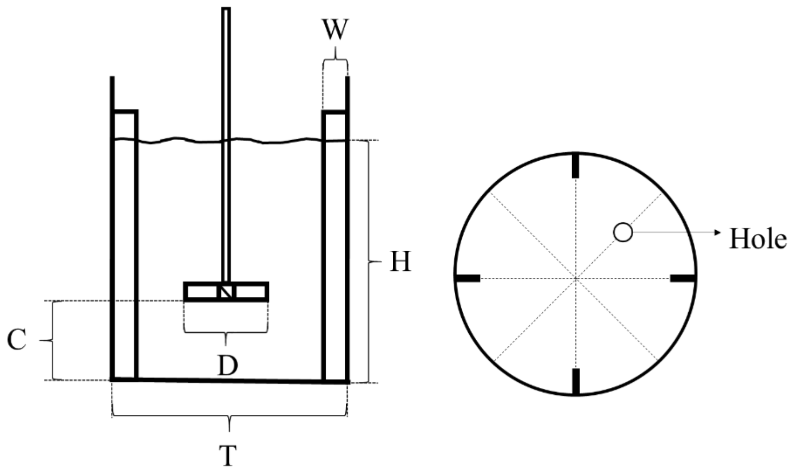

a. b.

Figure 6. The plot of the cylindrical tank a. Front view b. Bottom view

A mirror was placed below the tank to observe the tank bottom and determine N_{js} visually. As shown in Figure 6b there was a hole at the tank bottom to place a pressure sensor to apply the pressure gauge measurement method. The overall view of the experimental setup can be seen in Figure 7. The hole was located on a mid-baffle plane, at a radial location midway between the axis and the sidewall. The pressure sensor used for the measurements was MESENS MPS530 with 0-100 mBar measurement range and accuracy ± % 0.5 of the full scale.

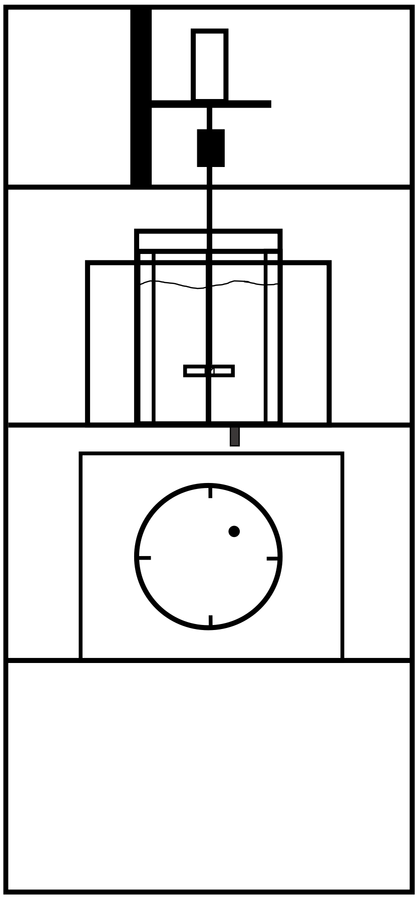

Figure 7. Front view of experimental setup

3.2 Particles Used in Experiments

Twelve different types of particles with various densities, sizes and shapes were used in the experiments. A Malvern Mastersizer 3000 instrument was used for size analysis of the particles smaller than 1 mm. The sizes of the particles whose dimensions that can easily be seen were measured with a ruler. The list of the particles and their physical properties are given in Table 4 and Figure 8 shows their images. The dimensions for the large particles given in Table 4 -BG, TPE, ABS, Akulon, Rod Cp, Plt Cp- are the maximum dimensions. The minimum dimensions of ABS, Akulon, Rod Cp and Plt Cp are 1500, 1500, 500 and 100 µm, respectively.

Table 4. Physical properties of particles used in experiments

Particle Name	**Shape**	**Size (µm)**	**Density (kg/m^3)**
Small Aluminum Oxide (SAl)	Grit	90	3600
Large Aluminum Oxide (LAl)	Grit	244	3600
Grit Steel (Grit St)	Grit	329	7000
Spherical Steel (Sph St)	Sphere	175	7650
Small Glass (SG)	Sphere	85	2500
Large Glass (LG)	Sphere	714	2500
Big Glass (BG)	Sphere	2000	2500
Thermoplastic Elastomer (TPE)	Sphere	3000	1165
Acrylonitrile Butadiene Styrene (ABS)	Cylinder	3000	1263
Akulon (Aku)	Ellipsoid	2200	1175
Rod Copper (Rod Cp)	Cylinder	3000	8000
Plate Copper (Plt Cp)	Plate	3000	8000

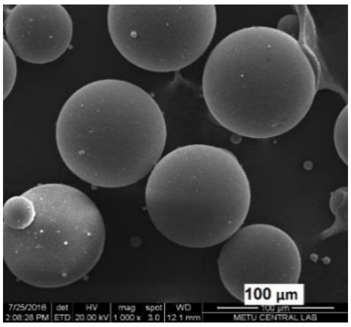

a. SG

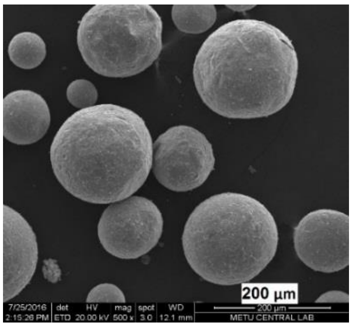

b. Sph St

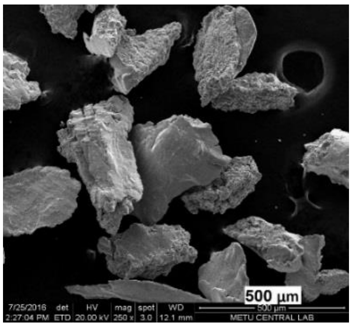

c. Grit St

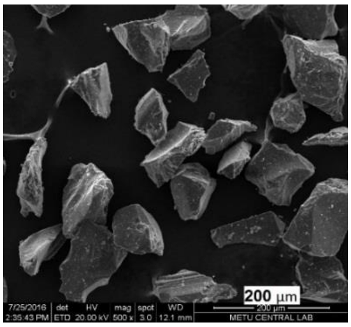

d. SAl

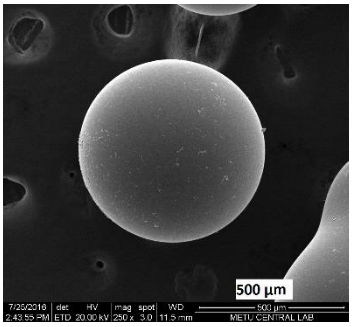

e. LG

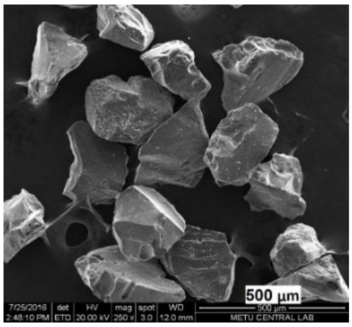

f. LAl

g. Plt and Rod Cp

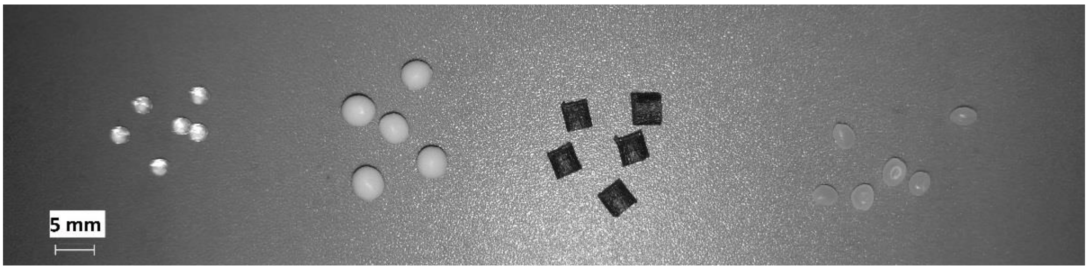

h. BG, TPE, ABS and Akulon

Figure 8. Images of the particles

Table 5. Properties of mixtures used in experiments

Mixture	More Dense Particle (wt %)	Less Dense Particle (wt %)	Particle Density Ratio	Particle Size Ratio	Particle Shape
1	Grit St (1.5-1.1)	SG (1.5-55)	~3:1	3.87	Grit Spherical
2	Grit St (1.5-1.1)	SAl (1.5-55)	~2:1	3.65	Grit Grit
3	Spherical St (1.5-1.1)	SG (1.5-55)	~3:1	2.17	Spherical Spherical
4	Spherical St (1.5-1.2)	SAl (1.5-55)	~2:1	2.05	Spherical Grit
5	Plate Cp (1.5-1.2)	LG (1.5-50)	~3:1	4.2	Plate Spherical
6	Plate Cp (1.5-1.2)	LAl (1.5-50)	~2:1	12	Plate Grit
7	Rod Cp (1.5-1.2)	LG (1.5-50)	~3:1	4.2	Cylindrical Spherical
8	Rod Cp (1.5-1.2)	LAl (1.5-50)	~2:1	12	Cylindrical Grit
9	BG (1.5-1.2)	Akulon (1.5-30)	~2:1	1.1	Spherical Ellipsoid
10	BG (1.5-1.2)	ABS (1.5-30)	~2:1	1.5	Spherical Cylindrical
11	BG (1.5-1.2)	TPE (1.5-30)	~2:1	1.5	Spherical Spherical

The results of the analysis with the Mastersizer device to determine the particle size distribution and particle size of the particles smaller than 1 mm are given in Appendix A. For grit shaped particles maximum and minimum sizes were measured with an image analysis program, Image J. The measurements were repeated for 50 different particles of each particle type: LAl, SAl and Grit St and the average for these 50 measurements was accepted as size of the particle. The minimum sizes of LAl, SAl and Grit St are 191, 61 and 167 μm and their maximum sizes are 310,122 and 385 μm, respectively.

The eleven mixtures given in Table 5 were used to investigate the effect of particle shape on suspension behaviour. In the experiments, the mass of the more dense phase was kept constant. In Table 5 the wt % of the more dense phase decreases slightly. This is due to the increase in the mass of the less dense phase for the same volume of the slurry. The visual N_{js} values of the mixtures which include particles have close densities and sizes but different shapes were compared.

3.3 Experimental Methods

3.3.1 Zwietering's Visual Observation Method

The complete off bottom suspension was characterized by Zwietering's "1 or 2 seconds" criterion. The bottom of the tank was observed and the impeller speed at which no particles remain motionless for more than 1-2 seconds was determined.

The impeller speed was increased with 100 rpm intervals up to a speed at which the bulk of the solids was suspended, and some remained at the back of the baffles only. At this point the just suspended speed is relatively closer; therefore, after this speed smaller increments were applied. The increments were as small as 1 rpm as the suspension approached N_{js}.

All experiments were repeated three times and averages were reported as N_{js} values. The results of experiments do not differ more than 1 % compared to the average value.

3.3.2 Pressure Gauge Measurement (PGM) Method

The pressure gauge measurement method was proposed by Micale et al. (2002) to remove the disadvantages of Zwietering's visual observation method. This method is based on the relationship between the pressure increase and mass of suspended solids. This relationship is shown with a representative plot in Figure 9. As the impeller speed increases, some of the particles get suspended and cause an increase in pressure at the bottom of the tank.

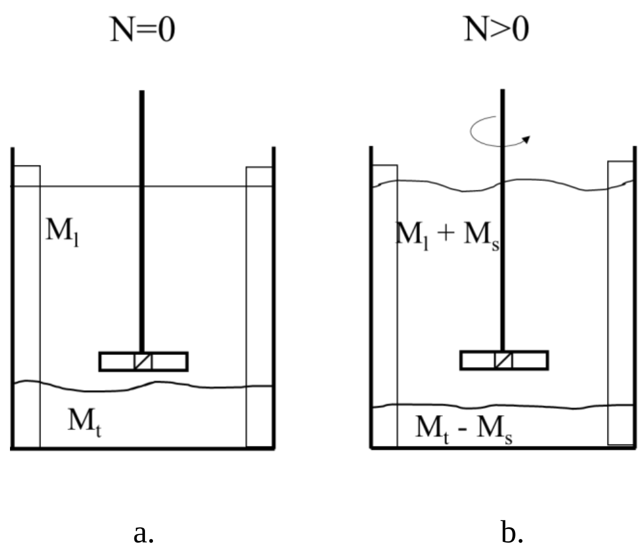

Figure 9. Particle mass distribution in a mixing tank. a. Particles lay on the bottom when N=0. b. Some of the particles are in motion when N>0. The measured pressure for a. is higher than b.

M_t is the total mass of the solid particles, M_l is the mass of liquid phase, M_s is the mass of the suspended solids. As the impeller speed is increased some of the solids - that were counted within M_t initially - get suspended, and are now a part of the moving side, and counted within M_s.

The solids and liquid in the tank apply a force to the tank bottom as expressed in Equation (3.1) for both N=0 and N>0 (Micale et al. 2002):

$$F_{total} = (M_l + M_t)g \tag{3.1}$$

The total force can be considered as the sum of the force due to direct contact of solid particles and the force due to the pressure exerted by the amounts of liquid and solid phases at height of H (Micale et al. 2002). These two contributions to the total force vary with increasing impeller speed while the total force is constant. The force due to direct contact can be written as Equations (3.2) and (3.3) for N=0 and N>0, respectively. As can be seen in Equation (3.2), the force due to direct contact is a result of the apparent mass of solids. Because of buoyant force of water, the mass of solids equals to $\left(1-{}^{\rho_l}/_{\rho_s}\right)g$. While the impeller speed increases, the mass of solids which lay on the bottom decreases. The mass of solids at the bottom at N>0 is expressed as: $(M_t - M_s)\left(1-{}^{\rho_l}/_{\rho_s}\right)$ and used in Equation (3.3)

$$F_{\substack{\text{direct contact}\\ N=0}} = M_t\left(1-\frac{\rho_l}{\rho_s}\right)g \tag{3.2}$$

$$F_{\substack{\text{direct contact}\\ N>0}} = (M_t - M_s)\left(1-\frac{\rho_l}{\rho_s}\right)g \tag{3.3}$$

The force due to the pressure exerted by the amounts of liquid and solid phases can be calculated by subtracting $F_{\text{direct contact}}$ from F_{total}. They are written in Equations (3.4) and (3.5).

$$F_{\substack{\text{pressure}\\ N=0}} = \left(M_l + M_t\frac{\rho_l}{\rho_s}\right)g \tag{3.4}$$

$$F_{\substack{\text{pressure}\\ N>0}} = (M_l + M_t)\,g - (M_t - M_s)\left(1-\frac{\rho_l}{\rho_s}\right)g \tag{3.5}$$

The pressure force difference due to increase of impeller speed can be calculated theoretically by subtracting Equation (3.4) from Equation (3.5) and the following equation is obtained:

$$\Delta F_{\text{pressure}} = M_s\left(1-\frac{\rho_l}{\rho_s}\right)g \tag{3.6}$$

Based on Equation (3.6), the pressure increase at the tank bottom due to solid suspension for N>0 can be written as:

$$\Delta P = \frac{M_s\left(1-\frac{\rho_l}{\rho_s}\right)g}{A_b} \tag{3.7}$$

From this derivation, it can be understood that the pressure measured at the tank bottom increases in proportion to M_s and (ρ_s - ρ_l). When the impeller speed reaches the just suspended speed, there are no particles remaining at the bottom and corresponding ΔP is called as ΔP_{js}: the pressure change at just suspended conditions. At impeller speeds higher than N_{js}, the pressure increase at the tank bottom is only due to the fluid motion. The effects of fluid motion may be axial force exchange between impeller and fluid or vertical friction forces on the tank lateral wall and baffles and they can be defined as dynamic head effects (Micale et al. 2002). The dynamic head effects cause pressure increase proportional to kinetic energy transferred from the impeller to the mixture, and it is proportional to the square of impeller speed. After the pressure data is collected, the pressure increase due to dynamic head effects can be determined for each impeller speed with the help of N^2- pressure relationship and just suspended speed can be determined. The steps of applying the method are given below in detail:

- The pressure change is measured per second over 2-3 minutes at an impeller speed. The speed is then increased gradually. The measurements were repeated three times and the average value of pressure data is calculated for each impeller speed. The change in pressure with respect to increasing impeller speed is plotted. Thus, **total pressure data** is obtained. A representative data is shown in Figure 10.
- It is necessary to take pressure data for the impeller speeds up to speeds above N_{js} to apply this method. To decide whether the impeller speed is sufficiently high, the following two criteria must be considered: The pressure curve should look like S-shaped curve (it should have two turning points) and there should be enough data points to fit a second-order parabola after the second turning point as shown in Figure 10. The **second-order parabola** was fitted on the last three or four points of pressure data.
- The equation of the parabola must be in the form of $\Delta \mathrm{P} = \mathrm{aN}^2 + \mathrm{b}$. It gives information about both dynamic head effects and ΔP_{js}. As shown in Figure 10, intercept of the parabola, b, equals to ΔP_{js} and the difference between ΔP_{js} and the parabola equals to **dynamic head effects** for each impeller speed.
- The ΔP_{js} also can be calculated from Equation (3.7) theoretically. The experimental ΔP_{js} which is obtained with the second-order parabola and theoretical ΔP_{js} can give different results. It was observed in this study that experimental ΔP_{js} values are up to 20 % higher than theoretical ones.

- When the pressure increase originating from dynamic head effects is substracted from total pressure data, **the corrected pressure curve** is obtained. This curve expresses the pressure increase only due to the amount of suspended solids; therefore, when all particles get suspended, the corrected pressure equals to ΔP_{js}. Thus, the intersection of the corrected pressure curve and the ΔP_{js} line is just suspended point and corresponding impeller speed to this point is N_{js} as shown in Figure 10.

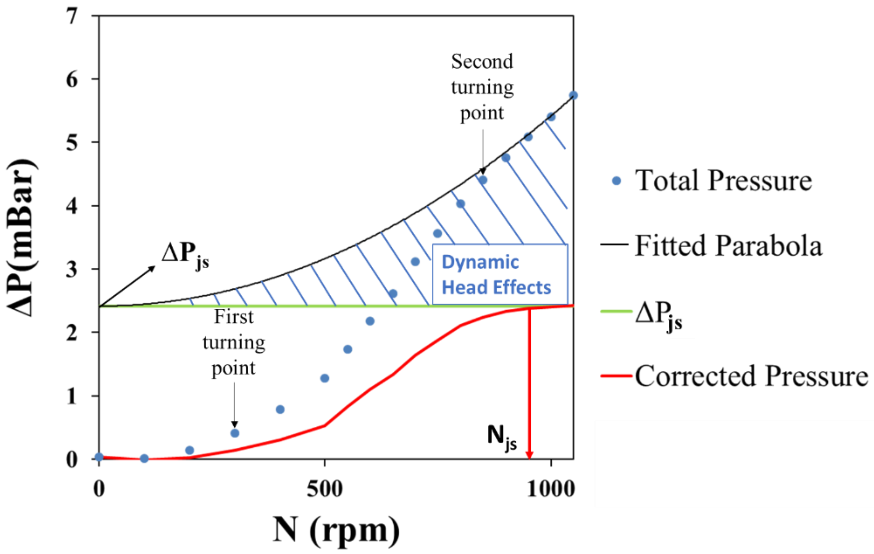

Figure 10. Representative graph of pressure versus impeller speed. The arrows show first and second turning points of the total pressure curve.

In this study, this method was applied to slurries that are more concentrated than the ones used in the literature. Therefore, the required impeller speeds are higher. Some issues related to these high impeller speeds were faced in the data analysis. These issues and how some applications of the method is modified is explained in Section 4.3.

CHAPTER 4

RESULTS AND DISCUSSION

4.1 Suspension Behaviour of Mixed Slurries with Spherical and Non-Spherical Particles

In this part, the effect of particle shape on the suspension behaviour and N_{js} of mixed slurries were investigated. The experiments included slurries that have two solid phases: a more dense and a less dense phase. In naming of the slurries in the text, the first one is the more dense and the second one is the less dense phase. For example in the mixed slurry of BG-TPE, the BG has a higher density; therefore, it is the more dense phase, and the TPE has a lower density; therefore, it is the less dense phase. The effect of particle shape was investigated by comparing mixed slurries that are composed of particles with the same/similar density and size, but different shapes.

In Figure 11 two slurries with the same more dense phase, BG, but different less dense phases, TPE and ABS, were compared. As the solids concentration of the less dense phase is increased mixed slurry N_{js} increases for both slurries. This increase is more pronounced above 15 wt % solids as seen with the larger slope for both slurries in the figure. However, this slope is significantly larger for the BG-TPE slurry compared to the BG-ABS slurry. At 30 wt % solids BG-TPE slurry N_{js} is 12 % higher than that of BG-ABS slurry. This shows that it is more difficult to suspend spherical particles than non-spherical particles. It is important to note that the sphericity and size of the two particles are in fact only slightly different. The height of the cylindrical ABS particles is equal to the diameter of the TPE particles, which is 3 mm. This shows that even a small difference in sphericity like this can have an effect on the suspension of the slurry. It is also important to note that the effect of particle shape is more visible when combined with the effect of increasing solids concentration.

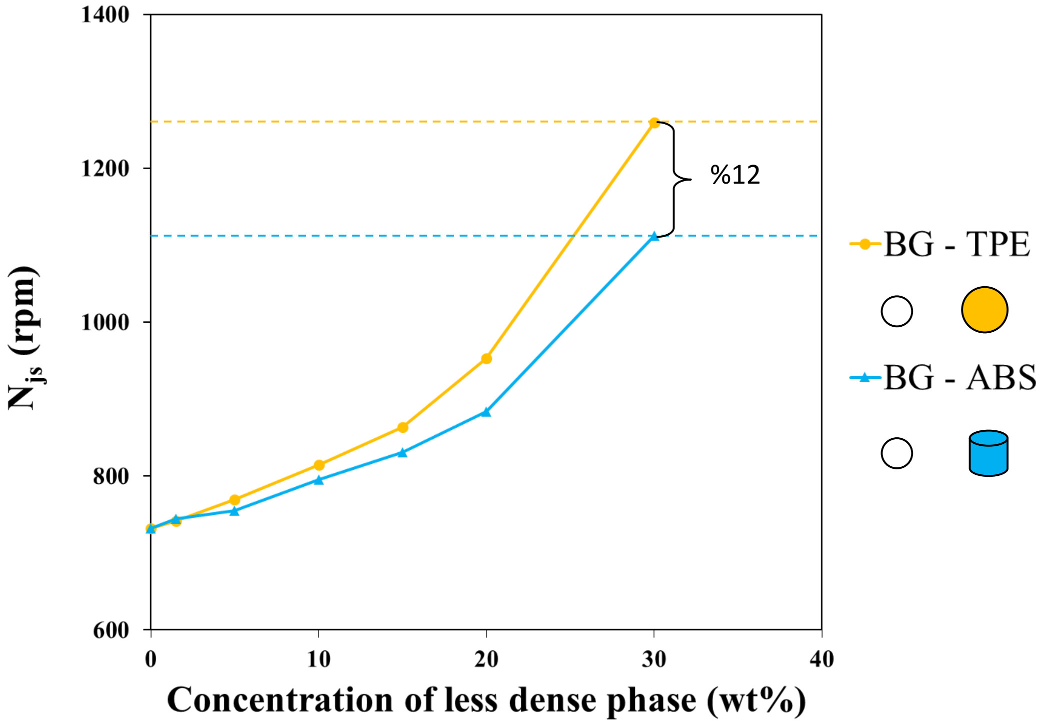

Figure 11. Comparison of mixed slurry N_{js} of BG and cylindrical ABS or spherical TPE at varying concentrations of ABS and TPE.

Figure 12 shows the effect of particle shape of more dense phase on N_{js}. The mass of the differently shaped steel particles was kept constant and the increase of solids concentration was provided with spherical SG. The steel particles are either spherical or grit shaped. Grit St is about two times larger than the Sph St; however, the Sph St needs 4 to 15 % higher N_{js}. The same conclusion is reached from this comparison: spherical particles are harder to suspend.

A comparison of the general trends of Figure 11 and Figure 12 shows that the N_{js} of slurries increase in Figure 11, but decrease in Figure 12 with increasing concentrations of less dense phase. While it is known that for most mixed slurries and for all unimodal slurries N_{js} increases with increasing solids concentration, Ayranci and Kresta (2011) reported a decrease in N_{js} for some mixed slurries. They proposed a networking mechanism for solids suspension for these cases. When the diameter of less dense solid phase is smaller than the more dense solid phase in a mixed slurry, the less dense and small particles are suspended at impeller speeds lower than large and more dense ones. Once they are suspended, these particles gain momentum with increasing impeller speeds. They collide with each other and with the more dense particles more frequently. Finally, the less dense and small particles form a network that prevents the more dense particles to contact with the tank bottom. This causes a drop in N_{js} of the mixed slurry. This decrease is more pronounced at higher solids concentrations. This is identical with the observation in this study: as the concentration of the less dense phase, SG, was increased, N_{js} of the mixture decreases.

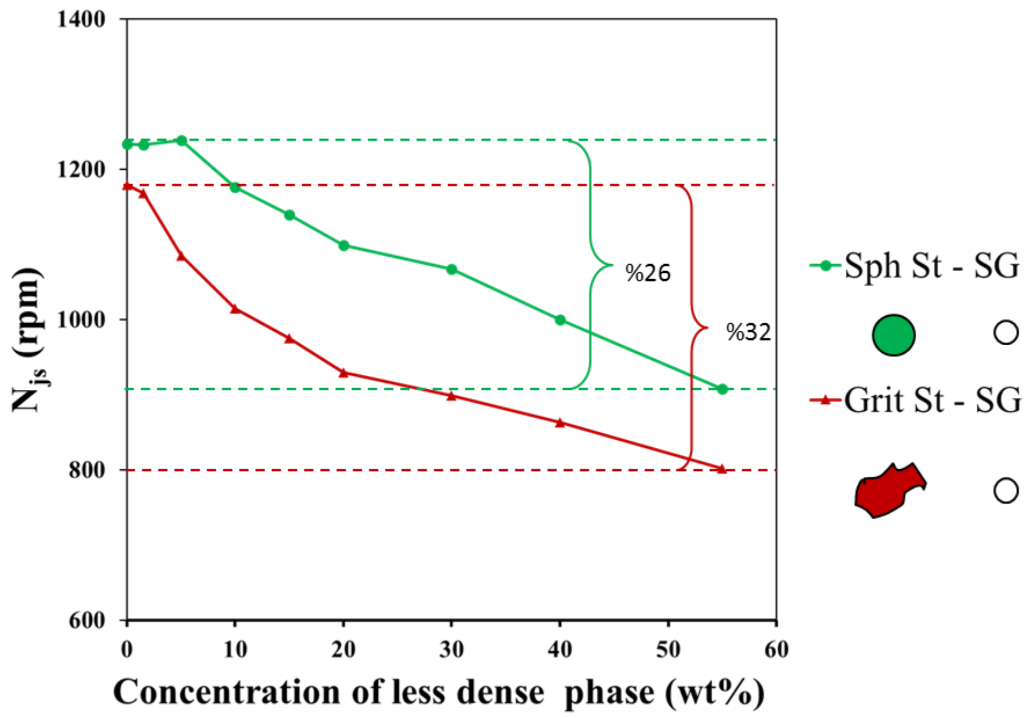

Figure 12. Comparison of N_{js} of Grit and Sph St in the presence of the less dense phase of spherical SG at varying concentrations.

The total decrease of N_{js} values from 1.5 to 55 wt % SG is 32 % for the slurry with Grit St and 26 % for the slurry with Sph St. This shows that the networking mechanism is more effective when the more dense solid phase is non-spherical. This highlights the importance of the particle shape for solids suspension.

A similar comparison is shown in Figure 13 for two mixed slurries in which grit shaped SAl is used as the less dense phase, and Grit and Sph St are used as the more dense phase. Once again, the Grit St was suspended at N_{js} values lower than that of Sph St. The N_{js} difference between the two slurries can reach up to 12 %.

As seen in Figure 13, the networking mechanism is more effective for the Grit St - SAl slurry where the two solid phases are grit shaped. This is shown with a total of 29 vs 26 % of drop in N_{js} with increasing concentrations of SAl. This is more likely a result of the possibility of the larger number of collisions between the Grit St and SAl compared to that of Sph St and SAl due to the larger projected area of Grit St. The SAl may also be getting under the steel particles more easily, taking advantage of the grit shape of the steel particles and therefore easing the suspension. Because of this, Grit St-SG mixture also has more effective mechanism than Sph St-SG mixture in Figure 12.

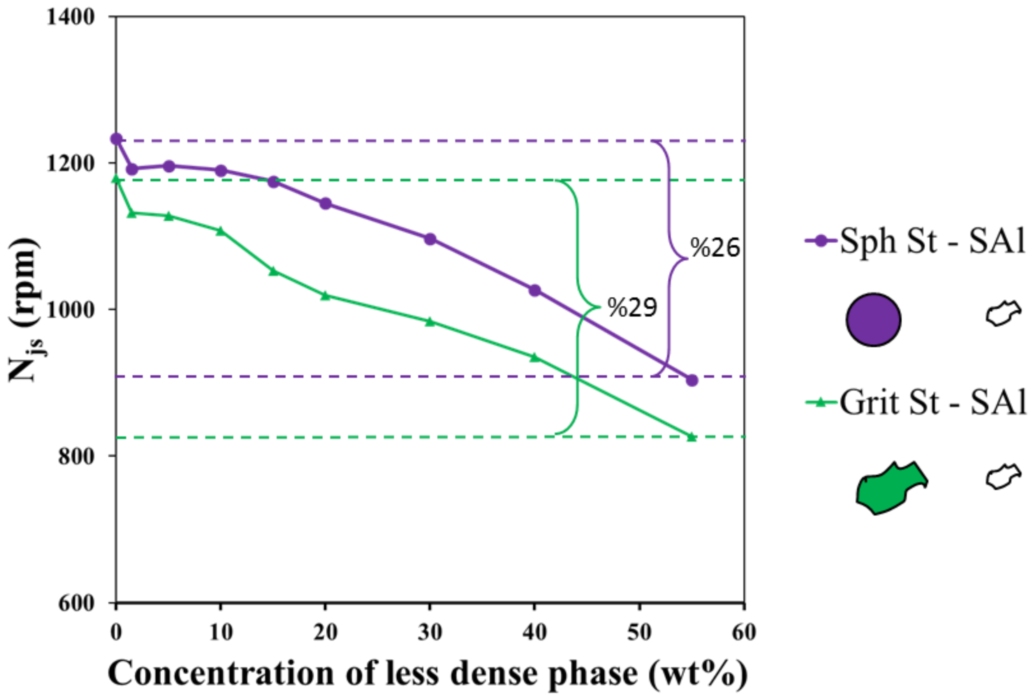

Figure 13. Comparison of N_{js} of Grit and Sph St in the presence of grit shaped less dense phase of SAl at varying concentrations

In Figure 14 two mixed slurries with the more dense phase of Sph St, and the less dense phase of SG and SAl are compared. It is surprising that the two data sets give very similar results. The density of aluminum oxide is 1.5 times of the density of glass. According to the most commonly used correlations in literature, N_{js} is proportional to $\rho_s^{\ 0.45}$ or $\rho_s^{\ 0.5}$. Based on this relation 20 % higher N_{js} is expected when the less dense phase is SAl. However; the data for the two slurries almost overlap. This is a result of the fact that the grit shape overcomes the effect of larger density and eases suspension.

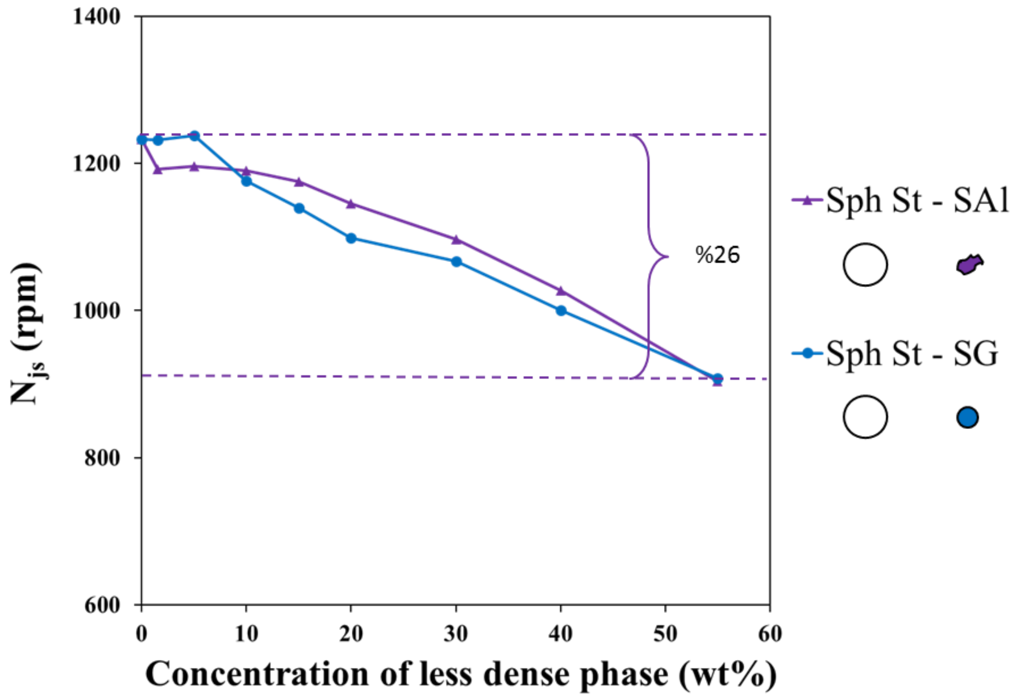

Figure 14. Comparison of N_{js} of Sph St with grit SAl or spherical SG at varying concentrations

In Figure 14 the grit shape of SAl also affects the networking mechanism. Both slurries are exposed to the networking mechanism: as the concentration of the less dense phase increases, the N_{js} of the mixture drops. The drop in N_{js} is almost identical at ~26 % for the two slurries. As SAl particles are more dense than SG they are expected to move slower in the liquid phase and collide with Sph St particles less frequently. This should cause a less effective network for Sph St-SAl mixture. The data; however, proves otherwise. Because of their shape, the SAl particles have larger surface area, and therefore drag coefficient, and they move faster.

In Figure 15, unlike the previous comparisons, two non-spherical particles which have different shapes were compared. The mixture with Plt Cp has lower N_{js} values. The difference between N_{js} of Rod and Plt Cp mixtures is maximum 9 % which is at 10 wt % solids. The difference decreases significantly at higher concentrations. When the surface area of copper particles are compared, it was seen that the surface area of Plt

Cp per unit volume is larger than the area of Rod Cp per unit volume; therefore, the Plt Cp has smaller sphericity. The drag force is one source that facilitates the suspension of particles. This force is proportional to drag coefficient. The drag coefficient increases as sphericity decreases. When a particle has larger drag coefficient, it is exposed to a larger drag force. Loth (2008) stated that the drag force of a non-spherical particle is higher than the drag force of a sphere which has the same volume as the non-spherical particle. It means that the drag force increases with surface area per volume because the surface area per volume of the non-spherical particle is higher than the surface area per volume of the sphere. In comparison of Rod and Plt Cp, plate shaped particles have larger surface area and higher drag force. Based on this information it is estimated that N_{js} of the Plt Cp slurry should be lower. The data in Figure 15 agrees with this estimation.

In Figure 15 when the trend of N_{js} at varying concentrations was examined, a significant increase is seen at concentrations of LAl higher than 20 wt %. Above 20 wt % the mass of the LAl present in the tank becomes much more significant; therefore, larger energy is required to suspend the solids. This results in an increase in the slope of N_{js} – concentration data.

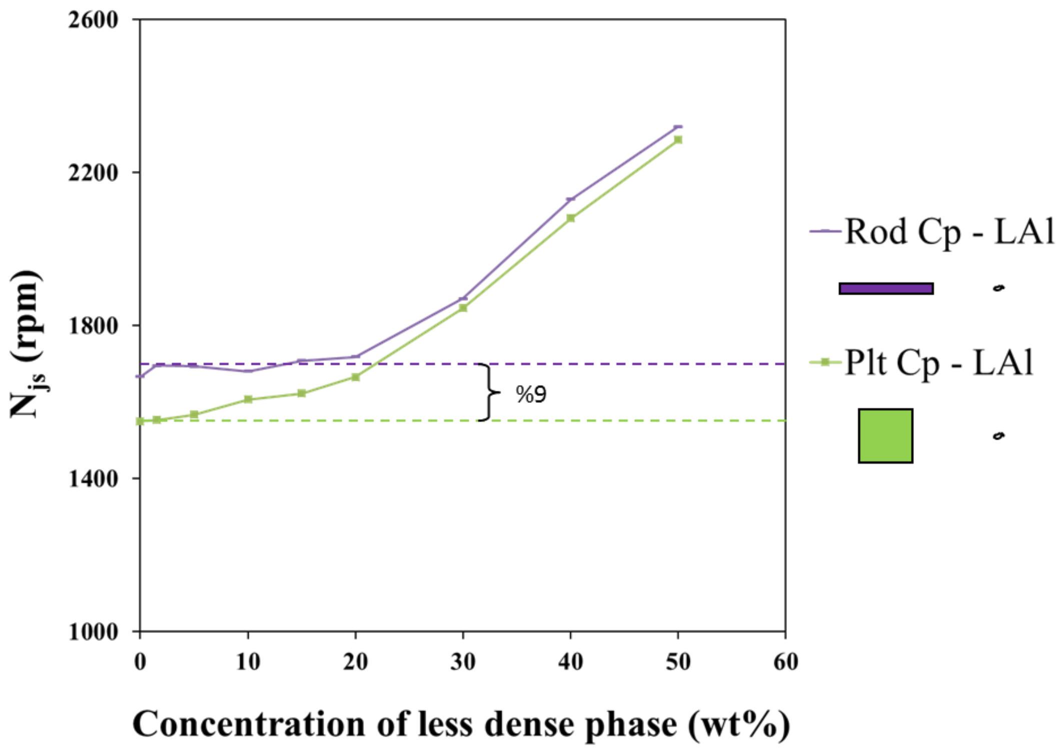

Figure 15. Comparison of N_{js} of Plt and Rod Cp with LAl at varying concentrations

Part of the mechanism observed in Plt and Rod Cp-LAl mixtures was seen in Ayranci et al. (2011) for the mixture of Nickel-SG. At the total slurry concentrations from 1.5 to 35 wt %, it was reported that the N_{js} of the mixture remained nearly constant with the addition of the second solid phase. This reported behaviour corresponds to our range of 0-20 wt % and it is seen more clearly for the Rod Cp-LAl mixture.

When the behaviour of mixtures in Figure 12 - Figure 14 and Figure 15 are compared, it was seen that their trends of N_{js} change with concentration are different. The difference results from density and size difference between less and more dense solid phases. LAl particles cannot form a network that prevents the copper particles to contact with the tank bottom.

In Figure 16 slurries of Plt and Rod Cp in the presence of LG particles were compared. It can be seen that the suspension behaviour was similar to mixtures of Plt Cp-LAl and Rod Cp-LAl. There are again two regions which are different in terms of slope of N_{js} change with concentration. N_{js} is increasing with a larger slope for concentrations larger than 20 wt %. The shapes of copper particles in the presence of LG particles caused 8 % difference in measured N_{js}, but again at higher concentrations this difference decreased.

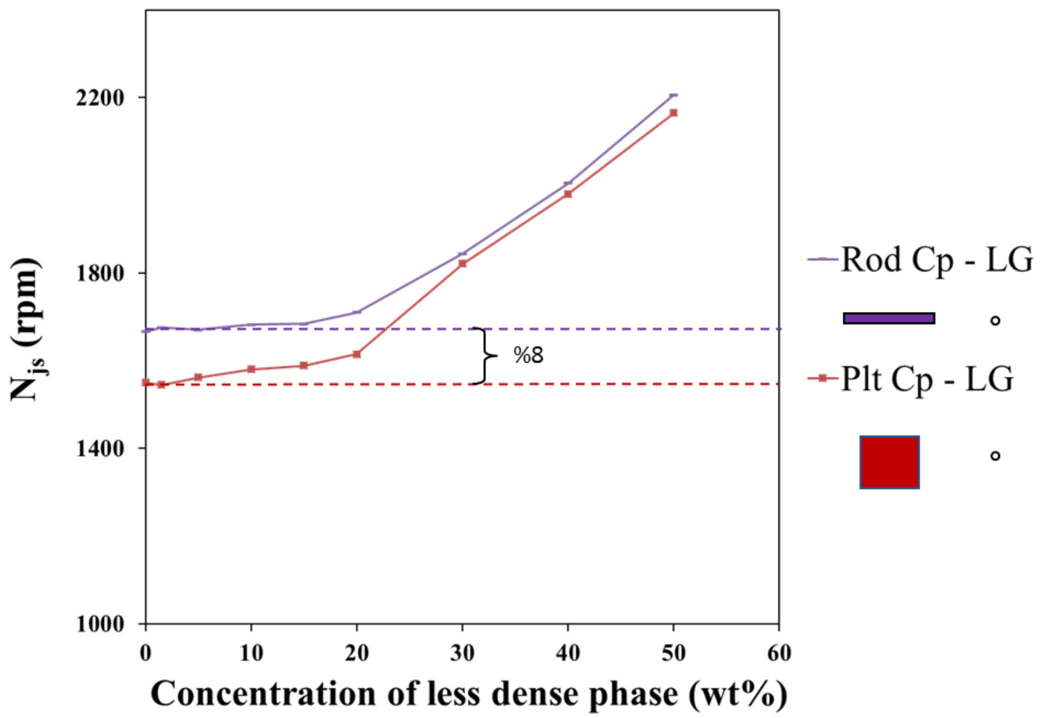

Figure 16. Comparison of N_{js} of Plt and Rod Cp with LG at varying concentrations

Prediction of N_{js} can be necessary for the design of a mixing system or for the applications that do not have an observable tank bottom. There are some equations to predict N_{js} in literature but these equations were obtained from experimental studies with spherical particles. Non-spherical particles are mostly used in industrial applications. In this section, it was seen that the shape of the particles has an effect on the suspension behaviour of the slurry. This shows the need to investigate whether a correction is required in the correlations for unimodal and mixed slurry N_{js} to take the effect of particle shape into account.

4.2 Assessment of Correlations in Literature

In this section, the correlations used for N_{js} predictions were tested with experimental data obtained in this study. First, the most commonly used correlations to predict N_{js} in literature, which were mentioned in Chapter 2, were assessed for unimodal slurries and the one that predicts N_{js} most accurately was determined. Then the results of the best correlation were examined in detail for the data in this study. Second, the mixture N_{js} data was analyzed. A concentration related factor was suggested to improve power model to obtain correct results for slurries with networking mechanism. Then the shape factors chosen in Chapter 2 were compared to determine which one represents the effect of particle shape on N_{js}.

4.2.1 Determination of the the Most Accurate Correlation

In this part, the correlations to be used for N_{js} prediction are compared with experimental N_{js} data. The N_{js} of unimodal slurries of particles listed in Table 4 at concentrations varying from 1.5 to 55 wt % was determined with visual observation method. The impeller speeds required to suspend steel and copper particles at increasing concentrations were too high for the current motor; therefore, these tests were run at only 1.5 wt % concentration for these two particles. After the determination of experimental N_{js} values, the corresponding predicted N_{js} values were calculated with the five correlations given in Section 1.3.2. These correlations are given below again:

Zwietering: $$N_{js} = S\left[\frac{g(\rho_s - \rho_l)}{\rho_l}\right]^{0.45} \upsilon^{0.1} X^{0.13} d_p^{0.2} D^{-0.85} \tag{1.1}$$

Baldi: $$N_{js} = \frac{1}{Z}\left(\frac{g(\rho_s - \rho_l)d_p}{\rho_l}\right)^{0.5} \frac{d_p^{\frac{1}{6}}}{N_p^{\frac{1}{3}} D^{\frac{2}{3}}} \frac{T}{D} \tag{1.2}$$

Davies:

$$N_{js} = 0.76\,(1 + \alpha C_b)(1 - C_b)^{\frac{x}{2}} N_p^{-\frac{1}{3}} d_p^{\frac{1}{6}} \left(\frac{g\Delta\rho}{\rho_l}\right)^{0.5} \left(\frac{H}{T}\right)^{\frac{1}{3}} \left(\frac{D}{T}\right)^{-1} D^{-\frac{2}{3}} \tag{1.3}$$

Ayranci: $$N_{js} = A'\left(\frac{g(\rho_s - \rho_l)}{\rho_l}\right)^{0.5} \frac{d_p^{\frac{1}{6}} X^n}{N_p^{\frac{1}{3}} D^{\frac{2}{3}}} \frac{T}{D} \tag{1.4}$$

GMB: $$N_{js} = \frac{z}{N_p^{0.333} D^{0.667}} \left(\frac{g(\rho_s - \rho_l)}{\rho_l}\right)^{0.5} d_p^{0.167} {X_v}^{0.154} \left(\frac{C}{D}\right)^{0.1} \tag{1.6}$$

Figure 17 shows the comparison of measured and predicted N_{js} for these five correlations. At solids concentrations lower than 5 wt % - which correspond to the lowest N_{js} values - Zwietering, Davies and Ayranci's correlations can predict N_{js} within or close to the ±20 % lines. As concentration is increased, at about 20 wt % solids and higher, Zwietering and Davies correlations begin to under-predict N_{js}. GMB and Baldi's correlations under-predict N_{js} for nearly all concentrations. Ayranci's correlation, on the other hand, predicts N_{js} close to the parity line for the full range of concentrations for all the tested slurries.

The main reason for the deviation between the correlations in Figure 17 is the difference in the concentration term in the equations. Table 6 gives the solids concentration terms used in each correlation, the solids concentration limits of applicability of each correlation and the testing range of solids concentration in this study corresponding to each solids concentration term. It is seen that range of solids concentrations used in this study is larger than the previous studies. The correlations which were developed for low concentrations failed to predict N_{js} for the higher concentration values. Ayranci's correlation, however, seems to be able to predict N_{js} even for solids concentrations above its limits of applicability.

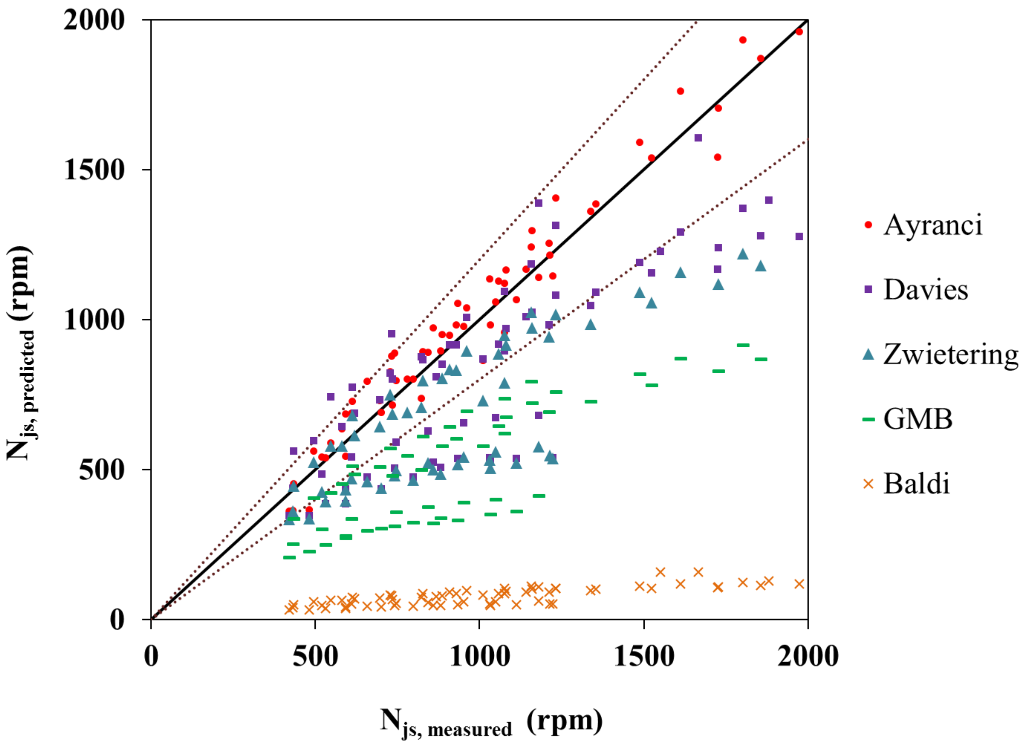

Figure 17. Comparison of predicted and measured N_{js} for five correlations. The data is for unimodal slurries of SG, SAl, LG, LAl, BG, TPE, ABS and Akulon particles at concentrations in the range of 1.5-55 wt % solids.

Table 6. The limits of correlations and concentration ranges used in this study

Correlation	Concentration term	Limits	Limits of this study
Zwietering	X	0.5-20	1.5-122
Baldi	X	0.002-0.02	1.5-122
Davies	C_b	0.08-0.10	0.02-0.32
Ayranci	X	0.1-54	1.5-122
GMB	X_v	0.04-20.2	2-32

This analysis was done for both spherical and non-spherical particles. In correlations the diameter of particles given in Table 4 was used as the particle size term. The normalized standard deviation of correlations was calculated with Equation (4.1) and results are given in Table 7.

$$\sigma = \sqrt{\frac{\sum_{n=1}^{n}\left(\frac{N_{js,predicted} - N_{js,measured}}{N_{js,measured}}\right)^2}{n-1}} \quad (4.1)$$

Table 7. Normalized standard deviation of predictions from measured N_{js}

Correlation	**Standard Deviation from Measured N_{js} (%)**
Zwietering	28.3
Baldi	91.4
Davies	27.8
Ayranci	**10.5**
GMB	45.6

The minimum standard deviation was obtained with Ayranci's correlation as 10.5 %. This is in line with the conclusions obtained by visual inspection of Figure 17. Therefore, this correlation was chosen as the correlation which can make the most accurate prediction.

Ayranci and Kresta (2014) proposed three possible exponents for the concentration term: 0.17, 0.23 and 0.32 for different particle groups. The exponent of 0.23 was proposed as the average exponent for all particle types tested. In the analysis up to now, the exponents that give the best fit were used for each particle type among three exponents in Ayranci's correlation. The values of these best exponents and how they are grouped are explained below.

The measured N_{js} is compared with the predictions using the three possible exponents for three different particles in Figure 18 a-c. The test particles can be divided into three groups regarding the particle size as given in Table 8. In the figure, three particles were chosen to represent these three groups. For SAl, LG and TPE the best fits were obtained with an exponent of 0.17, 0.23 and 0.32, respectively. Similar analyses were done for SG, LAl, and Akulon and ABS, and the exponents were found as 0.17, 0.23

and 0.32; respectively. It was observed that as particle size increases, the required exponents on concentration term increase. The reason for this increase can be the settling velocity. For particles used in this study, the larger particle size causes larger settling velocity. Settling velocity values of particles in the descending order is $V_{t, BG} > V_{t, ABS} > V_{t, TPE} > V_{t, Akulon} > V_{t, LG} > V_{t, LAl} > V_{t, SAl} > V_{t, SG}$. The particles which have larger settling velocity require more energy to be suspended and the increase in the concentration of these particles causes more energy need than the particles that have lower settling velocity. In Figure 18, the slope of the visual N_{js} curves of SAl, LG and TPE are different from each other because the increase in concentration affects N_{js} values differently according to their settling velocities.

Table 8. Particle groups regarding the particle size

Particle group	Diameter range (μm)	Type of particle
Small	85-90	SG, SAl
Large	240-1000	LG, LAl
Very Large	>1000	TPE, ABS, Akulon

Also, it is seen from Figure 18 that N_{js} predictions follow the experimental data closely up to 35 wt % for TPE (X=54) and 55 wt % for SG and LAl (X=122). The concentrations of SG and LAl is above the given upper limit of the correlation. This shows that the correlation is in fact applicable over a wider range of solids concentrations than developed initially.

Ayranci and Kresta (2014) stated that the three exponents proposed can be used whether the solids concentration is defined in terms of the Zwietering solids loading (X), weight percent (X_w) or volume percent (X_v). Zwietering's solids loading, X, takes the inertia of particle and the probability of particle-particle interactions into consideration. X_w is easy to use and includes the inertia of particles. X_v gives information about the distance between the particles. Since this study showed that Ayranci's correlation can be used at concentrations above 35 wt %, a test of whether the three concentration terms can still be used interchangeably is required. Figure 19 and Figure 20 shows the results for X_w and X_v, respectively. The results up to 35 wt % (X=54 and X_v=25-32) agree with Ayranci and Kresta (2014): any one of the solids concentration terms can be used with the given exponents. However, as the solids concentration is increased, this observation does not hold true. A larger exponent is required for the larger X_w and X_v values. The average representative exponent is 0.26 for X_w and 0.27 for X_v for these three particles. Since Zwietering solids loading, X, represents the entire solids concentration range with one exponent, it is recommended to use this term in the correlation as the solids concentration term.

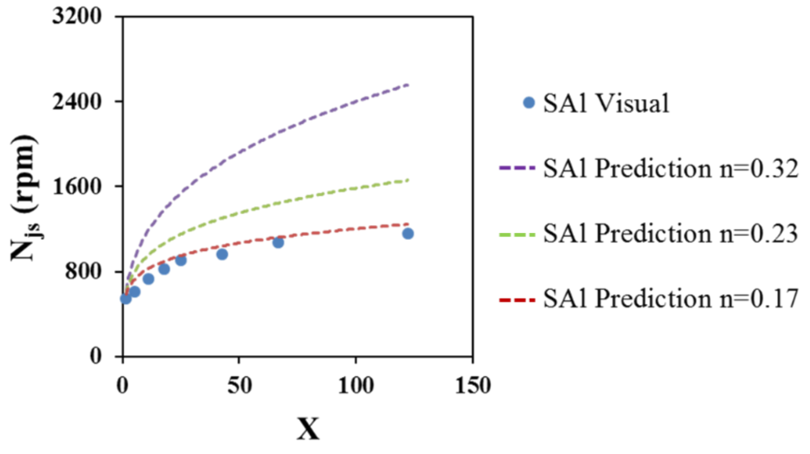

a.

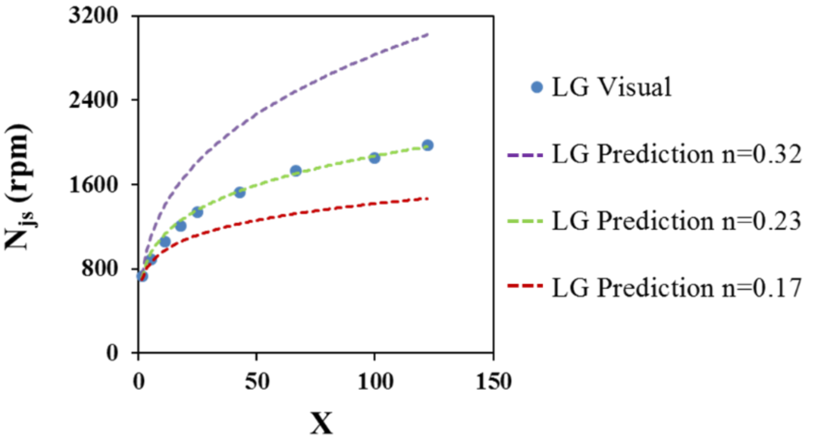

b.

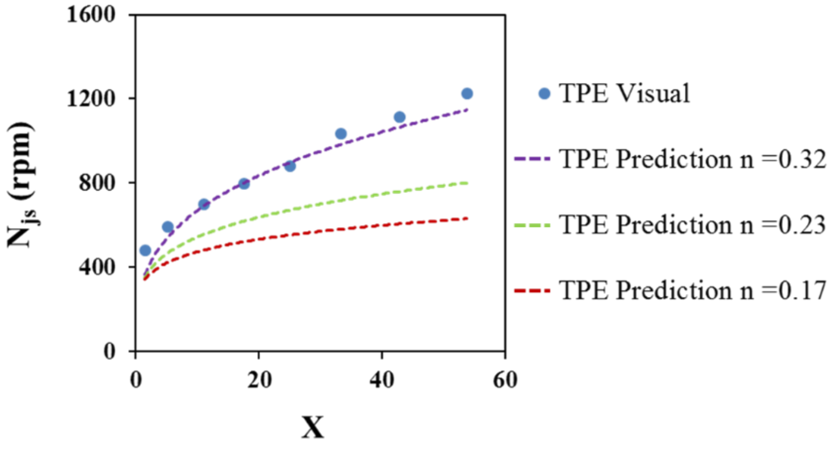

c.

Figure 18. Comparisons of measured and predicted N_{js} using Ayranci's exponents of 0.17, 0.23 and 0.32 for three different types of particles a. SAl b. LG c. TPE

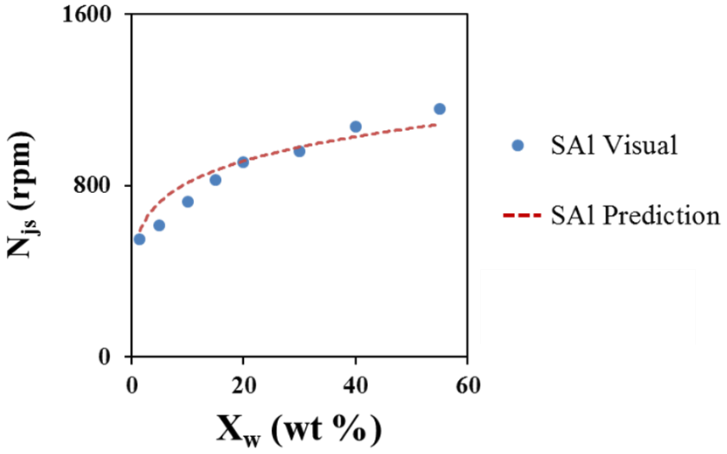

a.

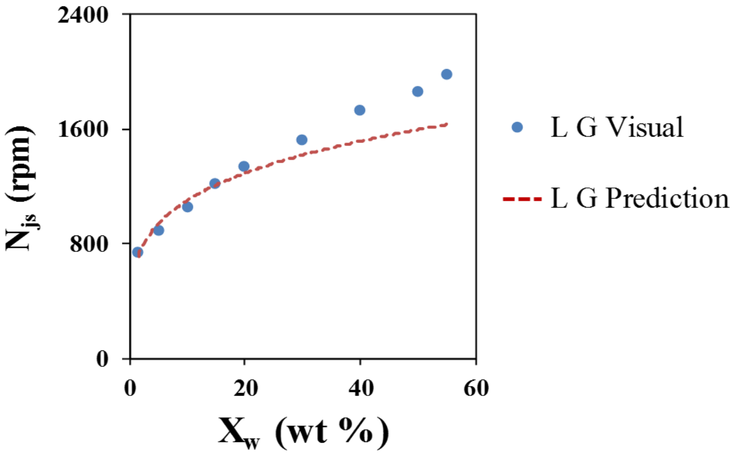

b.

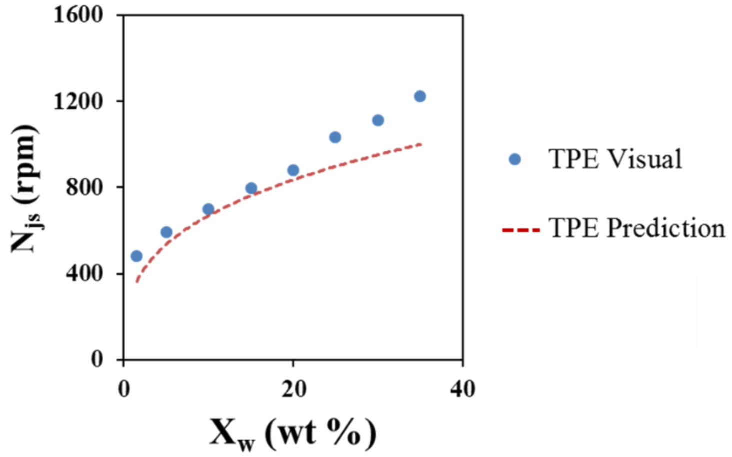

c.

Figure 19. The change of predicted N_{js} with concentration as weight percent (X_w)

a. SAl, b. LG, c. TPE

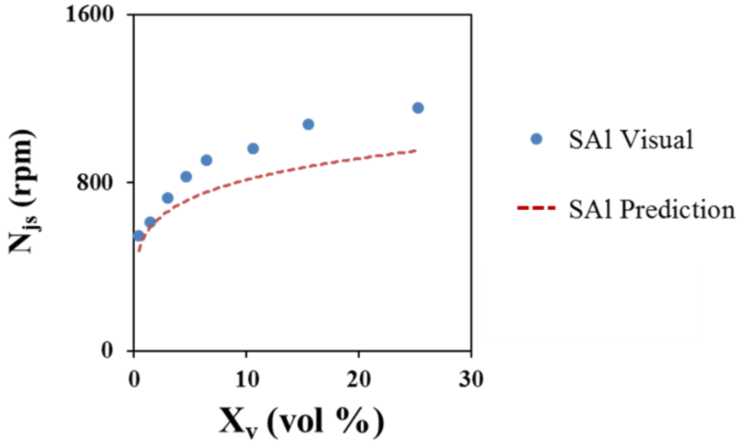

a.

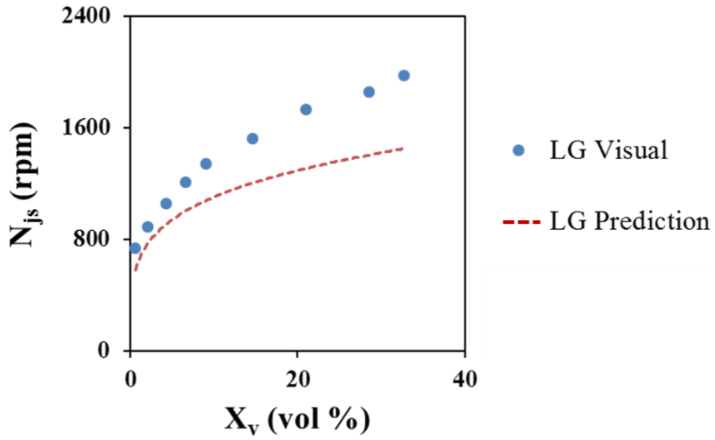

b.

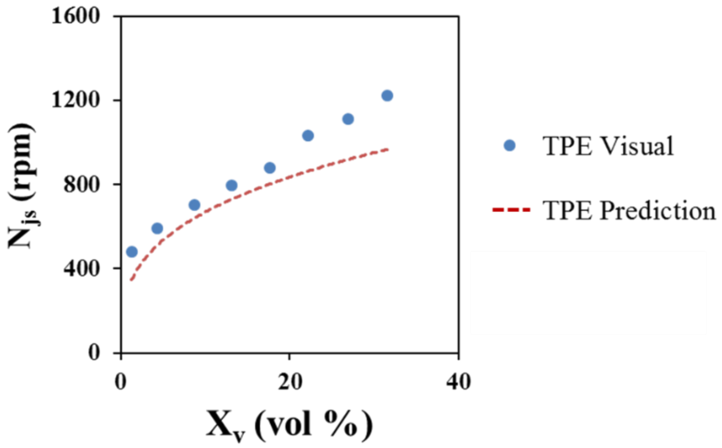

c.

Figure 20. The change of predicted N_{js} with concentration as volume percent (X_v)

a. SAl, b. LG, c. TPE

4.2.2 Comparison of the Measured and Predicted N_{js} of Mixed Slurries

In this section, the improvements on the predictions of N_{js} of binary mixtures are given. These improvements are obtained by taking the effect of networking mechanism and particle shape into account in the power model.

4.2.2.1 The Networking Mechanism in Power Model

As mentioned in the literature survey the power model cannot predict N_{js} of mixed slurries for which the networking mechanism is observed. These slurries are Sph St-SAl, Sph St-SG, Grit St-SAl and Grit St-SG. It was also seen for the mixture of Bronze-SG in Ayranci and Kresta (2011). The comparison of measured and predicted N_{js} of mixed slurries is shown in Figure 21. For these predictions, the unimodal slurry N_{js} in the power model was obtained experimentally. As seen in Figure 21, mixture N_{js} of the slurries for which the networking mechanism is active does not follow the parity line. The networking mechanism causes a drop in N_{js} as the solids concentration is increased. The data shows that the measured N_{js} drops while the power model predictions continue to increase.

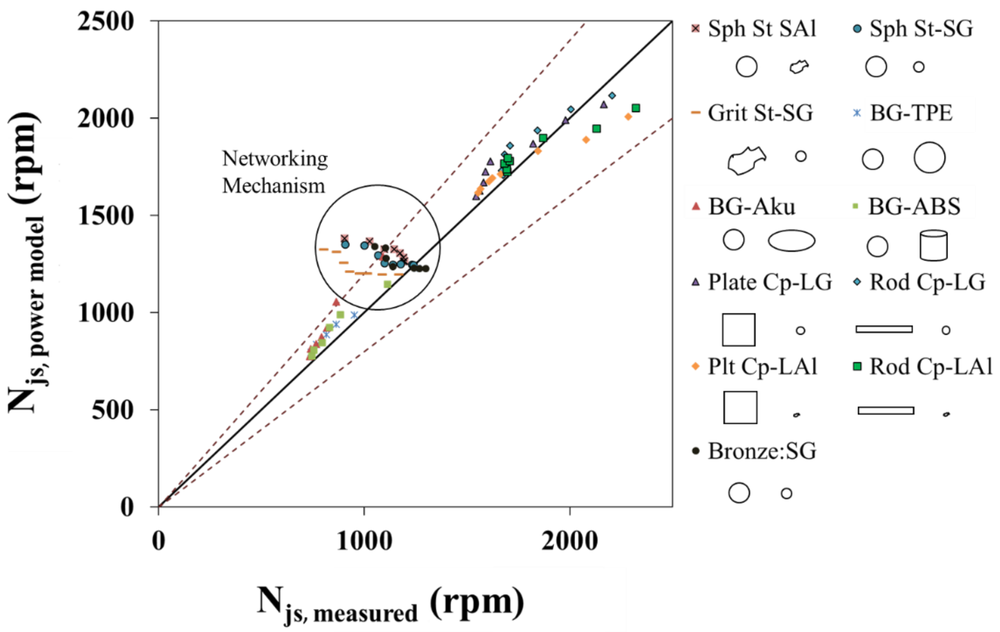

Figure 21. The parity plot of predicted and measured N_{js} of mixed slurries. N_{js} of unimodal slurries obtained experimentally. The slurries with networking mechanism are circled.

Table 9. The experimental and predicted N_{js} data for mixture of Grit St- SG at solids concentrations of less dense solid phase, SG, varying from 1.5 to 55 wt %

$X_{w,less\ dense}$ (wt %)	$\frac{X_{w,less\ dense}}{X_{w,more\ dense}}$	$N_{js,measured}$ (rpm)	$N_{js,predicted}$ (rpm)	$\frac{N_{js,measured}}{N_{js,predicted}}$
1.5	1	1168	1059	1.1
5	3	1085	1076	1
10	6	1015	1090	0.93
20	13	929	1107	0.83
30	20	899	1122	0.80
40	26	863	1138	0.75
55	36	802	1169	0.68

The measured N_{js} of the mixtures for which the networking mechanism is observed decreases in proportion to the concentration ratio of the less and more dense solid phases. This is seen for Sph St-SAl, Sph St-SG, Grit St-SAl, Grit St-SG and Bronze-SG mixtures. The data of these five mixtures were analyzed and a relationship was found between the concentration ratio of solid phases and ratio of measured and predicted N_{js}. A representative data is shown in Table 9 for Grit St-SG. For example, if $X_{w,\ less\ dense}$ / $X_{w,\ more\ dense}$ is 20, $N_{js,\ measured}$ is 80 % of $N_{js,\ predicted}$. While the amount of less dense and smaller particles increases, the possibility of more dense particles sitting at the bottom of the tank decreases because of the network formed by the less dense particles. This results in a decrease in N_{js}. The power model was modified with the given correction factor to account for the drop in N_{js} due to the networking mechanism as following:

$$N_{js,mix} = C\left(\frac{\rho_{sl,1}N_{js,1}^3 + \rho_{sl,2}N_{js,2}^3}{\rho_{sl,mix}}\right)^{1/3} \tag{4. 2}$$

$$C = (100 - \frac{X_{less\ dense}}{X_{more\ dense}})/100 \tag{4. 3}$$

Figure 22 shows the use of Equation (4.2) and (4.3). A significant improvement was obtained compared to Figure 21. The data now follows the parity line.

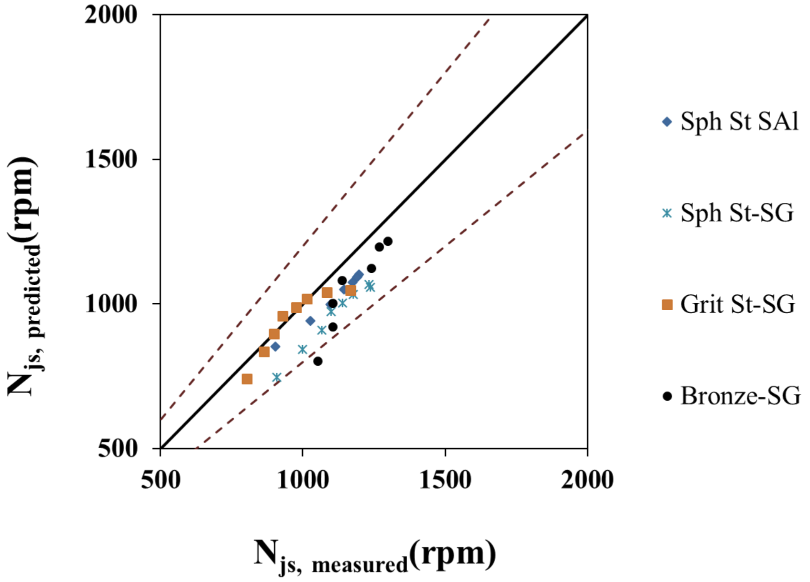

Figure 22. The modified power model predictions. Unimodal N_{js} within the power model is experimental data.

Up to now, the unimodal slurry N_{js} in power model was the measured N_{js}. For the full prediction of mixture N_{js}, the unimodal slurry N_{js} should also be predicted using correlations. Figure 23 a and b show the mixed slurry N_{js} predictions with the use of experimental and predicted unimodal slurry N_{js} in power model, respectively. The modified version of the power model was used when necessary. The data in Figure 23a is closer to parity line compared to Figure 23b. It seems that there are three groups of mixtures. The first group consists of BG-TPE, ABS, Akulon mixtures whose data is above the parity line and have similar trends. The second group is Grit St - SG, Sph St - SG, Grit St - SAl and Sph St – SAl whose data was corrected to take the networking mechanism into consideration. The third group consists of Plt Cp - LG, Rod Cp - LG, Plt Cp - LAl and Rod Cp – LAl mixtures whose data at low concentrations is above the parity line, but as the solids concentration increases it passes below the parity line. The standard deviations of these groups in Figure 23a are 10.3 % for BG-TPE, ABS, Akulon mixtures, 6.05 % for Grit St - SG, Sph St - SG, Grit St - SAl and Sph St - SAl mixtures and 5.95 % for Plt Cp - LG, Rod Cp - LG, Plt Cp - LAl and Rod Cp - LAl mixtures. The deviations of these three mixture groups are 24.1 %, 10.4 % and 18.3 %, respectively for the data shown in Figure 23b. As a result, it can be said that using the correlation to determine unimodal N_{js} in power model causes some increase in deviations from measured N_{js} of mixed slurries, which is expected.

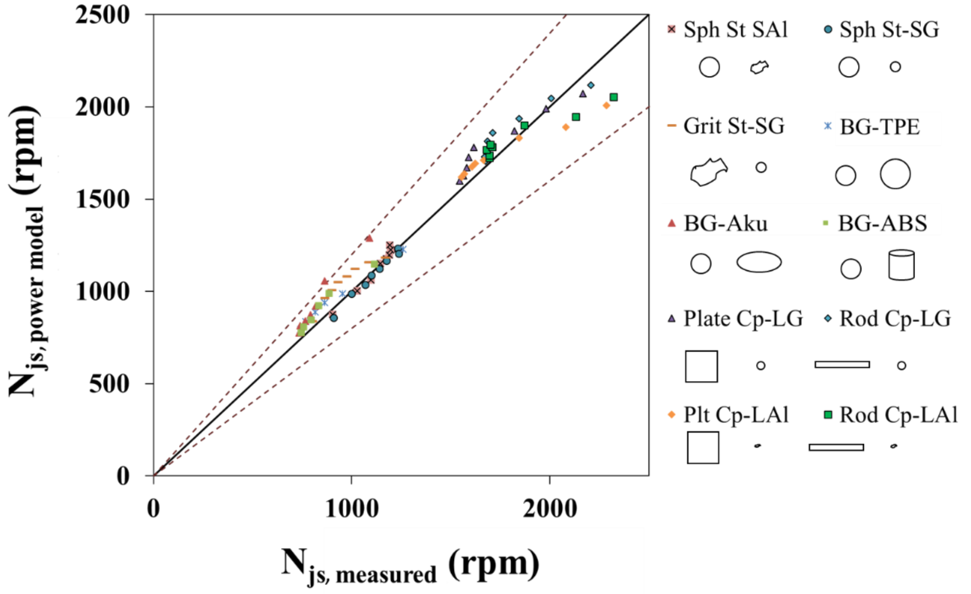

a.

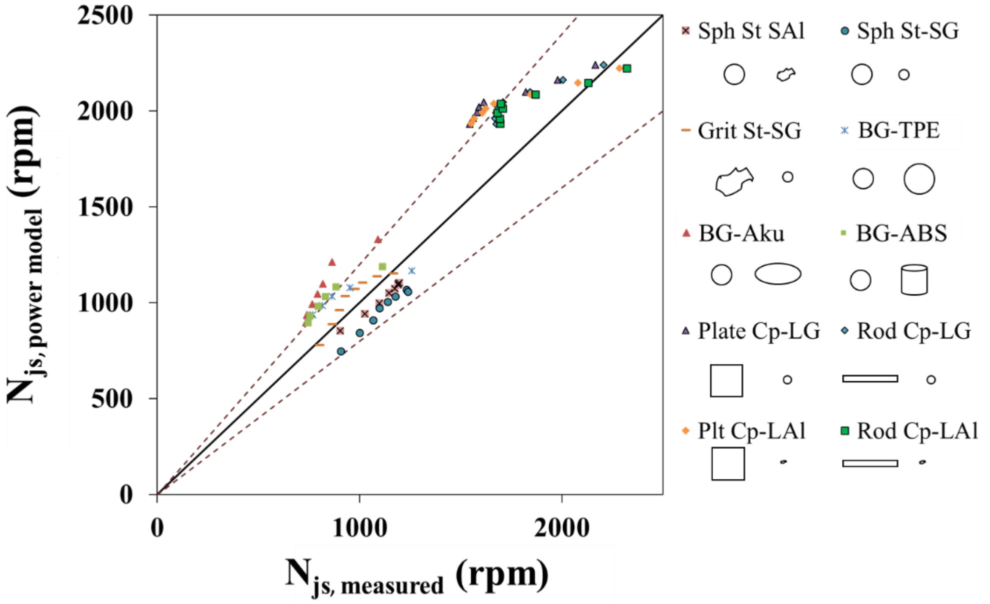

b.

Figure 23. Mixed slurry N_{js} predictions using power model and the modified power model when necessary. a. Unimodal N_{js} obtained experimentally b. Unimodal N_{js} obtained from Ayranci's correlation

As mentioned above, N_{js} predictions of mixtures which contain TPE, ABS and Akulon show largest deviations from measured N_{js} values. Measured N_{js} of these slurries are close to measured N_{js} of unimodal BG slurry at concentrations lower than 15 wt %. When the mixed slurry N_{js} is calculated from power model, the contributions which come from power required to suspend less dense phases - ABS, TPE, Akulon- cause high predictions. The same tendency was seen in slurries that include copper particles because their mixed slurry N_{js} is also close to N_{js} of unimodal Plt or Rod Cp slurry for concentrations of less dense phase lower than 15 wt % where the less dense phase is LAl or LG.

The high predictions of power model mentioned above do not cause significant standard deviations. The largest standard deviation is obtained as 24.1 % for mixtures of BG with TPE, ABS or Akulon, when unimodal N_{js} values in power model are determined with the use of Ayranci's correlation.

While the correction for the networking effect made the predictions much better, there is still some deviations from the parity line. The data shown in Figure 23b was predicted by use of particle sizes in Table 4 and the effect of particle shape was not considered. As the next step, the effect of particle shape on N_{js} was analyzed to improve the predictions.

4.2.2.2 Particle Shape Factors

In this section, the prediction of N_{js} of unimodal and mixed slurries which include non-spherical particles is analyzed in terms of the effect of particle shape. As mentioned in section 4.2.1, Ayranci's correlation predicts N_{js} of unimodal slurries of all particles used in this study with 10.5 % standard deviation. For this calculation, particle sizes given in Table 4 were used as d_p, and the exponent of 0.17 on the concentration term was used for SG and SAl, 0.23 was used for LG and LAl, and 0.32 was used for TPE, Akulon and ABS. The data was shown in Figure 17 among with the other five correlations. In Figure 24a and b it is shown separately for spherical and non-spherical particles, respectively. This separate analysis showed that the standard deviation for spherical particles is 9.7 % and for non-spherical particles is 11.7 %. The accuracy of Ayranci's correlation is almost the same for both spherical and non-spherical particles. It should, however, be noted that the same accuracy for non-spherical particles as spherical ones was obtained with the use of particle sizes in Table 4. The use of different sizes of non-spherical particles could give different results.

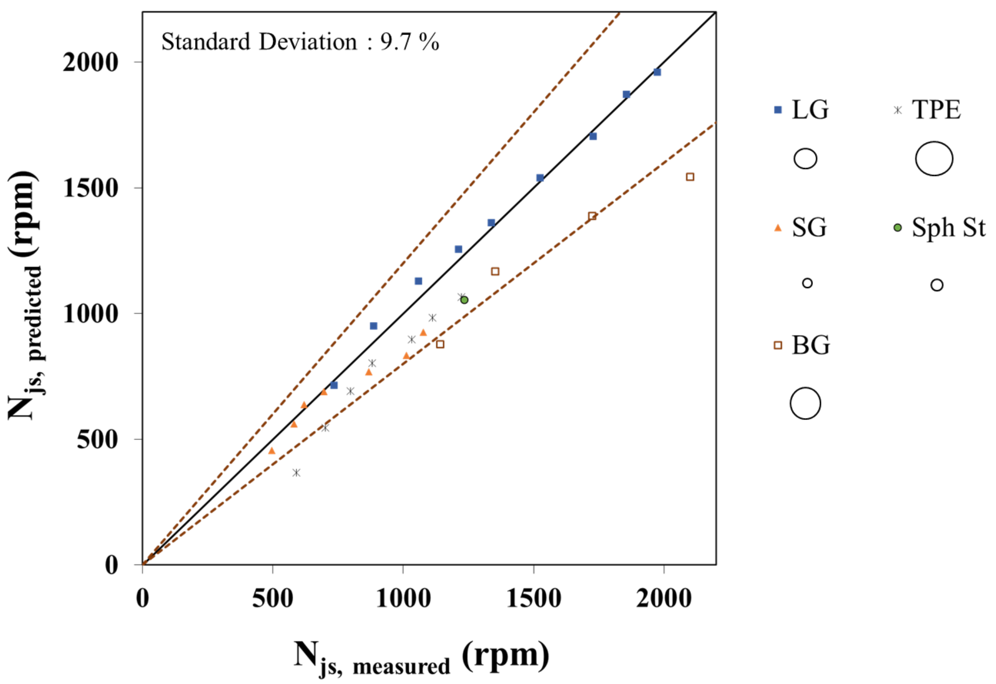

a.

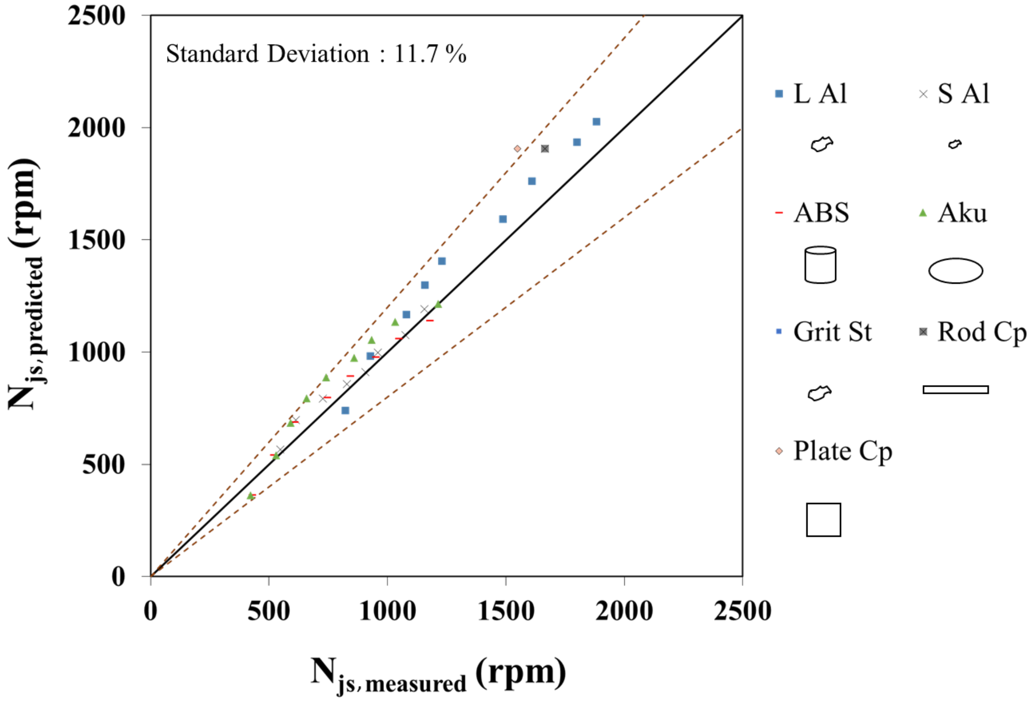

b.

Figure 24. The comparison of measured and predicted N_{js} for unimodal slurries a. spherical particles b. non-spherical particles

The choice of dimension to use as the particle diameter in correlations is simple when spherical solids are used: it is the one and only length, the particle diameter. The choice of representative d_p is much more complicated for a non-spherical particle: there is possibly a largest and a smallest dimension one of which might be the thickness of the particle.

Ditl and Naumann (1992) stated that the controlling dimension is the thickness of the plate and disc-shaped particles and largest dimension has no effect. This inference should not be interpreted as a suggestion of using the smallest size as d_p in correlations because all correlations are based on experimental data with spherical particles. When the smallest size – the thickness – of a plate is used as the size term in the correlation, the result would be the N_{js} of a sphere which has a diameter equal to the thickness of the plate shaped particle. When the individual mass of the plate and a sphere with a diameter of the thickness of the plate are compared, the difference is significant. Individual mass of a particle is an indication of the suspension characteristic of the particle; therefore, N_{js} calculated by using the smallest size of a particle would likely give inaccurate results, possibly too low N_{js}.

Figure 25 shows the N_{js} predictions when the smallest dimension of the non-spherical particles was used as d_p. The minimum and maximum sizes of particles are given in Chapter 3. N_{js} of the slurries of the plate and rod-shaped copper particles are under-predicted in both Figures 25 a and b. In Figure 25a the most noticeable deviation is the data of Plt Cp: its prediction is 23 % lower than measured. The thickness cannot be used as $d_{p,}$ but it can be controlling dimension for thin particles because thickness affects the definition of particle shape. As the thickness of a plate increases, its surface area per unit volume and sphericity increases. In fact, these properties of particles may affect N_{js} directly.

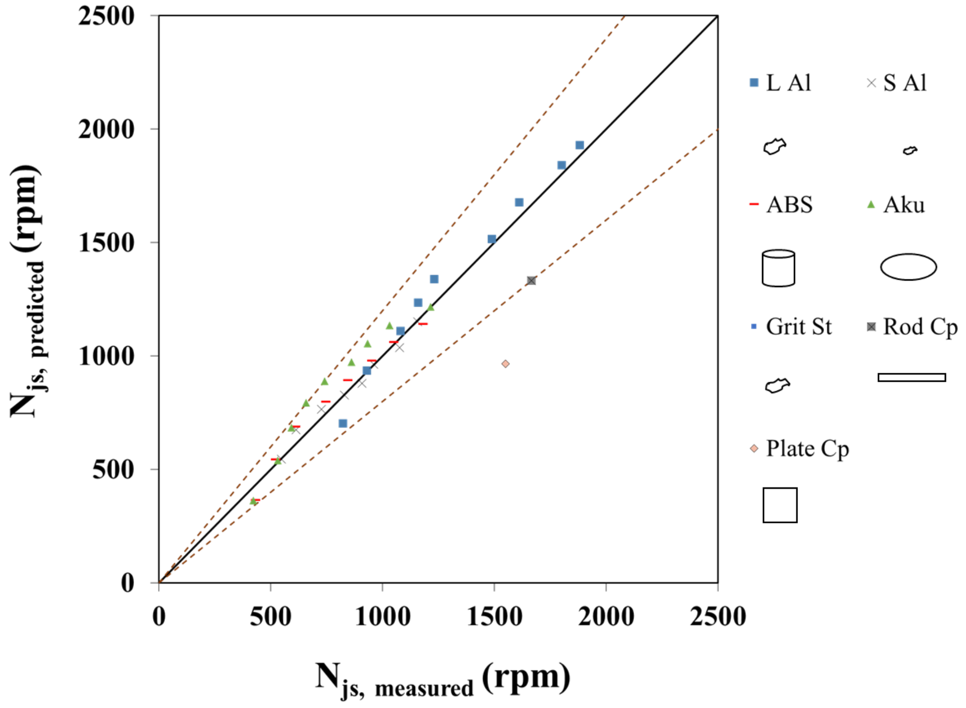

a.

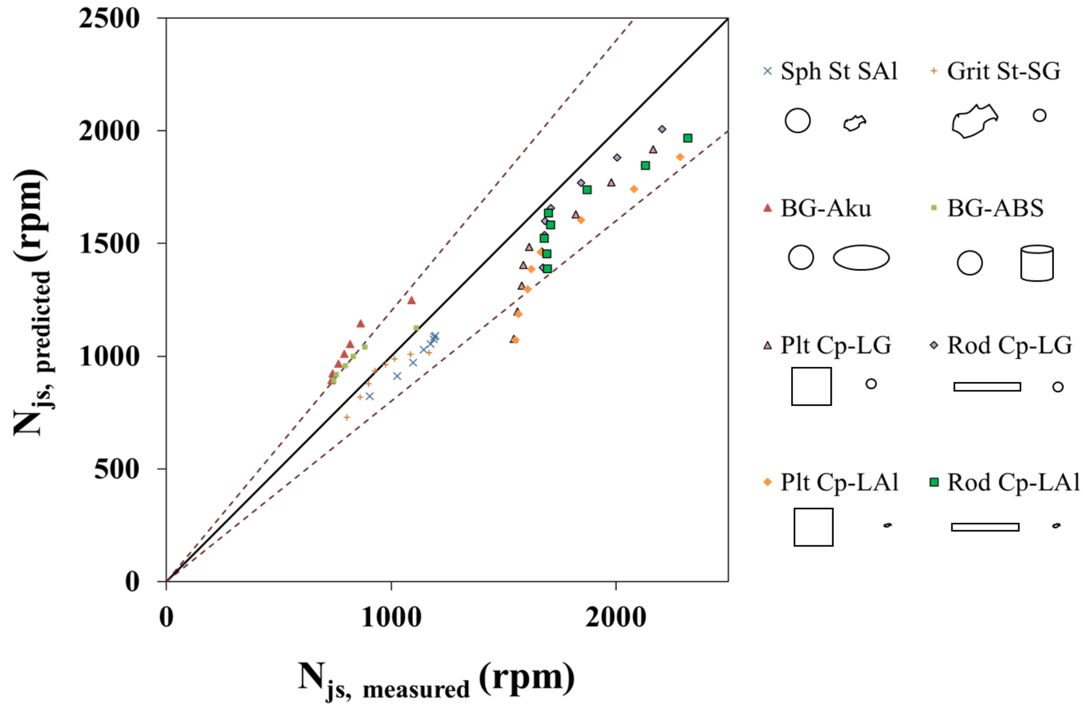

b.

Figure 25. The parity plot of predicted and measured N_{js} with the use of minimum dimension in Ayranci's correlation a. Unimodal slurries b. Mixed slurries

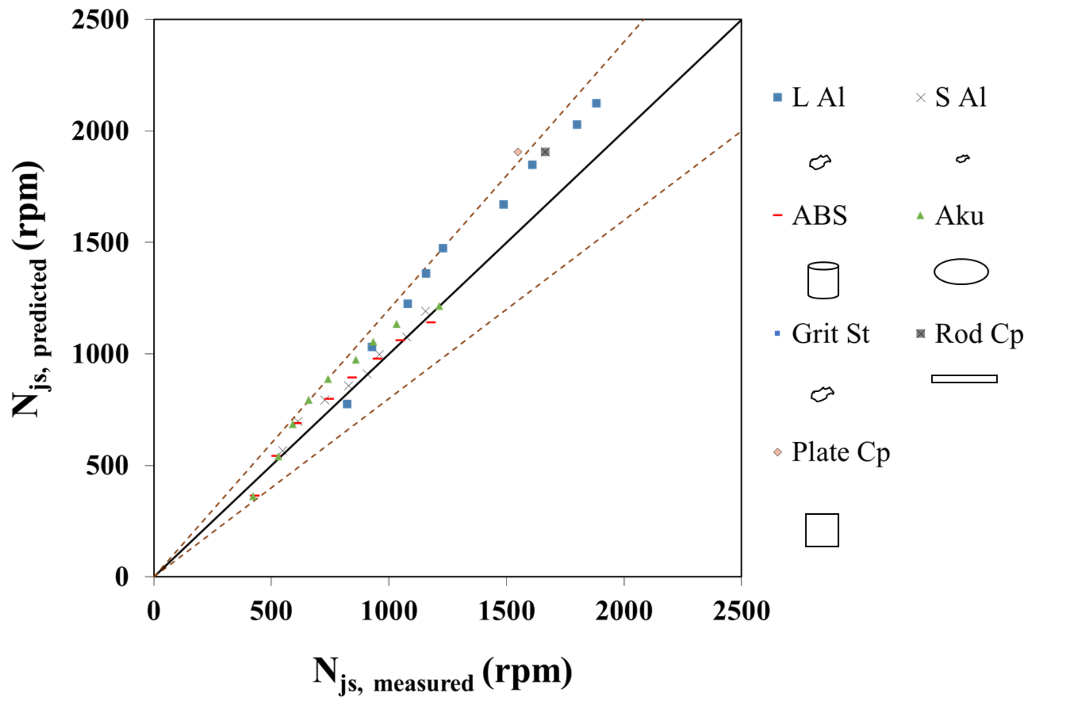

a.

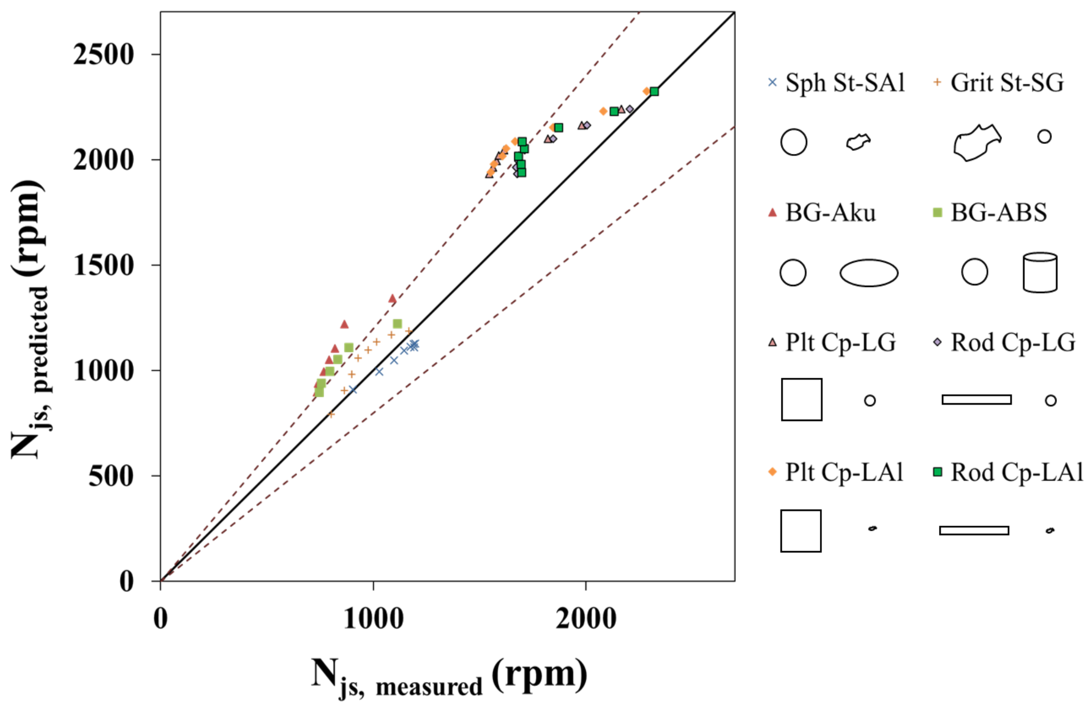

b.

Figure 26. The parity plot of predicted N_{js} with the use of maximum dimension in Ayranci's correlation a. Unimodal slurries b. Mixed slurries

Another option is to use the maximum diameter of a non-spherical particle as d_p. Figure 26a and b shows the predictions with this approach. The use of maximum dimension of non-spherical particles causes very large N_{js} for copper particles in both unimodal and mixed slurries because the correlation predicts N_{js} of a sphere which has a diameter equal to the maximum dimension of non-spherical particle and this imaginary spherical particle has larger individual mass and volume than the real non-spherical particle.

The use of the minimum dimensions caused predictions lower than and the use of the maximum dimensions caused predictions higher than measured N_{js}, but these results are within ±20 % lines. For more accurate prediction, however, the particle shape should be taken into account.

In
Figure *27* the particle shapes which have different projected areas but the same maximum dimensions are given. As their particle shape definition becomes different from a sphere, their projected areas become smaller. Drag force acting on a particle depends on its projected area (Henthorn et al., 2005). This relationship may be important to predict N_{js}. With this thought, it can be considered that maximum dimension of non-spherical particles should be used as d_p in the correlation but a correction should be done according to the shape of the particle. This way a representative size that is smaller than the maximum size, but larger than minimum size can be obtained.

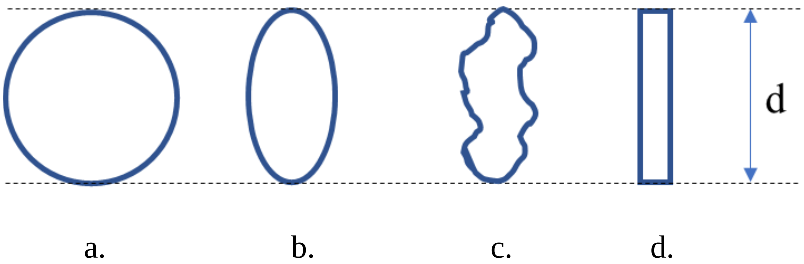

Figure 27. The different projected areas of particles. a. Spherical, b. Ellipsoid, c. Grit d. Rod shaped

To express this relationship mathematically, a shape factor term, φ, was added to Ayranci’s correlation and its effect was represented exponentially as for the rest of the terms. The modified form of the correlation is given in Equation (4.4).

$$N_{js} = \varphi^m A' \left(\frac{g(\rho_s - \rho_l)}{\rho_l}\right)^{0.5} \frac{d_p^{1/6} X^n}{N_p^{1/3} D^{2/3}} \frac{T}{D} \tag{4. 4}$$

The selected shape factors among the ones found in the literature were calculated for non-spherical particles. Table 10 shows these factors for all the non-spherical particles tested.

Table 10. The values of shape factors of non-spherical particles

Name of non-spherical particle	AR	Circularity	Convexity	Wadell’ s Sphericity	Corey’s shape factor
Grit St	0.52	0.56	0.462	0.52	-
SAl	0.65	0.69	0.479	0.65	-
LAl	0.7	0.72	0.482	0.7	-
Rod Cp	0.268	0.48	0.5	0.66	0.13
Plt Cp	0.811	0.73	0.5	0.23	0.033
ABS	0.819	0.76	0.5	0.82	0.67
Akulon	0.818	0.86	0.5	0.95	0.5

Aspect ratio, AR, and circularity were calculated with the help of Image J software for all particles. Convexity was calculated with the help of Image J for only concave particles: Grit St, SAl and LAl. Convexity value of the already convex particles is 0.5 based on the definition of convexity. These particles are Plt Cp, Rod Cp, ABS andAkulon. This definition does not allow for taking the differences in shapes into account for these particles. Corey’s shape factor requires the measurement of all three dimensions, minimum, maximum and medium, of the particle. It was not possible to measure these for the small particles; therefore, these factors were calculated only for particles of dp >1 mm for which a ruler could be used in measuring all three dimensions. Similarly, Wadell's sphericity could also be calculated for only dp>1 mm particles. However, this issue was overcomed by using Image J program.

Image J provides roundness values which is defined as ($\pi \times$ Major axis^2)/(4 × Area). We proposed that roundness can be used as the Wadell's sphericity. The analysis showed that with the assumption that the surface area of a sphere, which has the same volume as particle, equals to $\pi \times$ (Major axis)^2 and the surface area of particle equals to 4 × (Area), the roundness gave similar results as the Wadell's sphericity. Image J can analyze images of particles only in 2D; therefore, it cannot give any volume related results. The assumption of roundness being equivalent to Wadell's sphericity for non-spherical particles was verified by comparing the results with the results of Hua et al. (2015) which used a different method. Hua et al. (2015) conducted an experiment in a fluidized bed with alumina particles which have the same shape as SAl particles used in this study as shown in Appendix B. In the experiments, the pressure drop along the bed was measured. Then the sphericity of the particles was determined by using the Ergun equation. They determined sphericity of the alumina particles as 0.625. This value is close to the value of 0.65 determined by using the roundness in Image J for SAl particles; therefore, the assumption that roundness and sphericity give the same results can be accepted.

The shape factors given in Table 10 were placed in Equation (4.4) to calculate unimodal slurry N_{js}, and then the mixed slurry N_{js} were calculated by using the power model. The performance of shape factors to account for the effect of particle shape on N_{js} was analyzed by comparing the measured and predicted N_{js} values. The standard deviation of predictions from measured N_{js} was calculated for each shape factor using different m values. The changes of standard deviations with m for the five shape factors are given in Figure 28a and b for unimodal and mixed slurries, respectively. The optimum m values which give minimum standard deviations were determined for all five shape factors. The value of m which can give the most representative results for each shape factor and minimum standard deviations of predictions from measured N_{js} are given in Table 11 and Table 12. The parity plots of predicted N_{js} with the use of each of the five shape factors using the optimum m values that provide minimum standard deviations from experimental N_{js} are given in Figure 29-Figure 33.

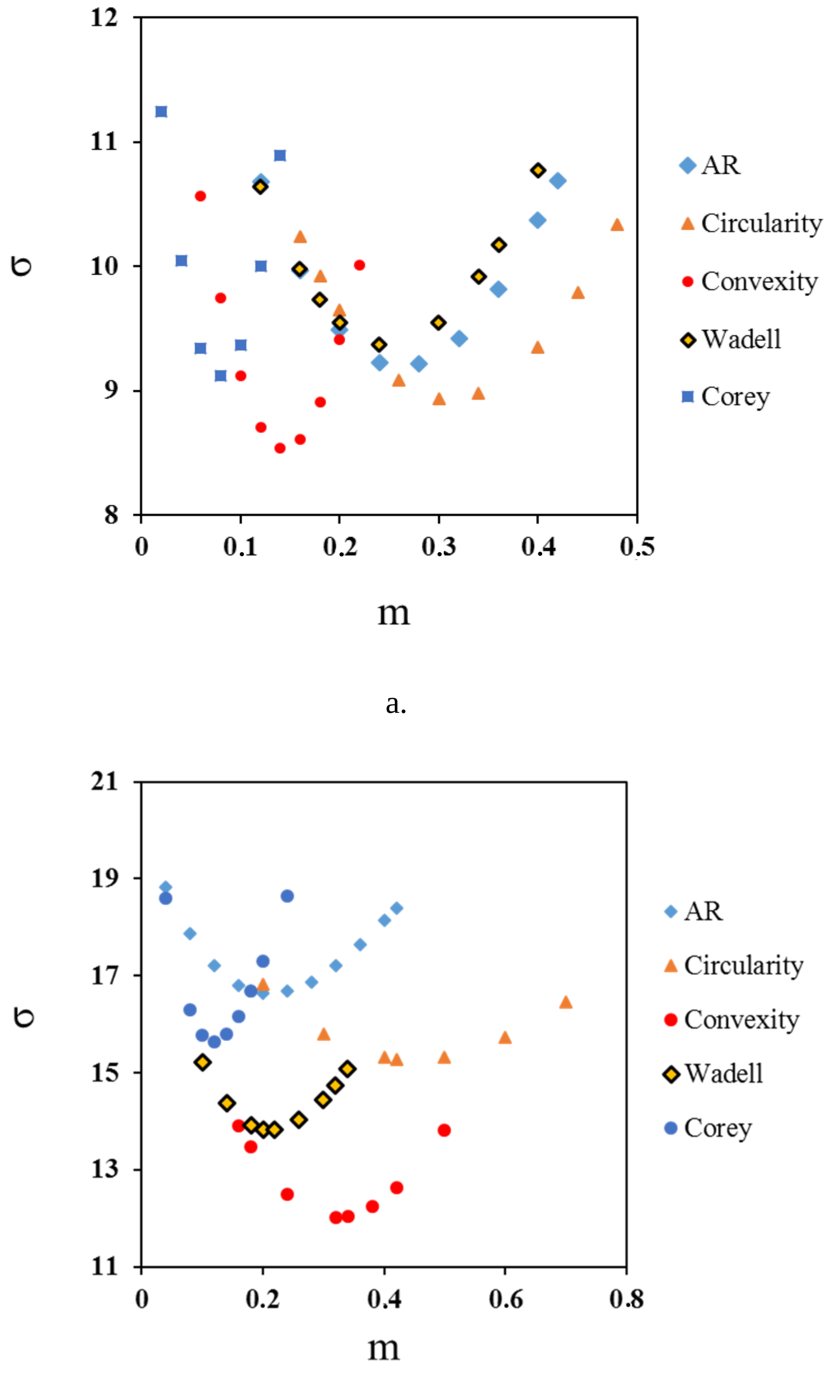

a.

b.

Figure 28. Variation of the standard deviation of predicted N_{js} with the exponent of shape factor (m). a. Unimodal slurries, b. Mixed slurries

Table 11. The minimum standard deviations of unimodal slurry $N_{js,\ predicted}$ from $N_{js,measured}$ with the use of minimum and maximum dimension, and shape factors. Optimum exponents (m) are given for the five shape factors.

φ	m	Standard Deviation (%)
Minimum	1	11.79
Maximum	1	12.07
AR	0.24	9.23
Circularity	0.3	8.94
Convexity	0.14	8.54
Wadell	0.24	9.37
Corey	0.08	9.12

Table 12. The minimum standard deviations of mixed slurry $N_{js,\ predicted}$ from $N_{js,measured}$ with the use of minimum and maximum dimension, and shape factors. Optimum exponents (m) are given for the five shape factors.

φ	m	Standard Deviation (%)
Minimum	1	15.76
Maximum	1	19.27
AR	0.2	16.64
Circularity	0.42	15.28
Convexity	0.32	12.01
Wadell	0.2	13.84
Corey	0.12	15.64

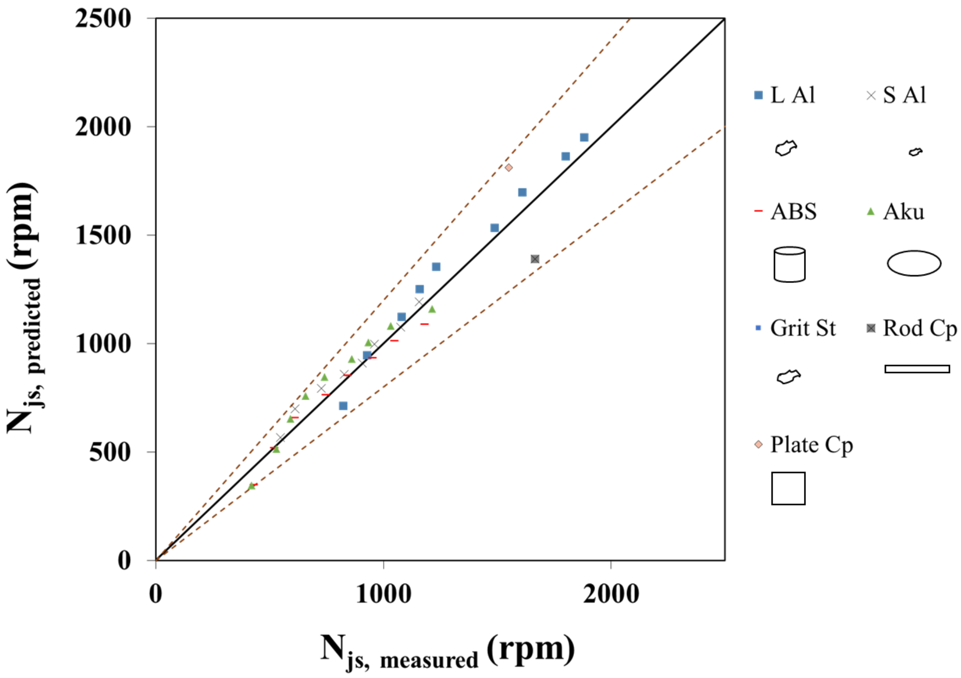

a.

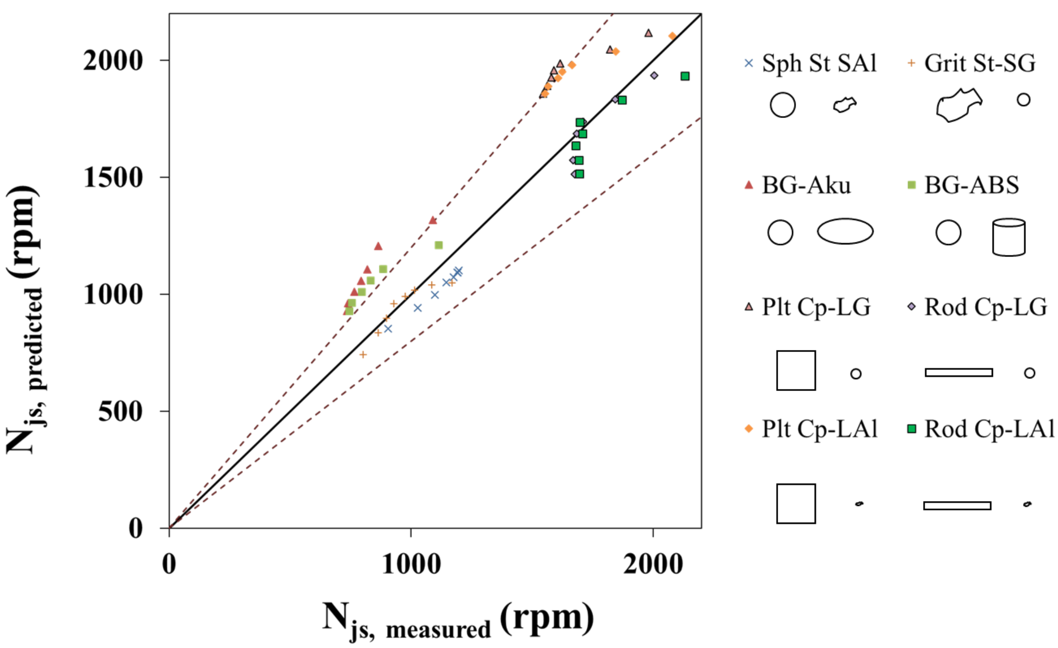

b.

Figure 29. The parity plot of predicted N_{js} with the use of AR in Ayranci's correlation a. Unimodal slurries b. Mixed slurries

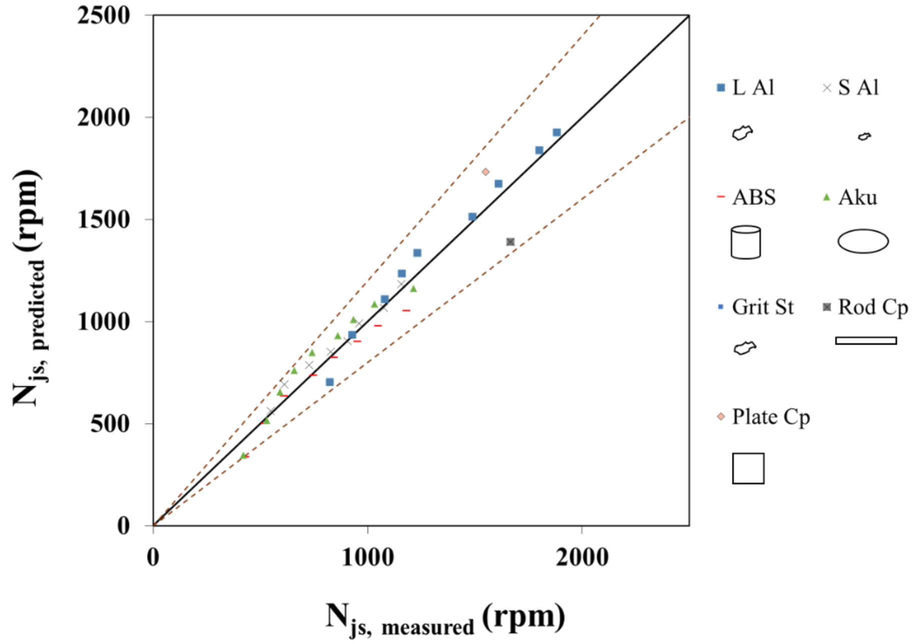

a.

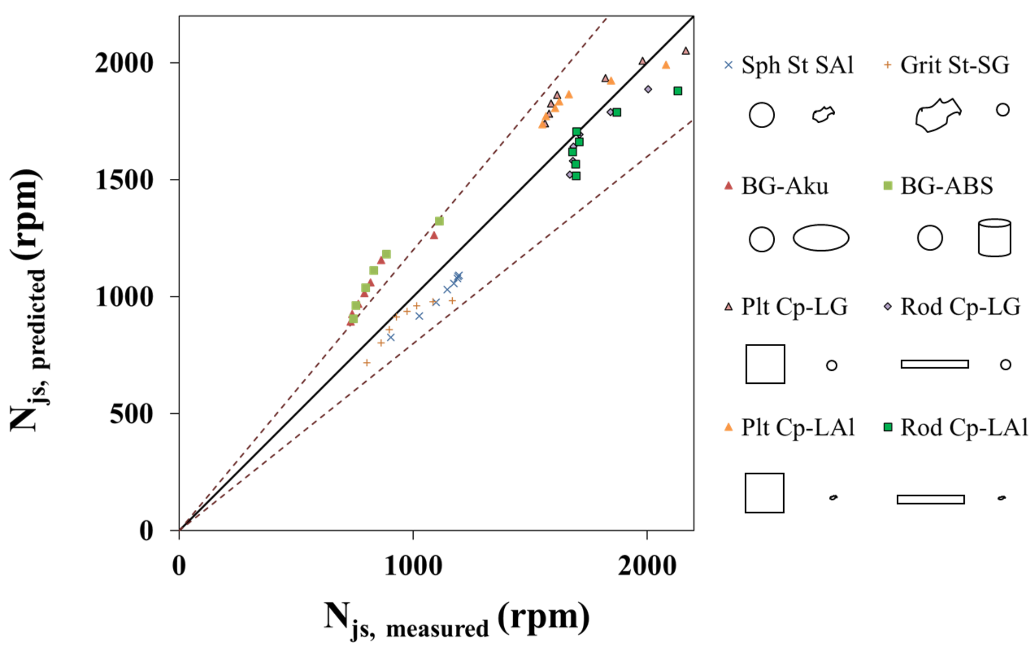

b.

Figure 30. The parity plot of predicted N_{js} with the use of circularity in Ayranci's correlation a. Unimodal slurries b. Mixed slurries

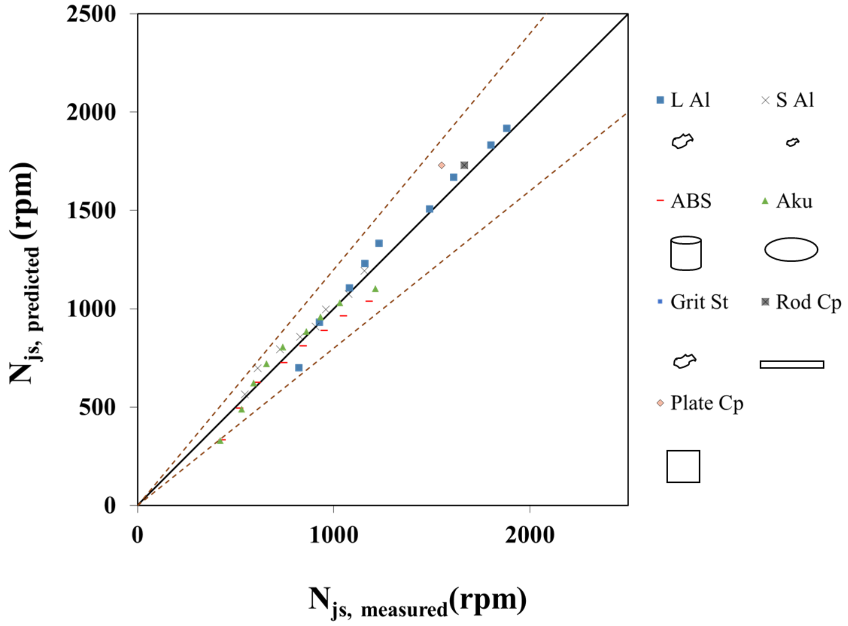

a.

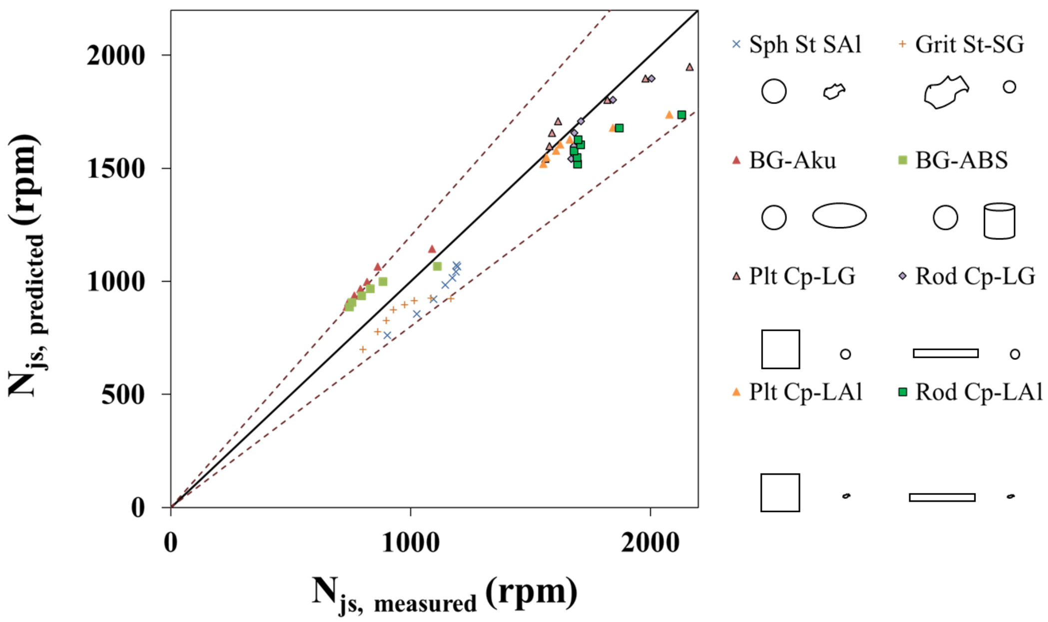

b.

Figure 31. The parity plot of predicted N_{js} of mixed slurries with the use of convexity in Ayranci's correlation a. Unimodal slurries b. Mixed slurries

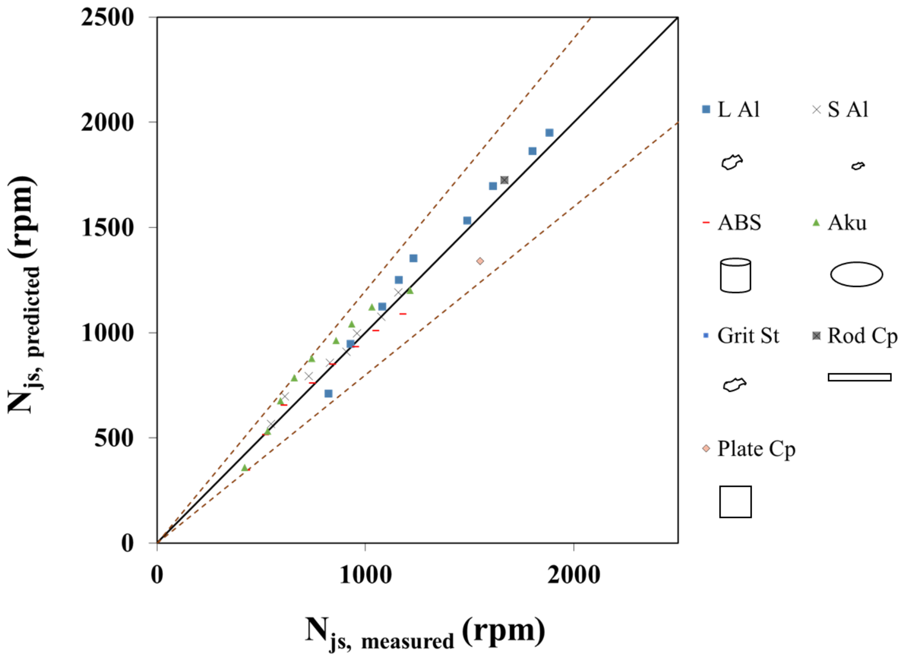

a.

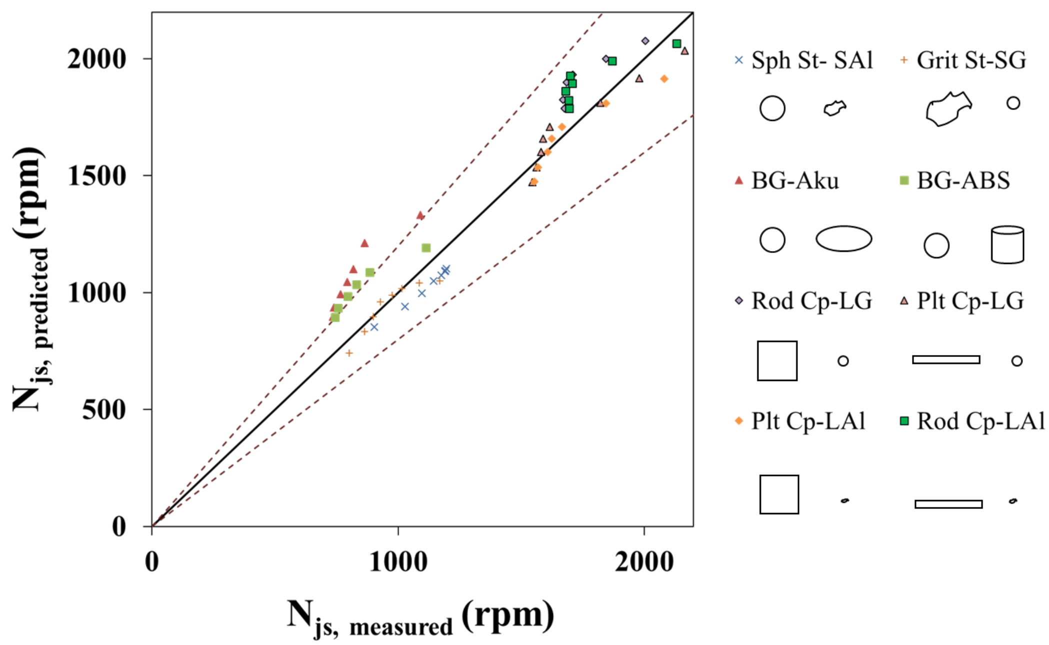

b.

Figure 32. The parity plot of predicted N_{js} of with the use of Wadell's sphericity in Ayranci's correlation a. Unimodal slurries b. Mixed slurries

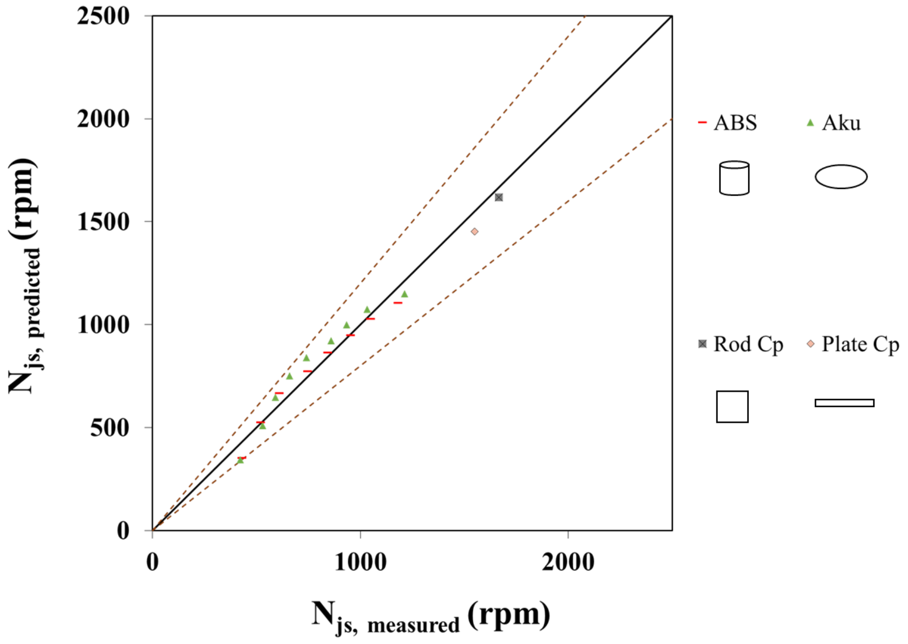

a.

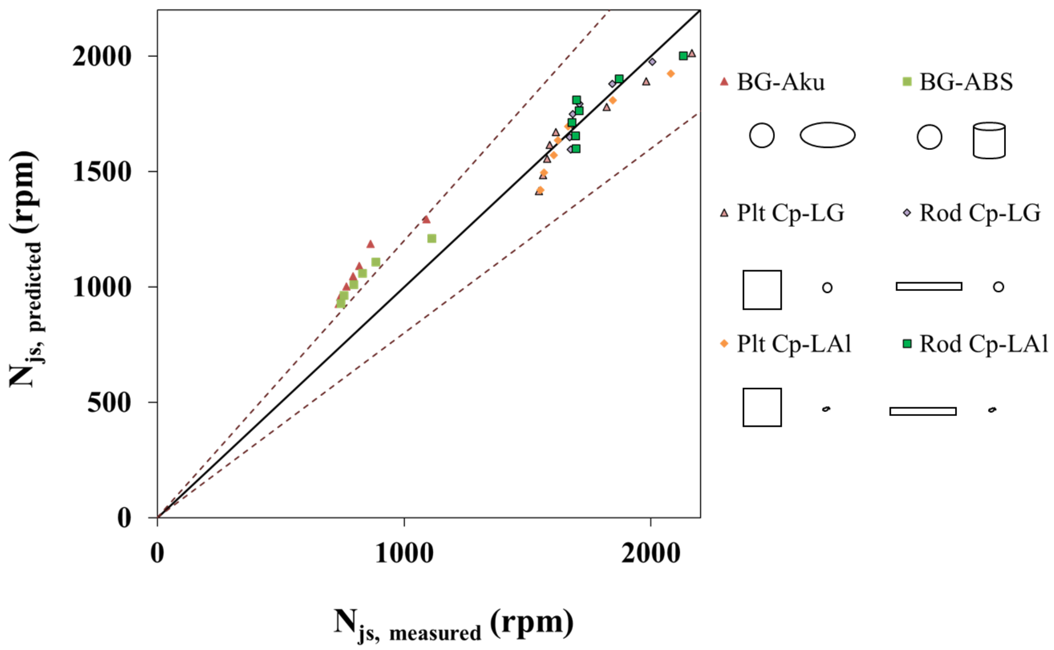

b.

Figure 33. The parity plot of predicted N_{js} of mixed slurries with the use of Corey's shape factor in Ayranci's correlation a. Unimodal slurries b. Mixed slurries

The use of five shape factors; AR, circularity, convexity, Wadell's sphericity and Corey's shape factor, gave lower standard deviations for unimodal slurries compared to mixed slurries because using one more correlation, power model, to determine N_{js} causes an increase in deviations. Thus, the standard deviation of mixed slurries is higher than unimodal slurries independent of the effect of particle shape. The use of minimum dimension, maximum dimension or the five shape factors results in standard deviations varying from 8.5 to 12 % for unimodal slurries and 12 to 19 % for mixed slurries.

It was found that the use of convexity minimizes the standard deviation for both unimodal and mixed slurries but as mentioned above convexity is not distinctive for convex non-spherical particles. Similarly, Corey's shape factor is not distinctive for particles whose all three dimensions cannot be measured separately. It could be calculated for only very large (dp>1mm) particles. AR and circularity lead to lower standard deviations compared to Wadell's sphericity and Corey's shape factor for unimodal slurries, but they cause higher standard deviations for mixed slurries because they cannot represent the shape of copper particles in the correlation correctly. This can be seen in Figure 29b and Figure 30b for Plt Cp more clearly. N_{js} predictions of slurries of Plt Cp-LG and Plt Cp-LAl are close to +20 % line due to AR and circularity values of Plt Cp. Wadell's sphericity is the most convenient factor which can reduce the deviations originated from particle shape. Determining Wadell's sphericity is possible and N_{js} predictions with the use of this factor are reasonable, for all particles.

Wadell's sphericity is a ratio related to volume and surface area of a particle. In section 4.1 the conclusion is reached that as the surface area per volume of particle increases, drag force acting on the particle increases and N_{js} decreases; therefore, a factor which contains information of volume and surface area of the particle like Wadell's sphericity may be used to interpret behaviour of particles in solid suspension applications. Based on the analyses done in this section, the use of Wadell's sphericity as the shape factor in Equation (4.4) with exponents of 0.24 for unimodal and 0.2 for mixed slurries is recommended. Figure 34 shows parity plots of unimodal and mixed slurries for all particles – spherical ones, and non-spherical ones with shape modification. The modified power model was used when necessary. The standard deviation values are 9.4 % and 15.6 %, respectively.

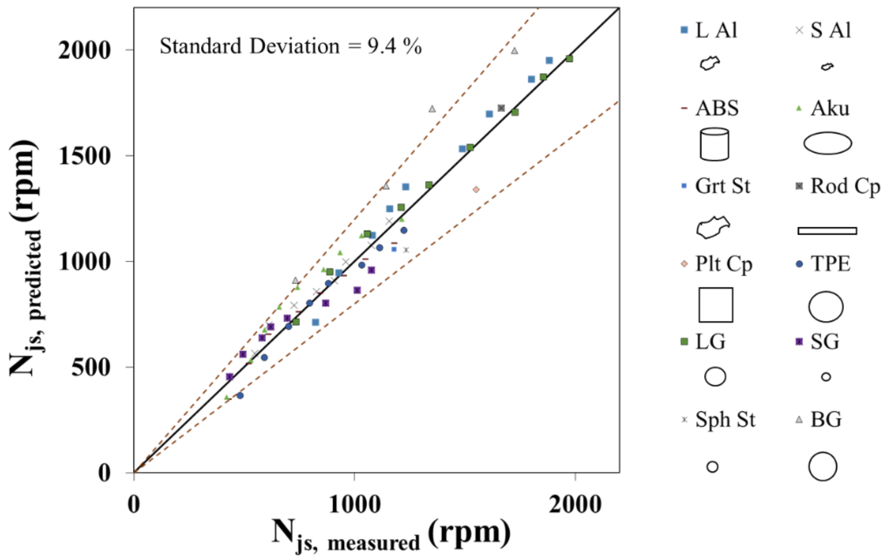

a.

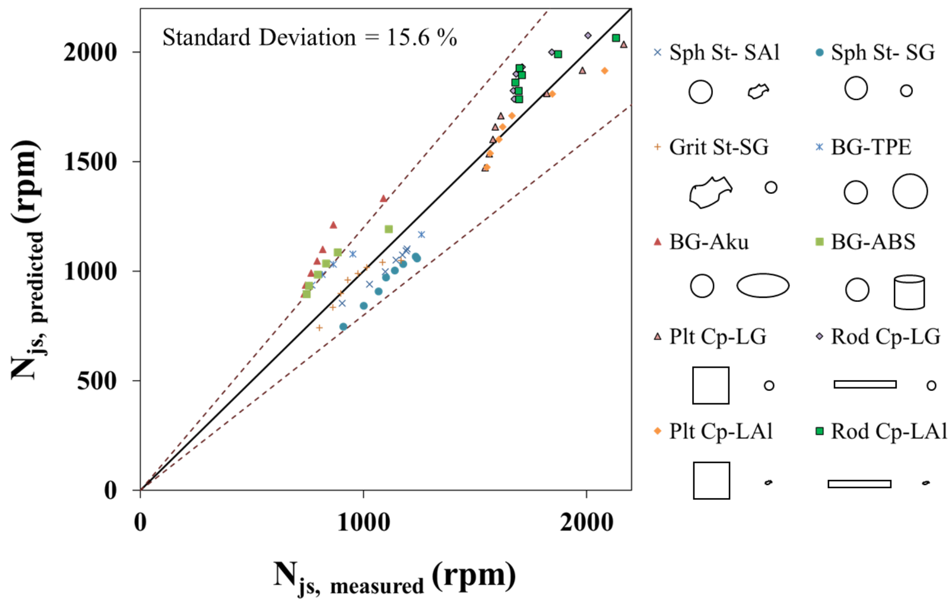

b.

Figure 34. The parity plots of slurries of spherical and non-spherical particles with the use of Wadell's sphericity in modified Ayranci's correlation. a. Unimodal slurries b. Mixed slurries

4.3 Application of Pressure Gauge Measurement Method to Determine N_{js} Experimentally

In this study, the application limits of PGM method was different than the limits in the literature regarding the range of impeller speeds, solids concentration, particle size and density of solids. N_{js} was also measured for both unimodal and mixed slurries in this work, but in literature all the reported data was for only unimodal slurries. Thus, the application of PGM was tested for slurries that are close to industrial applications regarding the number of solid phases. The conditions of previous studies and this study are compared in Table 13. This shows that in this study PGM method was applied beyond its limits of application in the literature. Some difficulties were encountered with the collection and analysis of data at these out-of-limit applications. These difficulties are seen at high impeller speeds and at low concentrations. In this section, how to overcome these problems are reported. Then, the PGM data was compared with the visual data and correlation results to test the accuracy and applicability of the method.

Table 13. Comparison of the test system conditions for PGM method in literature and this study

Study	**Slurry Type**	**X_w (wt %)**	**Impeller speed (rpm)**	**Density of Solids (kg/m^3)**	**Viscosity of Liquid (Pa.s)**	**Particle Size (µm)**
Micale et al., 2002	Unimodal	3.77-33.8	0-800	2500	1	180-1000
Selima et al., 2008	Unimodal	6-10	0-350	2650	1	74-300
Lassaigne et al., 2016	Unimodal	10-35	0-800	2500	1-4	500-3000
This study	**Unimodal and Mixed**	**1.5-40**	**0-1700**	**1200-8000**	**1**	**85-3000**

4.3.1 Applying PGM to Slurries at High Impeller Speeds

Figure 35 shows the increase in pressure with increasing impeller speeds for three replications for the same slurry. The results are the same for all of the tests up to 900 rpm. At impeller speeds higher than 900 rpm, fluctuations are observed. At these speeds, the repeated experiments begin to deviate up to 11 % from the average.

The pressure data in Figure 35 is the average of the pressure data taken during a time period of 2-3 min for each impeller speed. In Figure 36a and Figure 36b, the raw pressure data is shown for low and high impeller speeds, respectively. The pressure change in Figure 36a at smaller impeller speeds, the pressure data is more smooth and the points at which impeller speed is increased can be identified more easily. In Figure 36b; however, the fluctuations in pressure prevent the observation of increase of pressure with impeller speed. For especially slurries at solids loadings lower than 20 wt %, the pressure measurements are noisy at high impeller speeds as seen in Figure 36b. When this data is averaged over time, the fluctuations at high impeller speeds in Figure 35 are obtained. These fluctuations prevent fitting a meaningful second order parabola to the pressure data. A meaningful parabola gives a ΔP_{js} value close to the theoretical one. If it is much larger or much smaller than the theoretical ΔP_{js} an accurate prediction of N_{js} is not possible. This is why the fluctuations in the pressure data should be smoothed.

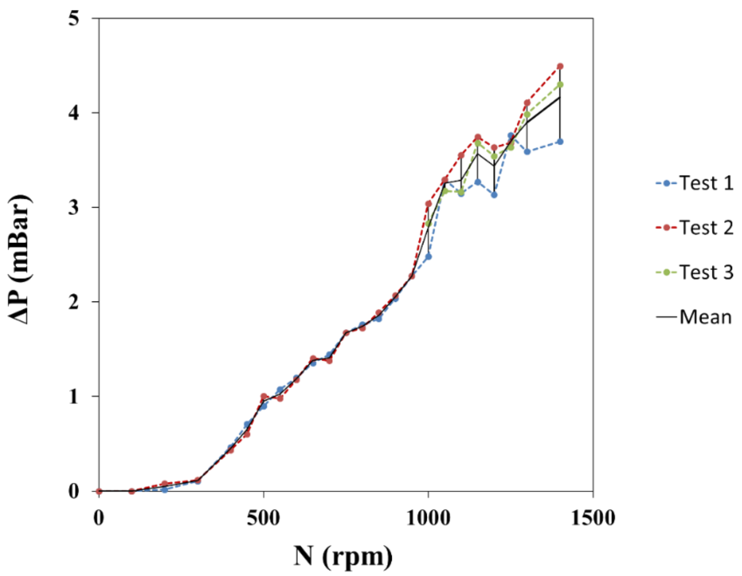

Figure 35. Reproducibility tests for the pressure measurements of the mixture of 1.5 wt % Sph St and 5 wt % SG

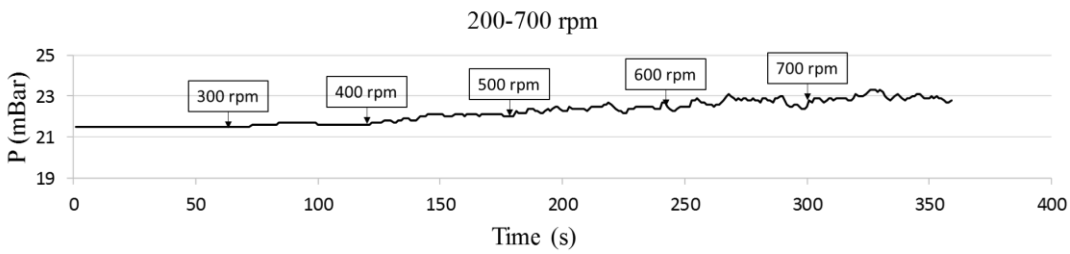

a.

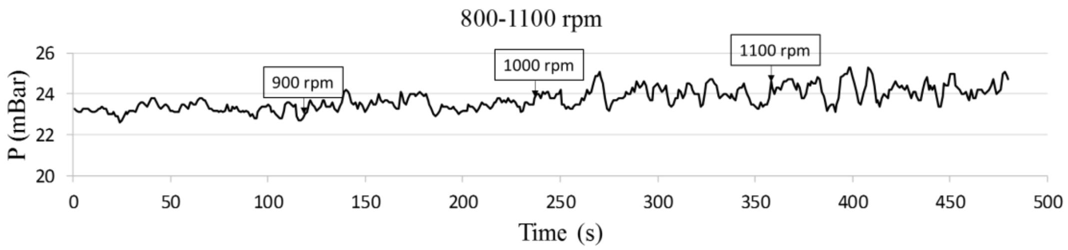

b.

Figure 36. Effect of impeller speed on fluctuations of pressure with time. Data is taken for the mixture of 1.5 wt% Sph St and 5 wt % SG a. For 200-700 rpm b. For 800-1000 rpm

The smoothing was obtained by filtering the pressure data using Savitzky-Golay filter which is a function in Matlab. The filter applies a regression with the least squares method to small data groups. When it was used, a smoothed pressure increase was obtained like in Figure 37. Other filter algorithms in Matlab were also tested, but the Savitzky-Golay filter represented the data most closely. Figure 37 shows the smoothed pressure curve for the same slurry in Figure 35 and Figure 36.

The literature studies listed in Table 13 were in the lower range of impeller speeds; therefore, a post-processing was not required. This study shows that the PGM method can be applied beyond its limits of development by applying a filter to the data.

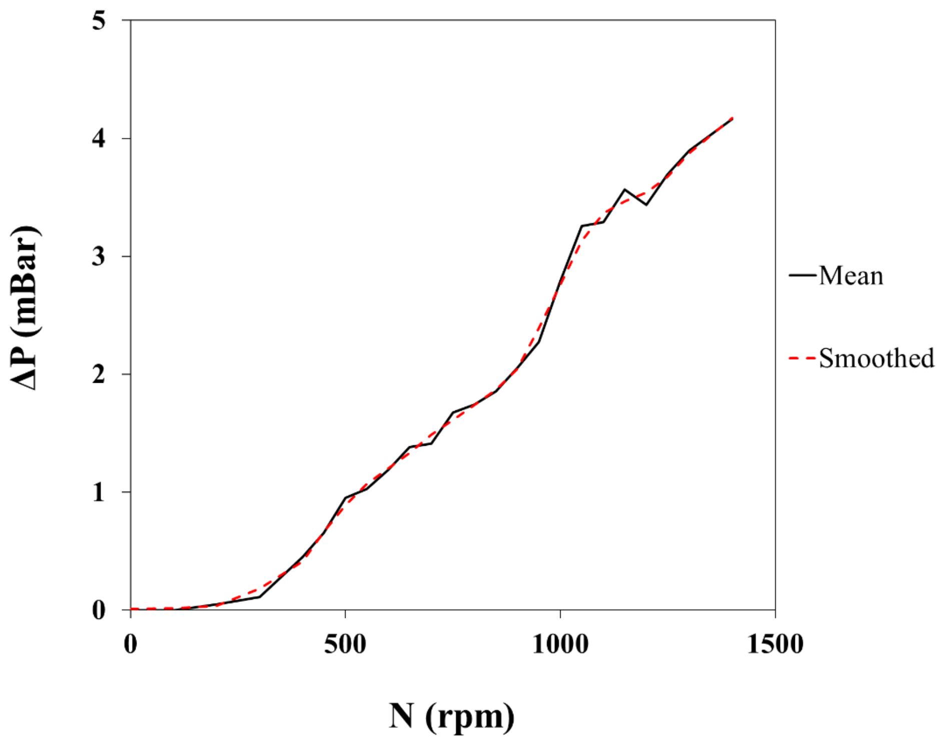

Figure 37. Smoothed pressure change graph of the mixture of 1.5 wt% Sph St and 5 wt % SG

4.3.2 Applying PGM to Slurries at Concentrations Lower and Higher than Previous Studies

Micale et al. (2002) stated that dynamic head effects are the major source of uncertainties of the PGM method. They anticipated that the ratio of pressure increase due to dynamic head effects to the pressure increase due to the mass of suspended solid particles will increase in the case of higher solids loadings, denser solid phases or larger tanks than the ones they used.

The experiments in this study were conducted with both higher and lower solids loadings, denser solid phases and in a larger tank than the ones used in Micale et al. (2002). In this section, first, the effect of concentration on the dynamic head effects was investigated. Second, findings about the application of the PGM method to mixed slurries were given. Third, the effect of settling velocity on dynamic head effects at low solids concentrations was expressed.

4.3.2.1 The Effect of Concentration on Dynamic Head Effects

As the impeller speed is increased in solid-liquid mixtures, the measured pressure increases due to the dynamic head effects and the mass of suspended solids. Figure 38 shows the determination of N_{js} graphs for mixture of Sph St and SAl at varying concentrations.

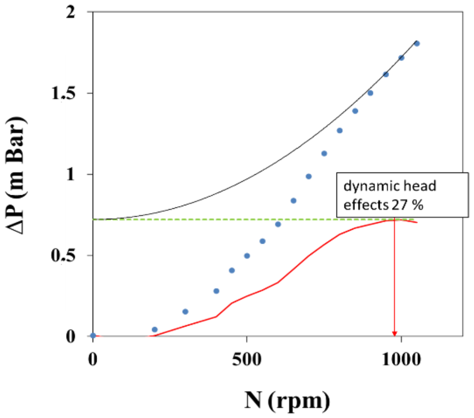

a. 1.5 wt % Sph St-1.5 wt % SAl
N_{js} = 900 rpm

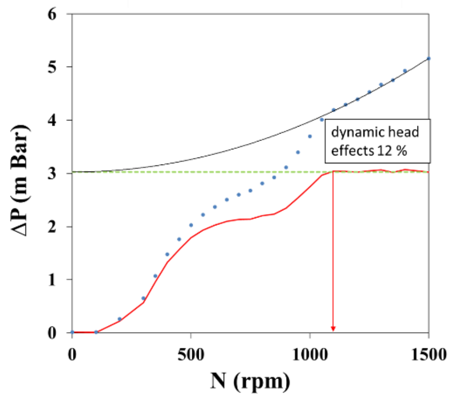

b. 1.5 wt % Sph St-10 wt % SAl
N_{js} = 1100 rpm

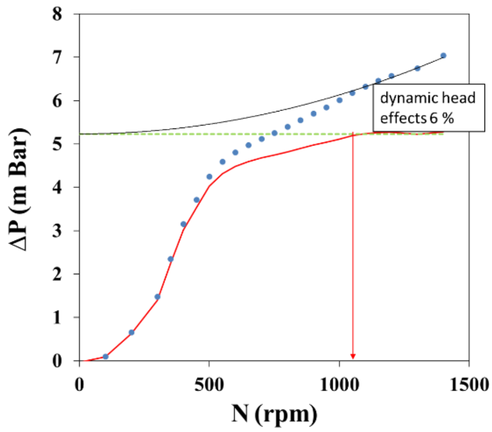

c. 1.5 wt % Sph St-20 wt % SAl
N_{js} = 1050 rpm

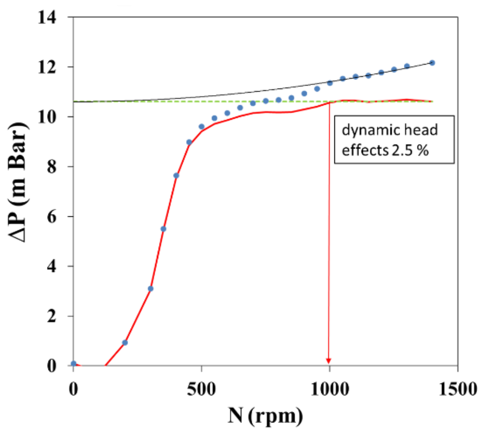

d. 1.5 wt % Sph St-40 wt % SAl
N_{js} = 1000 rpm

Figure 38. Effect of solids loading on dynamic head effects for the mixture of 1.5 wt % Sph St with varying concentrations of SAl: a. 1.5 wt %, b. 10 wt %, c. 20 wt %, d. 40 wt %

It was seen that the pressure increase due to dynamic head effects is higher at lower concentrations. This finding confirms Micale's anticipation mentioned above. In Figure 38, it is seen that the ratio of pressure change due to the dynamic head effects to total pressure change decreases as solids loading increases. The ratios are 27, 12, 6 and 2.5 % for the slurries with SAl concentrations of 1.5, 10, 20 and 40 wt %; respectively.

The relationship between dynamic head effects and concentration is analyzed in terms of raw pressure data in Figure 39. The figure shows pressure change with time for two slurries at different solids concentrations at the same impeller speed. The variation of pressure is generally in ±1 mbar for the concentrated mixture, while the pressure of low concentration slurry shows larger fluctuations, up to ±3 mbar. It should be noted that these fluctuations are observed only at high impeller speeds like explained in Section 4.3.1.

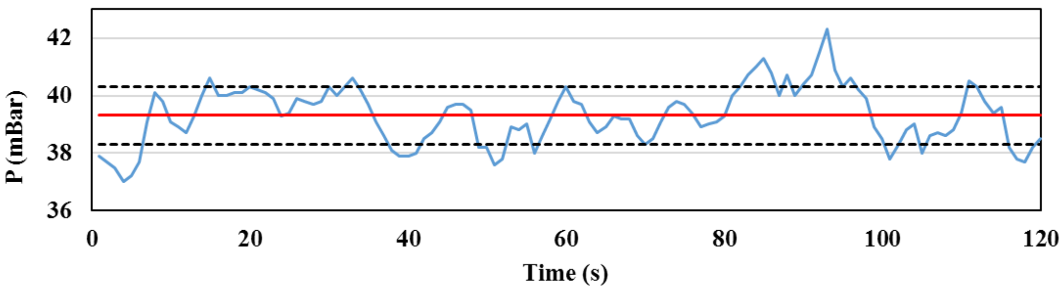

a.

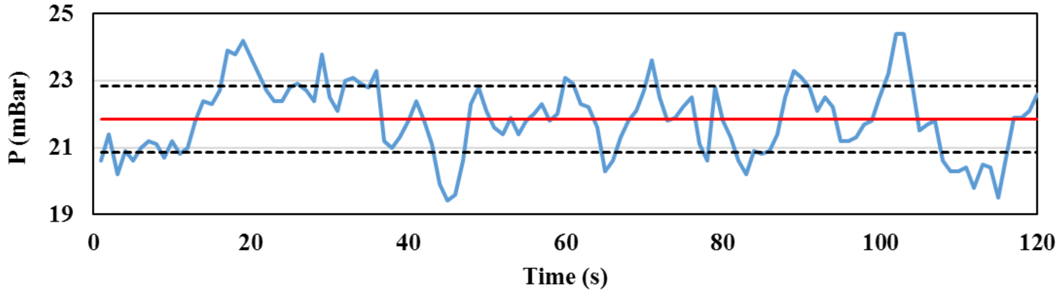

b.

Figure 39. Effect of solids concentration on fluctuations of pressure with time. Data is taken at 1300 rpm for the mixture of 1.5 wt % Sph St and SAl concentration of:

a. 55 wt % b. 1.5 wt %

These fluctuations are a result of fluid motion and the interactions between the solid and the fluid phases. The fluid, which moves axially towards the bottom of the tank due to pumping of the impeller, causes fluctuations inversely proportional to the concentration of particles: the larger the solids concentration, the smaller the fluctuations. Kinetic energy, that is transferred from the rotation of the impeller to the fluid provides energy for the particles motion and collisions (Ayranci et al. 2013b). When a larger number of particles exist at unit volume, the energy of the fluid is transferred to the particles more; therefore, the velocity of slurry would be lower. The force applied to the bottom of the tank varies with velocity of slurries and this force is low for high concentration slurries because the kinetic energy transferred from the impeller to the fluid does not lead to high slurry velocity.

4.3.2.2 The Effect of Concentration of Less Dense Phase on the Application of PGM for Mixed Slurries

The PGM method was applied to both unimodal and mixed slurries in this study. In this part, the pressure curves of mixed slurries are analyzed.

In Figure 40, the total pressure curves of mixtures of Sph St and SAl at varying concentrations and two curves of unimodal SAl are given. The curves at concentrations of 1.5, 5 and 10 wt % SAl are different from S-shaped curves of unimodal slurries: they include two waves because the two solid phases are suspended at different impeller speeds. Thus, the total pressure curves of mixed slurries at concentrations lower than 20 wt % give information about the suspensions of each solid phases and at concentrations higher than 20 wt % the total pressure curves become similar to the standard S-shaped. For instance, the total pressure curve of the slurry of Sph St-SAl which includes 30 wt % SAl is standard S-shaped. It is because the suspension of SAl begins at quite low impeller speeds and is completed at a large impeller speed. The suspension of Sph St particles begins before the suspension of SAl particles is completed. Although the N_{js} of the unimodal slurry of 30 wt % SAl is measured as 960 rpm, the N_{js} of the unimodal slurry that contains 1.5 wt % Sph St is measured as 1233 rpm. The total pressure curve of the slurry is S-shaped because of the overlap of suspensions mentioned above: a portion of the Sph St particles are suspended before all the SAl particles are suspended.

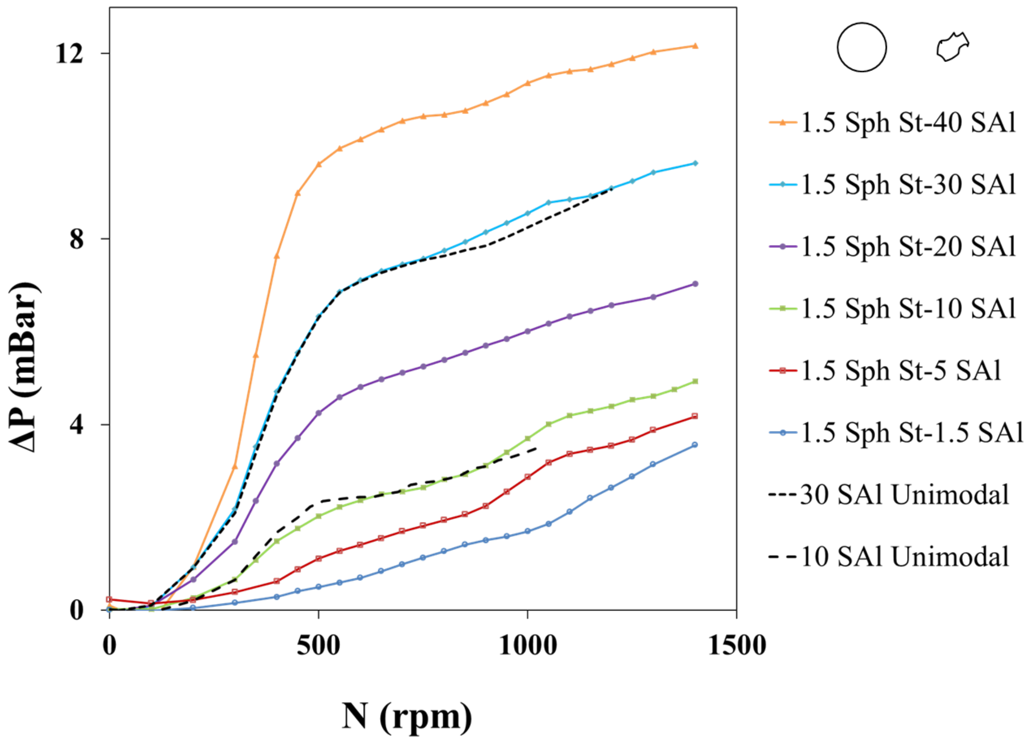

Figure 40. The total pressure curves of Sph St and SAl mixed slurries at varying concentrations and SAl unimodal slurries at 10 and 30 wt %

At low concentrations of mixed slurries where two waves are observed in the total pressure data, the N_{js} of the less dense solid phase can be approximated using the PGM method. Figure 41 shows an example of this for the Sph St-SAl mixture. Since the suspension of SAl is much easier compared to the much denser steel particles, initially the SAl particles are suspended. The suspension of the SAl particles corresponds to the first S-shaped curve. The pressure data after the first S-shaped curve correlates with the square of the impeller speed. This allows for the application of the PGM method to determine N_{js} of SAl. The N_{js} was found as 650 rpm. When the PGM method is applied to 10 wt % SAl only, the N_{js} was found as 690 rpm. The two data are very close.

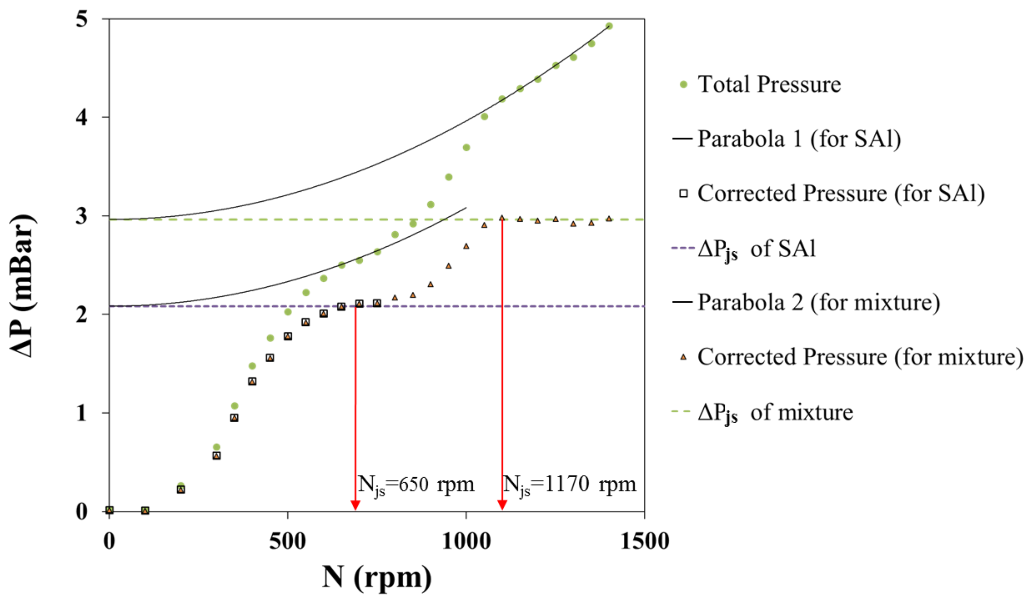

Figure 41. N_{js} of less dense solid alone and mixture can be determined with PGM method at low concentrations. The slurry is the mixture of 1.5 wt % Sph St and 10 wt % SAl

4.3.2.3 The Effect of Settling Velocity on the Application of PGM Method at Low Concentrations

According to the definition of the PGM method, pressure increase should be proportional to N^2 for impeller speeds higher than N_{js}; therefore, a second-order parabola can be fitted to the pressure data. Figure 42 shows an example of a case for which this procedure is not valid for the full range of pressure data above N_{js}. In this study it was observed that when the PGM method was used for unimodal slurries of particles which have settling velocities lower than 0.15 m/s and solids concentrations lower than 5 wt %, a second-order parabola could not represent the total pressure curve for N values higher than N_{js}. Instead, the pressure increase becomes a larger function of N. Figure 42 shows an example of this pressure increase for a unimodal TPE slurry at a solids concentration of 5 wt %. To determine N_{js} with PGM, a second-order parabola was fitted to data which corresponds to 450-600 rpm, but this parabola could not represent the total pressure data at impeller speeds higher than 600 rpm. If a parabola is fitted to the higher impeller speeds -that is N>600 rpm- the intercept which corresponds to ΔP_{js} would be negative. This is physically not meaningful. This trend was seen for ABS, TPE, Akulon, LAl, LG, SAl and SG particles. When the data for all these particles was analyzed it was seen that this unexpected sudden increase began once N become 20 % larger than N_{js}.

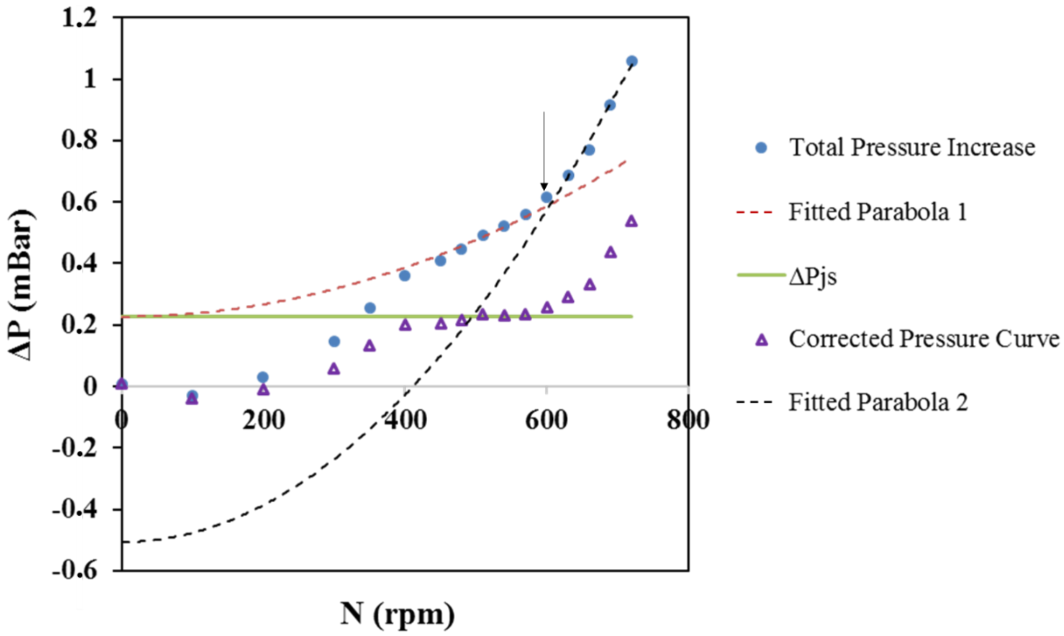

Figure 42. Sudden total pressure increase above N_{js} for the unimodal slurry of 5 wt % TPE. The arrow shows the onset of sudden pressure increase.

In order to investigate this trend, the trend of the total pressure curve with no solids in the tank was examined in the range of 0-2000 rpm. Figure 43 shows this data. The increase of ΔP is similar to the data in Figure 42 which is for low solids concentrations of low settling velocity solids. This shows that the presence of these solids does not affect the flow of the fluid. For the conditions at which this sudden pressure increase trend is seen, the dynamic head effects in the axial direction are larger than for the rest of the conditions. But this situation was not observed for mixed slurries because the presence of a second denser solid phase affects the flow of the fluid.

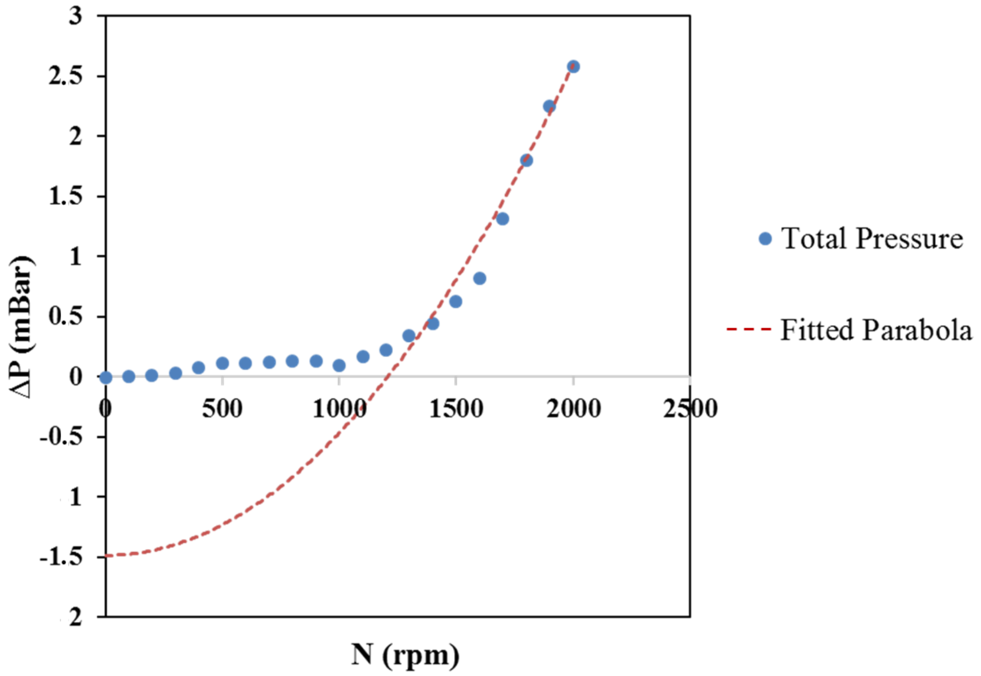

Figure 43. Pressure increase when there are no solids in the tank

As a result, the PGM method can be used to determine N_{js} of slurries with low settling velocity particles at low solids concentrations if the second-order parabola is fitted to total pressure data before the onset of sudden pressure increase.

4.3.3 Comparisons of PGM with Visual Method and Correlations

In this section, the PGM method was compared with the more commonly used visual observation method and with the correlation results. In Figure 44, the comparison of PGM method with the visual method is seen for all the mixed slurries used in this study at solids concentrations varying between 1.5 and 40 wt %. These two experimental methods give similar N_{js} results with 11.2 % standard deviation.

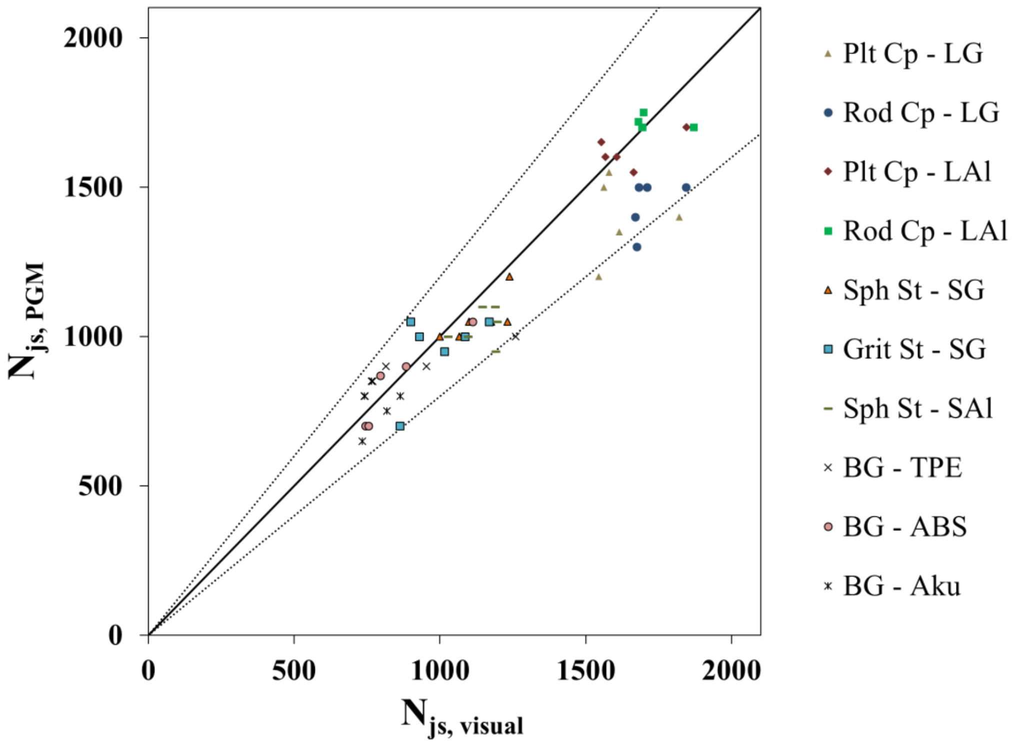

Figure 44. Comparison of N_{js} obtained with visual and PGM methods for mixed slurries. The data shows with ±20 % lines.

In Figure 44 it is seen that as visual N_{js} increases, PGM N_{js} remains constant for mixtures of Plt Cp-LAl, Sph St-SG and Sph St-SAl for subsequent 2 or 3 data points among which the solids concentration varies with small increments. The visual observation method is a more sensitive method in comparison with PGM about distinguishing small differences in N_{js}. According to the PGM method, the increase of apparent density of slurry affects the pressure measured at the bottom of the tank. To observe the changes due to small differences in the apparent density due to small increments in solids concentration, the precision of the pressure sensor should be sufficiently high. The sensor used in the experiments cannot measure these small differences in N_{js} of mixtures. This deficiency of PGM method can be eliminated by increasing the sensitivity of the pressure sensor. It should; however, be noted that the visual method may be sensitive to capture these small changes only based on the observer.

The comparison of visual and PGM N_{js} for all the unimodal slurries is given in Figure 45. The N_{js} values obtained with the two methods are again similar with 12.8 %

standard deviation. A similar observation can be made for some of the data: $N_{js, PGM}$ remains constant even though visual N_{js} increases because N_{js} of mixed slurries is close to each other at increasing concentrations up to 15 wt %. As can be seen in Figure 13-Figure 15 at low concentrations of less dense solid phase, N_{js} of the mixture does not change more than 50 rpm for slurries of Plt Cp-LAl, Sph St-SG and Sph St-SAl.

The fact that this trend is seen more in the data for mixed slurries could be thought to relate this behaviour to the number of solid phases present; however, the PGM method is based on the pressure increase and it should be proportional to N^2 for impeller speeds higher than N_{js} regardless of the number of solid phases present. The data given in Figure 45 helps proving this theory right, because the accuracy of this data is very close to the accuracy of the data of mixed slurries. Figure 44 and Figure 45 show that PGM method can be applied confidently to unimodal and mixed slurries at solids concentrations of 1.5 % to 40 wt % with a maximum deviation of 12.8 %.

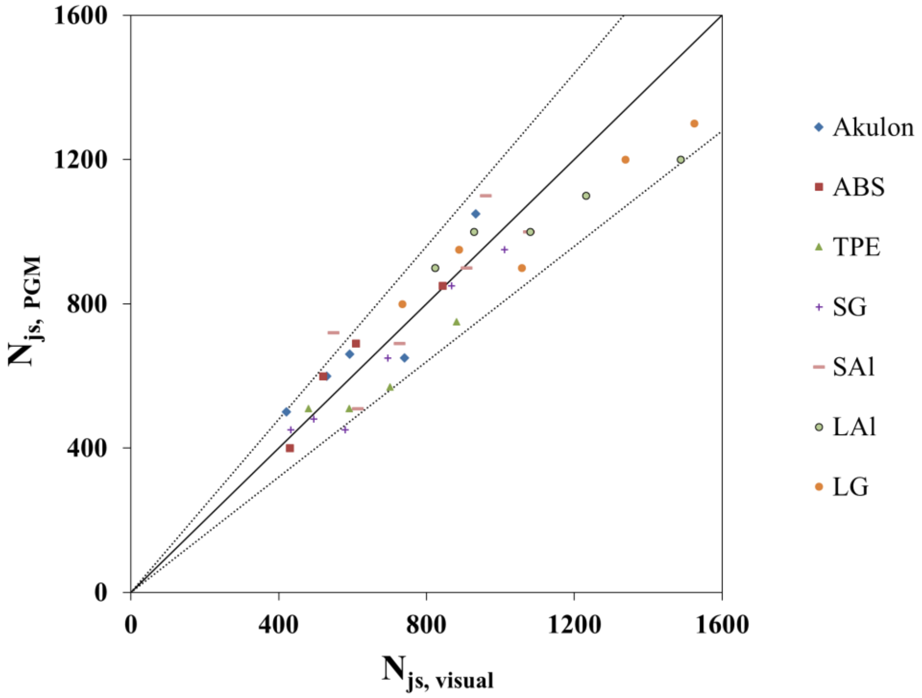

Figure 45. Comparison of N_{js} obtained with visual and PGM methods for unimodal slurries. The data shows with ±20 % lines.

If visual observation method cannot be used in a solid suspension application, N_{js} can be determined with correlations or PGM method. In Figure 46, the mixture N_{js} obtained from power model in which modified Ayranci's correlation was used for unimodal slurry N_{js}, and from PGM was compared. For some slurries, the data follows the parity line but for most it does not. However, most of the data lies between ±25 % lines, which is an indication that the correlations and PGM method provide similar results. The standard deviation from the parity line is found as 16.7 %.

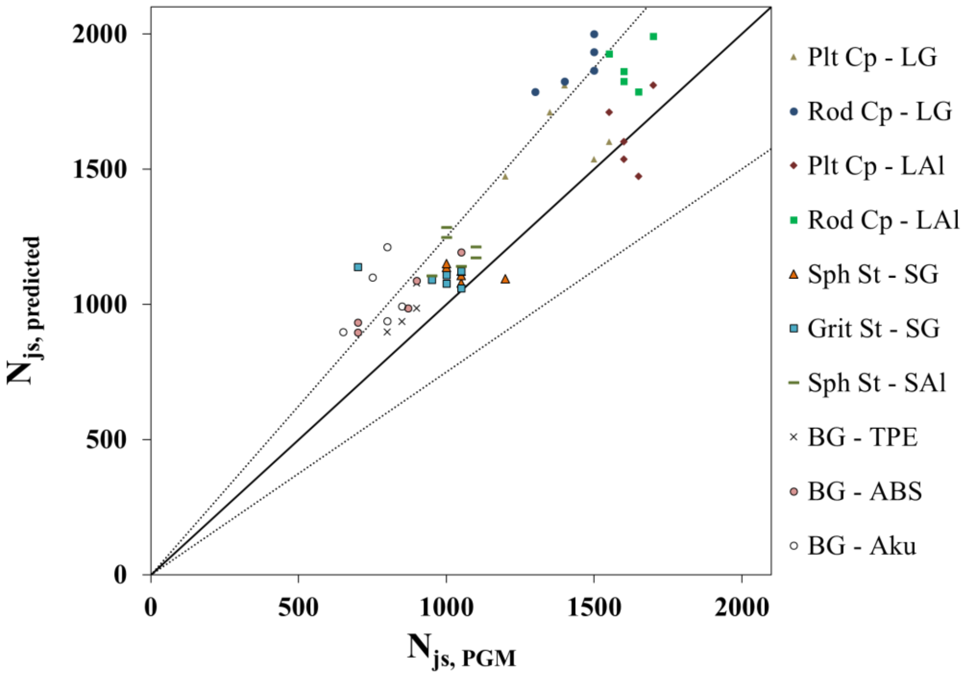

Figure 46. Comparison of N_{js} obtained with PGM method and obtained from correlations for mixed slurries. In power model predictions Ayranci's correlation was used for unimodal slurry N_{js}. The data shows with ±25 % lines.

Figure 47 shows the comparison of $N_{js, predicted}$ and $N_{js, PGM}$ for unimodal slurries. At the lowest concentrations of unimodal slurries, there are predictions outside the ±25 % lines. But in general, $N_{js, predicted}$ and $N_{js, PGM}$ are compatible. The standard deviation from the parity line is 19.1 %. The conclusion is reached that when N_{js} is determined by PGM experimentally, Ayranci can predict within ±25 % lines.

The results in this section show that PGM method can be applied beyond the limits that it was developed for. The conditions in this study are closer to industrial applications, thus the applicability of the PGM was tested for these conditions. As a result, PGM method which can eliminate the error based on the observer was recommended to use in industrial mixing systems.

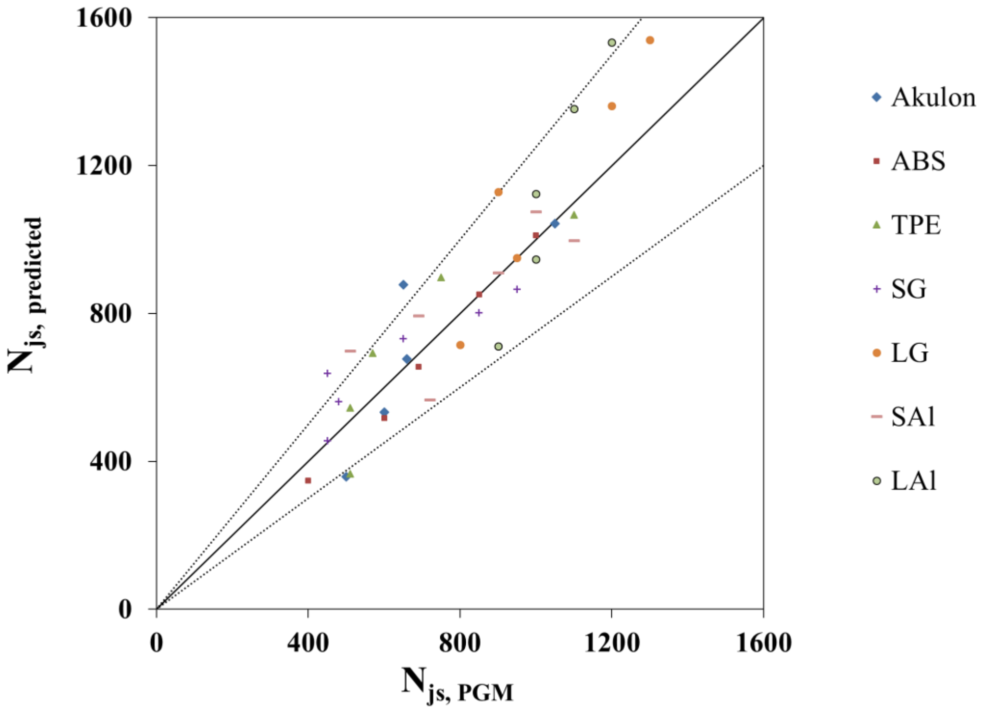

Figure 47. Comparison of N_{js} obtained with PGM method and obtained from Ayranci’s correlation for unimodal slurries. The data shows with ±25 % lines.

CHAPTER 5

CONCLUSIONS

For efficient operation of industrial applications of solids suspension, the maximum surface area between solid and liquid phases should be provided with minimum power consumption. The impeller speed that would provide this condition, N_{js}, for an application can be found experimentally, or by using correlations. The correlations in literature are empirical equations that are based on experiments conducted with spherical particles; however, the slurries include non-spherical and irregular shaped particles in actual industrial applications. Industrial applications also include mixed slurries at high concentrations. The aim of this study is to test the applicability of correlations for N_{js} prediction of concentrated mixed slurries in presence of non-spherical particles. To test the applicability of correlations at these conditions, N_{js} was determined by use of visual observation method. Then, another experimental method to determine N_{js}, PGM method, was tested. This method is an observer-independent and new method compared to visual observation method.

In this thesis following outcomes were obtained:

- When suspension behaviour of particles was examined by comparing solid phases which have similar size and density but different shapes it was seen that less spherical particles are easier to suspend.
- The mainly used five correlations for prediction of N_{js} in literature were compared with experimental N_{js} data. According to the result of the comparison, Ayranci’s correlation (Ayranci and Kresta, 2014) was the most accurate because it gave the smallest standard deviation – 10.5 % –for slurries with spherical and non-spherical particles.
- The experimental data that Ayranci’s correlation was based on was up to 35 wt % solids. The analysis of the data in this study showed that the correlation in fact provides reliable results (within ± 20 % error) up to 55 wt %.

- N_{js} of mixed slurries can be calculated with power model (Ayranci et al. 2013a, Bao et al. 2013). The power model, however, cannot take networking effect into consideration. To overcome this problem a factor, C was recommended based on the ratio of concentrations of solid phases:

$$N_{js,mix} = C\left(\frac{\rho_{sl,1}N_{js,1}^{3} + \rho_{sl,2}N_{js,2}^{3}}{\rho_{sl,mix}}\right)^{1/3} \tag{4.2}$$

$$C = (100 - \frac{X_{w2}}{X_{w1}})/100 \tag{4.3}$$

  After this modification the prediction of N_{js} of the slurries which show networking mechanism is improved significantly.

- It was found that Ayranci's correlation can predict N_{js} of slurries with spherical and non-spherical particles with similar accuracy. To obtain more accurate predictions for non-spherical particles, a particle shape term was added to Ayranci's correlation. Five different shape factors - AR, circularity, convexity, Wadell's sphericity and Corey's shape factor- were compared to define particle shape mathematically in the Ayranci's correlation. Wadell's sphericity was found as most convenient shape factor to take into account the effect of particle shape on N_{js}.
- After the modification of power model to account for networking mechanism and modification of Ayranci's correlation to account for particle shape, it was seen that N_{js} predictions are compatible with measurements with a deviation of 9.4 % for unimodal slurries and 15.6 % for mixed slurries.
- The PGM method was applied at conditions that are significantly different than literature conditions. The slurries resembled industrial applications in terms of solids concentration and the number of solid phases, and the required impeller speeds to suspend particles were higher than used in literature.
- The impeller speeds higher than 900 rpm caused fluctuations in pressure data. The PGM method could not be applied because of these fluctuations. This problem was solved by data filtering using Savitzky Golay filter.
- With increasing solids concentrations it was observed that the ratio of pressure increase due to the dynamic head effects to total pressure change decreased. But it is still possible to apply PGM method to slurries at concentrations up to 40 wt %.

- When PGM method was applied to mixed slurries, if the density difference between the solid phases is sufficiently high, the shape of the pressure-impeller speed curve gave information about the N_{js} of each solid component up to the concentration at which the interactions between the solid phases intensify.
- The total pressure data of the slurries which include particles that have settling velocity lower than 0.15 m/s showed a sudden increase at impeller speeds higher than 20 % of their N_{js}. But it is still possible to apply PGM method to these slurries if the second order parabola is fitted to data points before that sudden increase.
- When the results of visual measurements and PGM measurements were compared, it was seen that measurements are similar with 12.8 % maximum standard deviation for unimodal and mixed slurries. As a result, this study demonstrates that the pressure measurement method is also a reliable method for mixed slurries and at high impeller speeds – if the pressure data is filtered.

REFERENCES

Atiemo-Obeng, V.A, Penney W.R., Armenante P., 2004. Solid-Liquid Mixing. In: Paul EL, Atiemo-Obeng VA, Kresta SM, Eds. Handbook of Industrial Mixing: Science and Practice. *John Wiley & Sons.*

Ayranci, I., Machado, M.B., Madej, A.M., Derksen, J.J., Nobes, D.S., Kresta, S.M., 2012. Effect of Geometry on the Mechanisms for off-Bottom Solids Suspension in a Stirred Tank. *Chemical Engineering Science* 79:163–76.

Ayranci, I., Theodore, N., Arthur, W., Kresta, S. M., 2013a Prediction of Just Suspended Speed for Mixed Slurries at High Solids Loadings. *Chemical Engineering Research and Design* 91(2):227–33.

Ayranci, I., Kresta, S. M., Derksen, J. J., 2013b. Experiments and Simulations on Bidisperse Solids Suspension in a Mixing Tank. *Chemical Engineering & Technology* 36(11):1957–67.

Ayranci, I., Kresta, S. M., 2011. Design Rules for Suspending Concentrated Mixtures of Solids in Stirred Tanks. *Chemical Engineering Research and Design* 89(10):1961–71.

Ayranci, I., Kresta, S. M., 2014. Critical Analysis of Zwietering Correlation for Solids Suspension in Stirred Tanks. *Chemical Engineering Research and Design* 92(3):413–22.

Baldi, G., Conti, R., Alaria, E., 1978. Complete suspension of particles in mechanically agitated vessels. *Chem Eng Sci.* 33: 21-25

Bao T., Myers, K. J., Janz, E.E., Fasano, J.B. 2013. Just-Suspended Agitation of Solid Mixtures. *Canadian journal of Chemical Engineering* 91:1632–40.

Bouwman, A. M., Jaap, C. B., Vonk, P., Wesselingh, A., Hans, J., Frijlink, H. W., 2004. Which Shape Factor(s) Best Describe Granules? *Powder Technology* 146(1–2):66–72.

Corey, A.T., 1949. Influence of Shape on the Fall Velocity of Sand Grains. *Colorado A and M College, Fort Collins, Master Thesis*, p:102.

Cox, E.P., A method of assigning numerical and percentage values to the degree of roundness of sand grains. 1927 *Journal of Paleontology* 1 (3): 179–183.

Daniel, E., 1988. A Study of Factors Suspected of Influencing The Settling Velocity. *Mineral Industry Research Laboratory, University of Alaska Fairbanks*.

Davies, J., 1986. Particle Suspension and Mass Transfer Rates in Agitated Vessels. *Chem. Eng. Proc.* 20: 175–81.

Ditl, P., Nauman, E.B., 1992. Off-Bottom Suspension of Thin Sheets. *AICHE* 38(6):959–65.

Einenkel, W.D., Mersmann, A., 1977. Required rpm for suspending in agitators [Erforderliche drehzahl zum suspendieren in ruerhwerken], *Verfahrenstechnik*, 11(2): 90-94.

Emara, K., M., Ahmed, S. M., 2009. Characterizing Cavitation Erosion Particles by Analysis of SEM Images. *Tribology International*. 42:130–36.

Grenville, R. K., Giacomelli, J. J, Brown, D. A. R., 2016. Suspension of Solid Particles in Vessels Agitated by Rushton Turbine Imperllers. *Chemical Engineering Research and Design* 109:730–33.

Henthorn, K. H., Park, K., Curtis, J. S. 2005. Measurement and Prediction of Pressure Drop in Pneumatic Conveying: Effect of Particle Characteristics, Mass Loading, and Reynolds Number. *Industrial and Engineering Chemistry Research* 44(14):5090–98.

Heywood, H., 1962. Uniform and nonuniform motion of particles in fluids, *Proceedings of the Symposium on the Interaction between Fluids and Particles*, pp. 1–8.

Hilton, J.E., Mason, L.R., Cleary, P.W., 2010. Dynamics of gas–solid fluidised beds with non-spherical particle geometry. *Chem. Eng. Sci.* 65: 1584–1596.

Hua, L., Zhao, H., Li J., Wang, J., Zhu, Q., 2015. Eulerian – Eulerian Simulation of Irregular Particles in Dense Gas – Solid Fluidized Beds. *Powder Technology* 284:299–311.

Ibrahim, S.,Wong, S.D., Baker, F. I., Zamzam, Z., Sato, M., Kato, Y., 2015. Influence of Geometry and Slurry Properties on Fine Particles Suspension at High Loadings in a Stirred Vessel. *Chemical Engineering Research and Design* 94 (8): 324–36.

Ibrahim, S., Nienow, A. W., 1994. The Effect of Viscosity on Mixing Pattern and Solids, *in Proc. 8th European Conf. on Mixing, IChemE Symposium Series* 136: 25-32

Kasat, G.R., Pandit, A.B., 2005. Review on mixing characteristics in solid–liquid and solid–liquid–gas reactor vessels. *Canadian Journal of Chem. Eng.* 83: 618–643.

Kruggel-Emden, H., Oschmann, T., 2014. Numerical Study of Rope Formation and Dispersion of Non-Spherical Particles during Pneumatic Conveying in a Pipe Bend. *Powder Technology* 268: 219–36.

Kruggel-Emden, H., Vollmari, K., 2016. Flow-regime transitions in fluidized beds of non-spherical particles. *Particuology* 29: 1-15

Lambert, A., J.M., Smith, 1996. The Suspension of Flat particles in Stirred Tanks. *IChemE Research Event/Second European Conference for Young Researchers*, 1081–1083

Leith, D., 1987. Drag on Nonspherical Objects. *Aerosol Science and Technology* 6(2): 153–61.

Levenspiel, O., 1998.Chemical Reaction Engineering. Ind. Eng Chem., John Wiley & Sons, Oregon 97331 pp: 193-194

Liu, B., Zhang, X., Wang, L., Hong, H., 2008. Fluidization of Non-Spherical Particles: Sphericity, Zingg Factor and Other Fluidization Parameters. *Particuology* 6(2): 125–29.

Liu, Y., Park, J., Schnare, D., Hill, E., Taylor, L. A., 2008. Characterization of Lunar Dust for Toxicological Studies . II : Texture and Shape Characteristics. *ASCE* 21: 272–79.

Loth, E., 2008. Drag of Non-Spherical Solid Particles of Regular and Irregular Shape. *Powder Technology* 182(3): 342–53.

Mandø, M., Rosendahl, L., 2010. On the Motion of Non-Spherical Particles at High Reynolds Number. *Powder Technology* 202(1–3): 1–13.

Micale, G., Grisafi, F., Brucato, A., 2002. Assessment of Particle Suspension Conditions in Stirred Vessels By Means of Pressure Gauge Technique. *Trans. IChemE* 80 (A), 893–902.

Montante, G., Magelli, F., 2007. Mixed solid distribution in stirred vessels: experiments and computational fluid dynamics simulations. *Ind. Eng. Chem. Res.* 46: 2885–2891

Nikku, M., Jalali, P., Ritvanen, J., Hyppänen, T. 2014. Characterization Method of Average Gas – Solid Drag for Regular and Irregular Particle Groups. *Powder Technology* 253: 284–94.

Oldshue, J. Y. 1983. Fluid mixing technology and practice. Mcgraw Hill Inc, New York, 10020, pp. 83–108.

Parveen, F., Berruti, F., Briens, C., Mcmillan, J., 2013. Effect of Fluidized Bed Particle Properties and Agglomerate Shape on the Stability of Agglomerates in a Fluidized Bed. *Powder Technology* 237: 46–52.

Radoičić, K.T., Mihal, Đ., Garić-Grulović, R., Arsenijević, Z., Grbavčić, Z., 2014. Particle Characterization of Polydisperse Quartz Fi Ltration Sand. *Powder Technology*. 254: 63–71.

Saad, M., Sadoudi, A., Rondet, E., Cuq, B., 2011. Morphological Characterization of Wheat Powders , How to Characterize the Shape of Particles ? *Journal of Food Engineering* 102(4): 293–301.

Schaan, J., Sumner, R. J., Gillies, R. G., Shook, C. A., 1997. The Effect of Particle Shape on Pipeline Friction for Newtonian Slurries of Fine Particles. *Canadian Journal of Chem. Eng.* 78(4): 717–725

Schneiderhohn, P. 1954. Eine vergleichende Studie uber Methoden zur quantitativen Pestimmung von Abrundung und Form an Sandkornern, 1954. Heidelberger Beitrage zur Mineralogie und Petrographie 4: 172–191.

Selima, Y.S., Fangary, Y.S., Mahmoud, N.A., 2008. Determination of minimum speed required for solids suspension in stirred vessels using pressure measurements, *Can. J. Chem. Eng.*, 86(4): 661-666.

Thorpe, R. B., Stevenson, P., 2003. Suspension of Particles from the Bottom of Pipes and Stirred Tanks by Gassed and Ungassed Flows. *Can. J. of Chem. Eng.* 81: 351–59.

Wadell, H., 1934. The coefficient of resistance as a function of Reynolds number for solids of various shapes, *Journal of the Franklin Institute* 217 (4): 459–490.

Wong, S. D., Ibrahim, S., Zamzam, Z., Kato Y., Sato, M., 2015. Effect of Impeller-To-Tank Geometry on Particles Distribution and Just-Suspension Speeds for a Range of Solids Loadings. *Journal of Chemical Engineering of Japan* 48(5): 374–80.

Wu, J., Zhu, Y., Pullum, L., 2001. The Effect of Impeller Pumping and Fluid. C*anadian Journal of Chem. Eng.* (79): 177–86.

Zwietering, Th. N., 1958. Suspending of Solid Particles in Liquid by Agitators. *Chem. Eng. Sci.* 244–253.

APPENDIX

A. Particle Size Distribution

Table A 1. Sizes of particles determined by Malvern Mastersizer 3000

Sample Same	D (10)	D (50)	D (90)	D [3,2]	D [4,3]
SG	62.6	83.3	109	81.1	84.5
LG	552	701	890	692	714
Grit St	174	310	519	256	329
Sph St	88.6	168	276	109	175
S Al	53.5	87.4	139	81.3	92.3
L Al	166	238	335	228	244

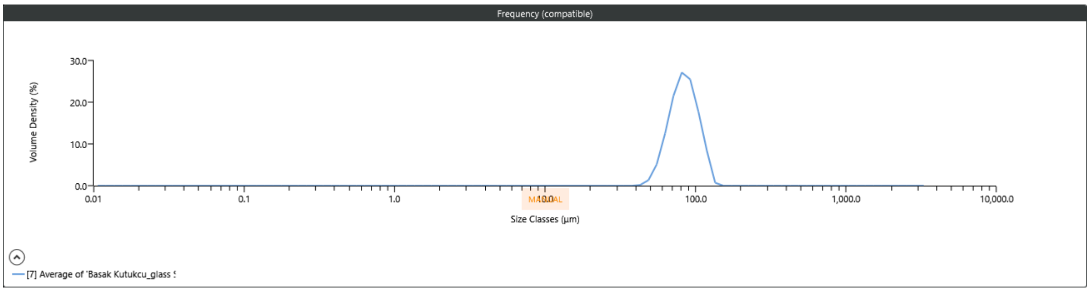

Figure A 1. Particle size distribution of SG

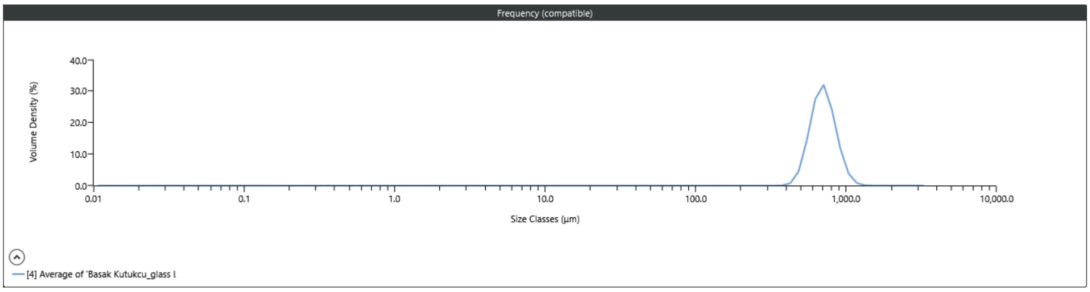

Figure A 2. Particle size distribution of LG

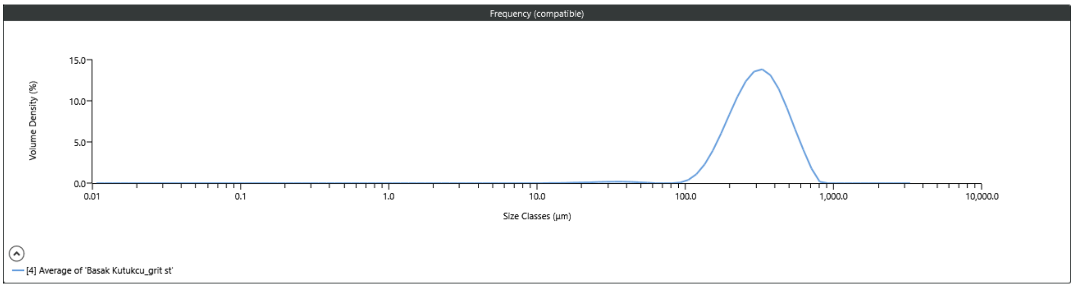

Figure A 3. Particle size distribution of Grit St

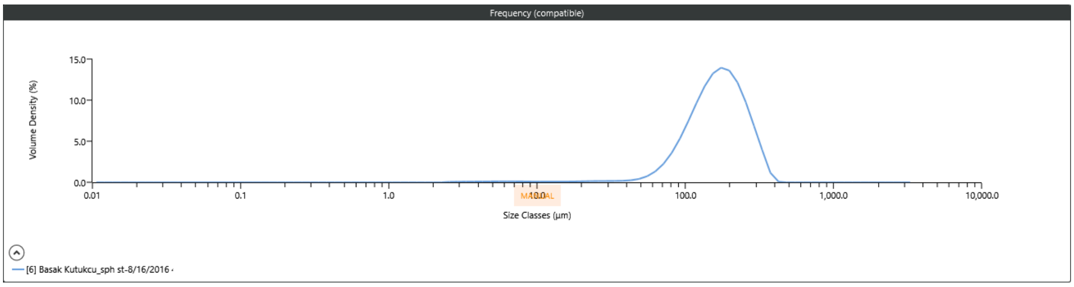

Figure A 4. Particle size distribution of Sph St

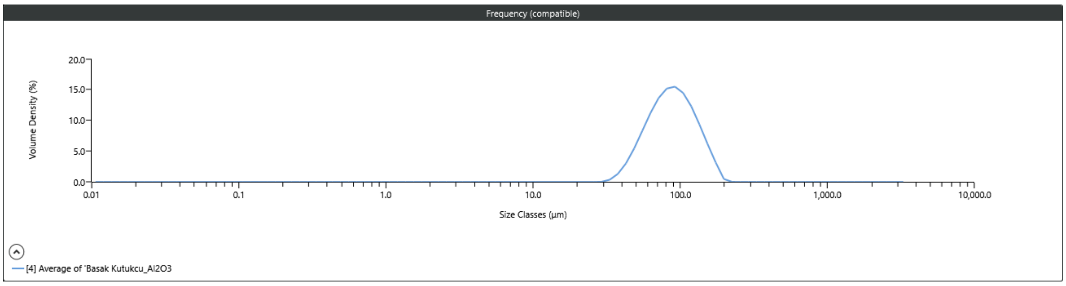

Figure A 5. Particle size distribution of SAl

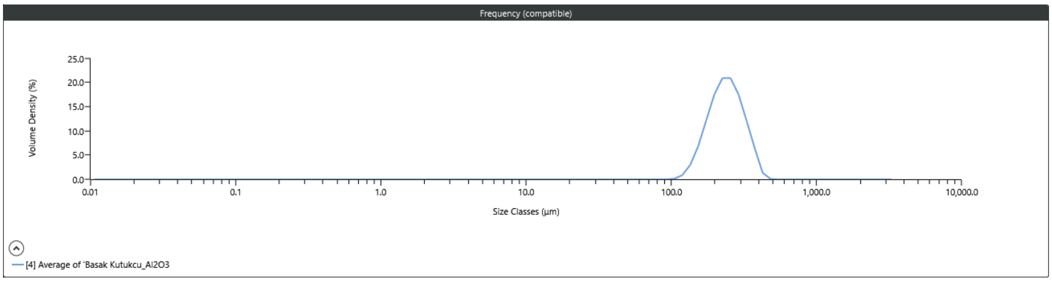

Figure A 6. Particle size distribution of LAl

B. Image Comparison

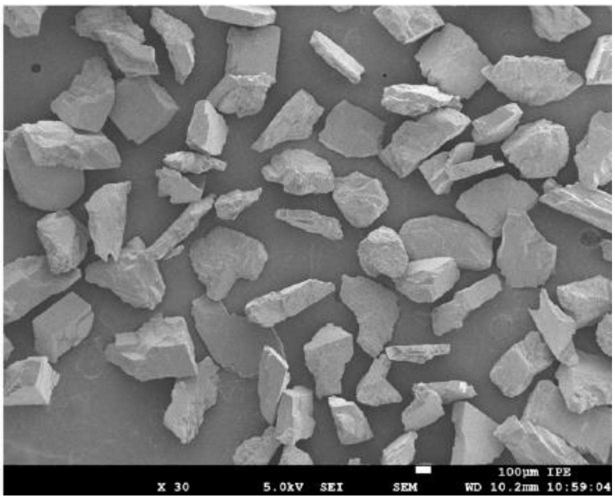

Figure B 1. SEM images of Alumni particles adopted from Hua et al. 2015

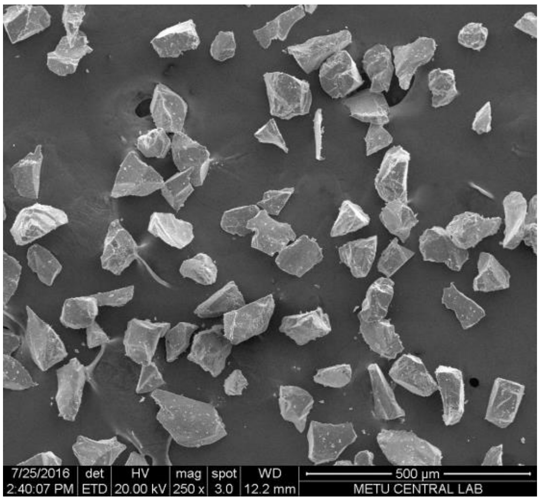

Figure B 2. SEM images of LAl particles used in this study